



Model for coupled ferroelectric hysteresis using time fractional operators : Application to innovative energy harvesting

Bin Zhang

► To cite this version:

Bin Zhang. Model for coupled ferroelectric hysteresis using time fractional operators : Application to innovative energy harvesting. Other [cond-mat.other]. INSA de Lyon, 2014. English. NNT : 2014ISAL0065 . tel-01175848

HAL Id: tel-01175848

<https://theses.hal.science/tel-01175848>

Submitted on 13 Jul 2015

HAL is a multi-disciplinary open access archive for the deposit and dissemination of scientific research documents, whether they are published or not. The documents may come from teaching and research institutions in France or abroad, or from public or private research centers.

L'archive ouverte pluridisciplinaire **HAL**, est destinée au dépôt et à la diffusion de documents scientifiques de niveau recherche, publiés ou non, émanant des établissements d'enseignement et de recherche français ou étrangers, des laboratoires publics ou privés.



Numéo d'ordre : 2014ISAL0065

Année 2014

THÈSE

Déivrée par

Institut National des Sciences Appliquées de Lyon (INSA Lyon)
Spécialité : Acoustique

DIPLÔME DE DOCTORAT

(Soutenue le 2 Juillet 2014 devant la Commission d'examen)

ÉCOLE DOCTORALE : MÉCANIQUE, ÉNERGÉTIQUE, GÉNIE CIVIL,
ACOUSTIQUE

Model for coupled ferroelectric hysteresis using time fractional operators: Application to innovative energy harvesting.

ZHANG Bin

Jury

BERNARD Yves	Professeur à Université Paris Sud	Rapporteur
DEU Jean-François	Professeur à CNAM	Président
DUCHARNE Benjamin	Maître de conférences à INSA Lyon	Co-directeur de thèse
GUYOMAR Daniel	Professeur à INSA Lyon	Directeur de thèse
LITAK Grzegorz	Professeur à LUT, Poland	Rapporteur
MELCHIOR Pierre	Maître de conférences à IMS	Examineur

INSA Direction de la Recherche - Ecoles Doctorales – Quinquennal 2011-2015

SIGLE	ECOLE DOCTORALE	NOM ET COORDONNEES DU RESPONSABLE
CHIMIE	CHIMIE DE LYON http://www.edchimie-lyon.fr Sec :Renée EL MELHEM Bat Blaise Pascal 3° etage Insa : R. GOURDON	M. Jean Marc LANCELIN Université de Lyon – Collège Doctoral Bât ESCPE 43 bd du 11 novembre 1918 69622 VILLEURBANNE Cedex Tél : 04.72.43 13 95 directeur@edchimie-lyon.fr
E.E.A.	ELECTRONIQUE, ELECTROTECHNIQUE, AUTOMATIQUE http://edeea.ec-lyon.fr Secrétariat : M.C. HAVGOUDOUKIAN eea@ec-lyon.fr	M. Gérard SCORLETTI Ecole Centrale de Lyon 36 avenue Guy de Collongue 69134 ECULLY Tél : 04.72.18 60.97 Fax : 04 78 43 37 17 Gerard.scorletti@ec-lyon.fr
E2M2	EVOLUTION, ECOSYSTEME, MICROBIOLOGIE, MODELISATION http://e2m2.universite-lyon.fr Insa : H. CHARLES	Mme Gudrun BORNETTE CNRS UMR 5023 LEHNA Université Claude Bernard Lyon 1 Bât Forel 43 bd du 11 novembre 1918 69622 VILLEURBANNE Cédex Tél : 06.07.53.89.13 e2m2@univ-lyon1.fr
EDISS	INTERDISCIPLINAIRE SCIENCES-SANTE http://www.ediss-lyon.fr Sec : Insa : M. LAGARDE	Mme Emmanuelle CANET-SOULAS INSERM U1060, CarMeN lab, Univ. Lyon 1 Bâtiment IMBL 11 avenue Jean Capelle INSA de Lyon 696621 Villeurbanne Tél : 04.72.68.49.09 Fax :04 72 68 49 16 Emmanuelle.canet@univ-lyon1.fr
INFOMATHS	INFORMATIQUE ET MATHEMATIQUES http://infomaths.univ-lyon1.fr Sec :Renée EL MELHEM Bat Blaise Pascal 3° etage infomaths@univ-lyon1.fr	Mme Sylvie CALABRETTO LIRIS – INSA de Lyon Bat Blaise Pascal 7 avenue Jean Capelle 69622 VILLEURBANNE Cedex Tél : 04.72. 43. 80. 46 Fax 04 72 43 16 87 Sylvie.calabretto@insa-lyon.fr
Matériaux	MATERIAUX DE LYON http://ed34.universite-lyon.fr Secrétariat : M. LABOUNE PM : 71.70 –Fax : 87.12 Bat. Saint Exupéry Ed.materiaux@insa-lyon.fr	M. Jean-Yves BUFFIERE INSA de Lyon MATEIS Bâtiment Saint Exupéry 7 avenue Jean Capelle 69621 VILLEURBANNE Cedex Tél : 04.72.43 83 18 Fax 04 72 43 85 28 Jean-yves.buffiere@insa-lyon.fr
MEGA	MECANIQUE, ENERGETIQUE, GENIE CIVIL, ACOUSTIQUE http://mega.universite-lyon.fr Secrétariat : M. LABOUNE PM : 71.70 –Fax : 87.12 Bat. Saint Exupéry mega@insa-lyon.fr	M. Philippe BOISSE INSA de Lyon Laboratoire LAMCOS Bâtiment Jacquard 25 bis avenue Jean Capelle 69621 VILLEURBANNE Cedex Tél :04.72 .43.71.70 Fax : 04 72 43 72 37 Philippe.boisse@insa-lyon.fr
ScSo	ScSo* http://recherche.univ-lyon2.fr/scso/ Sec : Viviane POLSINELLI Brigitte DUBOIS Insa : J.Y. TOUSSAINT	M. OBADIA Lionel Université Lyon 2 86 rue Pasteur 69365 LYON Cedex 07 Tél : 04.78.77.23.86 Fax : 04.37.28.04.48 Lionel.Obadia@univ-lyon2.fr

*ScSo : Histoire, Géographie, Aménagement, Urbanisme, Archéologie, Science politique, Sociologie, Anthropologie

Acknowledgements

With the accomplishment of this thesis, I have finished my PhD study for the past 3 years, as well as a ending of the past 20 years' schoolwork. I got a chance to come to France to continue my study 4 years ago to pursue the master degree and doctor's degree, which became a most precious journey in my whole life. I would remember this experience and treasure it in the rest of my life.

During the 4 years in France, I would like to show my thanks to my colleagues in LGEF, who act as my families and make me feel at home. Everyone in the lab is nice and is always ready to help me, either in science or in daily life. I also want to show the special appreciate to my supervisors, Prof. Daniel Guyomar and Benjamin Ducharne, who give me the opportunity to come to the lab and offer the most help in my research. We are colleagues at work, friends in life. They guided me with patience in every field we investigated. Prof. Guyomar's strong work ethic and creative thinking is contagious to me and will influence me throughout my professional career. And Dr. Ducharne's sense of responsibility, incredible patience, and numerous fruitful discussions. His enlightening guidance and encouragement is the powerful support for my work.

I would like to thank the committee members, who pay lots of time on my thesis and give me valuable opinions even though they are busy with their own work. Prof. Dr. Gaël Sebald also helps me to correct the manuscript with great patience and his suggestions make me further understand the fundamental knowledge of this subject.

I spent my happy childhood in the countryside in China until I passed the National College Entrance Examination to go to NWPU in Xi'an, where another new world welcomed me with its open arms. Soon after my graduation in the university, I got supported by the China Scholarship Council (CSC) to continue my study. This is the triple jump in my life who makes me believe that knowledge can change one's life. To be a scientist is always my dream since the childhood but I never think it came so smoothly. We are living in a world filled with information and technology and there are much more communication and exchanges than any time in the human history ever. The much more frequent and international contact makes the science more popular and active. I benefit from this system and it enable me communicate directly with the strongman in the field thanks to my laboratory.

Besides the profs Petit, Lebrun and Dr. Michaël's help, during my research, I can't do my work well without the help and support from Laurance, Veronique, Evelyne, Xunqian,

Yang and all my friends in the lab, where I am not able to list all the names for whom I am grateful.

I am also grateful for my family members, my parents, Yuan and Weiwei, who are always there helping me with courage, patience and comprehension. We didn't spend enough together during this period. In the following days, I will devote more time with them.

Abstract

Energy harvesting based on mechanical vibration has been a long time research topic for the last few decades. An experimental energy scavenging investigation was first conducted by Hasler et al [1] in 1984, in which a physiological converter made of polyvinylidene difluoride (PVDF) films was implanted on the ribs of a dog. By converting the energy expended for the respiration, a peak voltage of 18 V with a power of $17\mu\text{W}$ had been acquired. At that time, this amount of energy was not sufficient to power the desired electronic devices, which made it impossible to act as an implanted power supply. In 1995, Antaki et al made an energy harvesting shoe mounted piezoelectric generator made of PZT with the purpose of supplying artificial organs. [2] As it was found the ground reaction force associated with the heel strike and toe-off phases of the gait represent the greatest potential for usable energy, piezoelectricity had been chosen as the approach to convert mechanical energy to electrical energy. The shoe generator had two longitudinal barrels house cylindrical PZT piezoelectric stacks which were actuated by hydraulic amplifier at each end. The effective power transfer in the experiment vary from 200 mW to 700 mW depending on different conditions for walking while a simulated of 2 W could be estimated on jogging. Power at this level could easily support many electronic devices and the results of this feasible study motivate further development of this prototype. Nowadays the scientist use are making wider researches on the energy harvesting technologies in various categories. The decreased energy consumption of the IC circuit, processors & sensors, remarkable evolution in materials and new energy harvesting methods have greatly evolved. Besides the synthesis of new material (coefficients of coupling), other techniques developments including circuitry and power storage, e.g. the super capacitors, have got a considerable progress. The advancement of the past years' study makes the self-power for portable and wireless sensor achievable.

In addition to enhancing the energy conversion amount, another objective is to master and give a precise model with consideration of the disciplines of piezoelectric material behavior. In fact, these materials are in low electromechanical coupling and it's important to comprehend how they function under different kinds of external excitations. As in the case of [2], the author found the discrepancy between the simulation and experiment results. They also refereed the uncertainties of the rated of piezo constants could be a main cause of this differences. The constitutive equations are linear under moderate excitations, while the coefficients are nonlinear under relatively high excitation as it happened in this experiment.

The augment of the level of excitation power and the application of energy harvesting under large bandwidth always imply high amplitudes stimulation on the employed piezoelectric material, under which condition and coupling situation obvious nonlinearity begins to appear. A precise model for the ferroelectric material is mighty needed in the energy harvesting process, so as to give an instruction to the prototype designing and modelling optimizing. What's more, in the sensing and nano-positioning application, the model with

high accuracy can improve their resolution.

In this thesis, a model working on wide bandwidth considering the nonlinearity of the piezoceramic has been developed. The employment of the fractional derivative has broadened the usage of this model on expanded bandwidth. The model permit to predict the evolution of the dielectric polarization as well as the mechanical displacement, which has been tested on different samples under different kinds of stimulation (pure mechanical, pure electrical and hybrid of electrical & mechanical excitations). This fractional derivative factor has been first developed under electrical excitations to describe the dynamic behavior. The dynamic contribution takes effect when the excitation exceeds the quasi-static state and plays an important role under the high excitations. In the development of this model to mechanical field, the fractional derivative factor was found available as well under the mechanical excitation in the same value. In the following study, an inverse of mechanical model has been developed as well. To a given polarization, the inverse model could accurately control the mechanical stress should be applied on the piezoceramic. In the end, we stimulate the piezoceramic using both electrical and mechanical excitation to augment the energy harvesting amount which could become a promising method in energy harvesting field. Every model has been exhaustively demonstrated and specific measuring benches have been established to validate these models.

Taking the dynamic contribution factor, the fractional derivative factor, into the models make it possible to broad the working bandwidth for simulating the piezoceramic under various excitations. The fractional factor has been validated both in the mechanical and electrical field excitation proving its universality for a piezoceramic regardless its shape, but a material property. Experiments results and simulations in different kinds of excitations (amplitudes, frequencies) for every kind of the above models have been compared. Good approximation has been acquired indicating the model has a good accuracy in describing the material property and dynamic behavior.

Résumé

Les systèmes de récupération d'énergies basées sur les vibrations mécaniques environnantes suscitent l'intérêt depuis de nombreuses années. Des premières investigations expérimentales autour de la récupération d'énergie ont été menées en 1984 par Hausler et al. [1]. L'équipe de scientifiques avait alors implanté un convertisseur physiologique à base de film de polyfluorure de vinylidène (PVDF) sur les côtes d'un chien. En convertissant l'énergie dépensée par la respiration, une tension crête de 18V et une puissance de 17 μ W avaient été ainsi obtenues. Malheureusement, une si faible quantité d'énergie n'était pas suffisante pour alimenter les appareils électroniques déportés de l'époque. En 1995, Antaki et al. ont mis au point une chaussure dédiée à la récupération d'énergie à base de générateur piézoélectrique PZT avec comme objectif l'alimentation d'organes artificiels [2]. Lors de cette étude, il a été constaté que la force de réaction du sol à l'instant de l'impact représentait le plus grand potentiel d'énergie utilisable, la piézoélectricité a été choisie comme moyen de conversion pour transformer cette énergie mécanique en énergie électrique. Dans l'expérience proposée, la chaussure génératrice présentait deux barreaux cylindriques de PZT piézoélectriques et était actionnée par un bras hydraulique à chaque extrémité. La puissance utile issue de cette expérience variait entre 200 mW et 700 mW en fonction des conditions de marche. Et même des simulations prévoyaient jusqu'à 2 W pour de la course à pied. Une telle puissance pourrait facilement subvenir à nombreux appareils électroniques contemporains, ces résultats très encourageants ont fortement motivé la poursuite du développement de ce type de prototypes. Aujourd'hui encore, de nombreuses équipes scientifiques poursuivent des travaux sur l'amélioration des performances des techniques de récupération d'énergie, encouragés par la forte diminution de la consommation d'énergie des semi-conducteurs, des processeurs et des capteurs. Les propriétés des matériaux (coefficients de couplage...) et la mise au point de nouvelles méthodes de collecte de l'énergie ont elles aussi beaucoup évolué. Outre la synthèse de nouveaux matériaux, la mise au point de nouvelles techniques, l'apparition de nouveaux dispositifs de stockage de l'énergie tels que les super condensateurs ont également favorisé ce développement. Les progrès de ces dernières années sont tels que l'auto-alimentation de capteurs nomades, disséminés et sans fil est maintenant envisageable.

Augmenter l'efficacité de la conversion d'énergie est primordial, mais celle-ci pour être bien maîtrisée, passe par la mise au point de modèles précis et notamment par la prise en compte des lois régissant les matériaux piézoélectriques. En effet, ces matériaux sont à la base des couplages mécano/électriques et il est capital de comprendre comment ils fonctionnent quelque soit l'excitation externe. Ainsi dans [2], l'équipe de recherche avait constaté de nombreux écarts entre mesures et simulations, ces écarts étaient vraisemblablement liés à une mauvaise prise en compte des propriétés des matériaux. En effet, les équations constitutives de la piézoélectricité considérées comme linéaires dans l'article, ne le sont en réalité que sous excitations modérées ce qui n'était pas le cas de l'expérience.

L'augmentation des niveaux de puissance, couplée à la miniaturisation des systèmes

impliquent des sollicitations extrêmes sur les matériaux piézoélectriques utilisés, et donc de fortes non-linéarités au niveau des lois de couplages. En outre, la mise au point de techniques de récupération d'énergie large bande implique une grande gamme de fréquence d'utilisation. Un modèle précis du matériau ferroélectrique est indispensable pour établir des critères de conception des prototypes et leur optimisation. Par ailleurs, dans des applications de type détection ou nano-positionnement, un modèle avec une forte précision permet d'améliorer la résolution.

Dans cette thèse, un modèle précis, temporel, large bande tenant compte de l'ensemble des non-linéarités d'une céramique piézoélectrique a été développé. L'utilisation d'opérateurs fractionnaires a permis d'augmenter fortement la bande de fréquence de validité du modèle. Le modèle permet notamment de prévoir l'évolution de la polarisation diélectrique ainsi que le déplacement mécanique de l'échantillon testé et ceci quelque soit le type de stimulation (contrainte mécanique pure, champ électrique et même excitation hybride électriques/mécaniques). La dérivé fractionnaire a dans un premier temps été utilisée pour l'hystérésis sous excitation électrique pour décrire le comportement dynamique de la polarisation diélectrique. En effet, au delà d'un seuil de fréquence, lorsque l'état du matériau n'est plus quasi-statique, une contribution dynamique apparaît. Cette contribution joue un rôle primordial lorsque les niveaux de fréquence et d'amplitude sont élevés. La même étude a ensuite été menée sous contrainte mécanique, et le même opérateur fractionnaire a été utilisé avec succès. Nous avons entre autre constaté que sur un même échantillon les paramètres de simulation établis sous champ électrique étaient conservés sous contrainte mécanique. Ensuite, un modèle inverse permettant d'imposer la forme d'onde de la polarisation ou du déplacement a été proposé. Pour une polarisation ou un déplacement donné, le modèle inverse permet de déterminer avec précision l'effort mécanique à appliquer sur la céramique piézo-électrique. Ces modèles sont nécessaires pour optimiser une forme d'onde de contrainte mécanique ou électrique et obtenir un rendement supérieur des systèmes récupérateurs d'énergie. En effet, une nouvelle technique couplée champ électrique/contrainte mécanique de récupération d'énergie est présentée à la fin de la thèse, technique qui nous a permis de valider l'utilisation du modèle. L'utilisation du modèle permet d'optimiser la mise au point d'un prototype mais également d'obtenir la valeur exacte du rendement de la méthode en rendant compte notamment des pertes diélectriques. Dans la thèse, le modèle sous ses différentes variantes est décrit de manière exhaustive. De même des bancs de mesure spécifiques ont été mis en place pour la validation expérimentale.

Contents

Abstract	vii
Résumé	ix
Contents	xiii
List of Symbols	xv
1 Generality	1
1.1 Introduction	1
1.1.1 Origin of piezoelectricity	2
1.1.2 Piezoelectric materials	4
1.1.3 Physical coupling through a ferroelectric material	8
1.2 Piezoelectric, dielectric and mechanical properties of ferroelectric materials	9
1.2.1 Electrical boundary conditions:	9
1.2.2 Mechanical boundary conditions:	10
1.2.3 Piezoelectric coefficients	10
1.2.4 Hysteresis in a piezoceramic	14
1.3 Piezoceramic applications and justification of a non linear model	14
1.4 Energy Harvesting Technology	16
1.5 Natural energy sources and harvesting technology	19
1.6 Conclusion	21
2 Dielectric hysteresis model	23
2.1 Modeling of the Piezoceramic	23
2.2 Quasi-Static dielectric hysteresis model	26
2.3 Dynamic model	35
2.3.1 Fractional derivative	35
2.3.2 Dynamic model	38
2.4 Inverse Model	41
2.4.1 Quai-static inverse contribution	42
2.4.2 Dynamic inverse contribution	43
2.4.3 Polarization control	44

2.4.4	Strain control	44
2.4.5	Polarization contrl under mechanical-type excitation	44
2.5	Conclusion	45
3	Piezoceramic characterization – Experimental measuring bench	47
3.1	Introduction	47
3.2	Material processing	48
3.3	Experimental design	51
3.3.1	Measuring bench for the pure electrical excitation situation	51
3.3.2	Measuring bench for the pure mechanical excitation situation	54
3.3.3	Measuring bench for the hybrid situation, combination of simultaneous mechanical & electrical excitation	56
3.4	Experiment initialization & parameter validation	58
3.4.1	Under electrical field excitation	59
3.4.2	Under mechanical stress excitation	59
3.4.3	Under a combination of electrical field and mechanical stress	60
3.5	Conclusion	62
4	Results and Discussion	65
4.1	Introduction	65
4.2	Model for the dielectric polarization variation under external mechanical stress excitation $P(T)$	66
4.2.1	Description	66
4.2.2	Experimental results and analysis	67
4.2.3	Discussion and conclusions	69
4.3	Inverse model $T(P)$ for dielectric polarization under mechanical stress excitation	70
4.3.1	Introduction and applications	70
4.3.2	$T(P)$ inverse model	70
4.3.3	Experiment results	71
4.3.4	Conclusion and discussion	74
4.4	Energy harvesting based on Ericsson loop	75
4.4.1	Technique introduction and application	75
4.4.2	Basic Harvesting technique	75
4.4.3	Ericsson loops technique for the energy harvesting under synchronized electric field and mechanical stress	78
4.4.4	Simulation and experimental results	78
4.4.5	Discussion and conclusion	81
4.5	Conclusion	83

Conclusions and perspectives	85
Bibliography	90
List of figures	93
List of tables	95

List of Symbols and abbreviations

Latin letter

F	Force
E	Electric field
E_c	Coercive electric field
I	Current
P	Polarization density
P_{sta}	Saturation Polarization
P_r	Remnant polarization,
\mathbf{p}	An electric dipole moment
\mathbf{d}	A displacement vector pointing from the negative charge to the positive charge
q	Electric charge
T_c	Curie temperature
K^T	The material's dielectric constant
k	Electrical mechanical coupling factor or stiffness of a spring
d	Piezoelectric charge coefficient
g	Piezoelectric voltage coefficient
s	Elastic compliance
Q_m	The mechanical quality factor
f_r	The resonant frequency
f_1/f_2	The upper/lower 3dB frequency about the f_r
R	The resistance
C_a	The active capacity
C_b	The locked capacity
Y	Young's modulus or admittance
S_{ij}	Strain

D_i	Electric displacement field
T_{ij}	Stress
x	Deformation
L	Length
Th	Thickness
$u(t)$	Input voltage signal
$< A >$	Loop area of the hysteretic loop
n	Derivative operator

Greek letter

ϵ_0	Vacuum permittivity, $8.854 \times 10^{-12}(F/m)$
ϵ_r	Relative permittivity
$\tan\delta$	Dielectric loss factor
π	3.14
γ	Coefficient from the comparison between the simulation and measurement
σ	Coefficient from the comparison between the simulation and measurement
$\gamma_{\alpha\beta}[\cdot]$	Elementary hysteresis operators
$\mu(\alpha, \beta)$	Weighting function with switching values α and β
$\Gamma(z)$	Gamma function
ρ	Coefficient of material property
ϕ	Diameter

Abbreviations

USM	Ultrasonic motor
PZT	Lead zirconate titanate
CPU	Microprocessor
RAM	Random-access memory
TWS	Thermal Weapon Sight
CPE	Constant phase element
SPM	Scanning probe microscopy

Chapter 1

Generality

1.1 Introduction

Piezoelectric materials have the ability to generate an electric potential in response to a mechanical stress (the direct piezoelectric effect) and deform according to an applied electric field (the converse piezoelectric effect). The first demonstration of the direct piezoelectric effect was in 1880 by the brothers Pierre Curie and Jacques Curie. Soon after, they experimentally identified the converse effect. The first practical application of the direct piezoelectric effect has been sonar, during the World War I, developed by French scientist Paul Langevin and his co-workers. Current development of piezoelectric materials make it possible an employment in various industrial fields, such as underwater sound transducer, B-ultrasonic probe, ultrasonic motor (USM), piezoelectric pressure transducer and so on.

Successive researches have been conducted on piezoelectric, such as the developments of the material synthesis, understanding of the physical behaviour and improvement of the coupling performances. Electrostriction properties and pyro-electricity have also been highly studied. Because of its specific set of characteristic, its high nonlinear behaviour, its frequency dependence, a precise model describing correctly the correlation between polarization, electric field and mechanical stress is still missing.

To understand and model the hysteretic phenomenon in piezoelectric materials, one can base on theoretical support from ferromagnetic domain where theories are relatively more mature. Among them, Preisach model of quasi-static hysteresis (first suggested in the year 1935 by F. Preisach) is one of the most widely accepted and efficient for taking into account of the hysteresis property of ferromagnetic. Preisach model has already been used

with success for the quasi-static piezoelectric hysteresis property (comparison between our model and Preisach model will be done in the second part of this thesis). But concerning the dynamic hysteresis behaviour of piezoelectric materials, relatively few studies have already been done and we lack of understanding the piezoelectric behaviour under such working conditions.

In this thesis, even if the theory and model proposed can be adopted for large family of ferroelectric and ferromagnetic materials, we mainly concentrate on piezoceramic. First part of this thesis will deal with basic properties of piezoelectricity. Then second part will expose the modelling of piezoceramic dielectric hysteresis under mechanical and electric excitations of changing properties (amplitudes, frequencies, waveforms, ...); an experimental measuring bench specially developed for this thesis will be presented in section 3; the next part will talk about some industrial applications and the last part will give some conclusions about our work and some predictions.

1.1.1 Origin of piezoelectricity

The piezoelectricity behaviour is illustrated in Fig. 1.1.

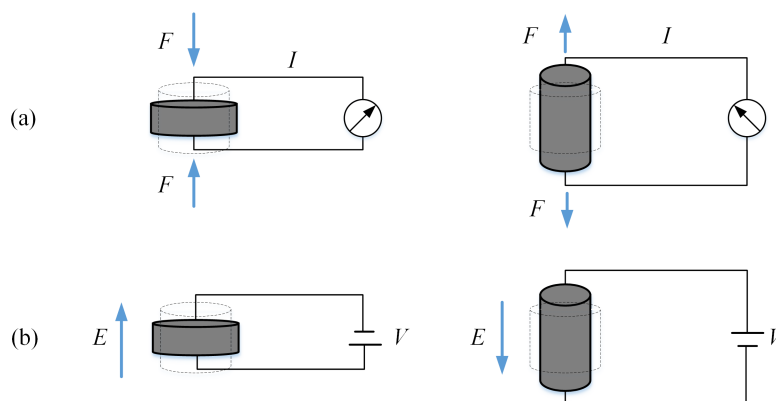


Figure 1.1: illustration of the piezoelectric effect.

The piezoelectric effect is a reversible process. A piezoceramic is a material where both direct piezoelectric effect (mechanical stress induces electric field) and converse piezoelectric effect (electric field induces mechanical stress) exist. Many ferroelectric materials can be chemically expressed as ABO_3 , see Fig.1.2(a), with an octahedron constructed by 6 oxygen atoms including a small metallic element in the center. Perovskite(see Fig.1.2(b)) type is the basic and the most common crystallographic structure in ferroelectric materials. In the cubic lattice structure, if it extends in the direction 001 under mechanical external force, the 100 and 010 directions will shrink as a response. As a consequence, the plus ions, the anions and their valence electrons will be separate from the center of gravity of the electric charges. When this displacement occurs, the positive and negative electric charges create an electric dipole moment as $\mathbf{p} = q\mathbf{d}$, where q is a pair of opposite electric charges magnitude; \mathbf{d} is a displacement vector pointing from negative electric charge to positive

one. The electric polarization density \mathbf{P} (C/m^2) is the average electric dipole moment \mathbf{p} in the volume. The induced polarization direction will be along the extended direction 001. If the cubic lattice is compressed along the direction 001, the electric charges move in the opposite direction (compared to the extended case) which means a converse electric field resulting and an induced polarization field in the inverse direction. [3] If the cubic lattice is submitted to an electric field whose direction is along 001, an electric dipole moment appears either in the extended orientation or in the compress one which also induces different polarization direction; this is the reverse piezoelectric effect.

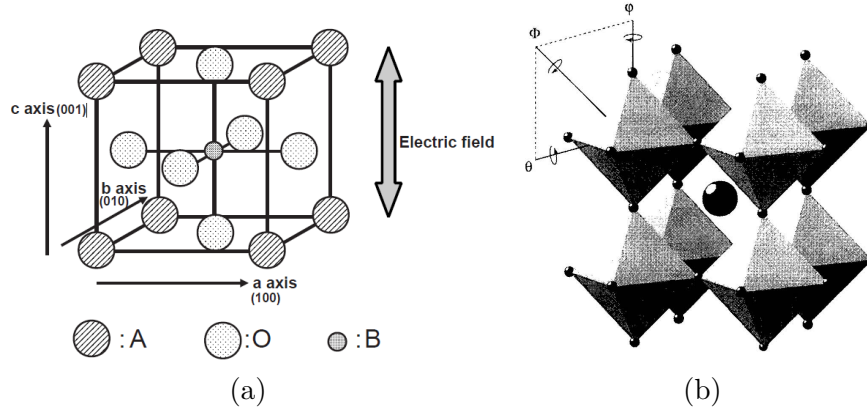
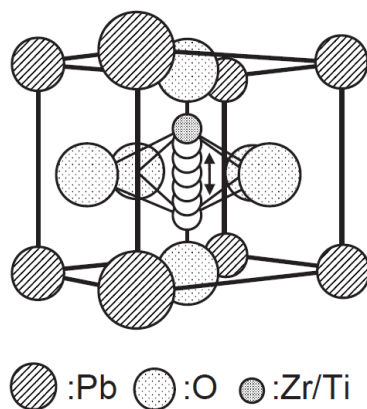


Figure 1.2: (a). ABO_3 crystal structure [3] (b). $CaTiO_3$ structure. [4]

Lead zirconium titanate (PZT) is one of the most representative ferroelectric material with perovskite crystallographic structure. It is an inter-metallic inorganic compound of $PbZrO_3$ and $PbTiO_3$ and its chemical formula is $Pb[Zr_xTi_{1-x}O_3]$ ($0 \leq x \leq 1$). Special properties of PZT are created by the addition of specific ions into the compound. Consequently, substantial changes will appear in the piezoelectric properties of the PZT according to the requirements. [3] By instant, one can get a soft PZT, by replacing Pb^{2+} with higher electro-valence ions, such as La^{3+} , Bi^{3+} or higher than Ti^{4+} , such as Nb^{5+} , W^{6+} , the dopant will cause a decrease of the coercive electric field E_c and an increase of the losses angle $\tan\delta$; As Q_m (the quality factor) is decreasing, ageing resistance will increase. On the contrary, by addition of Na^+ , K^+ and Fe^{2+} , Ni^{2+} or other element with electro valence lower than Pb^{2+} and Ti^{4+} , a hard PZT is obtained, accompanied to changing material properties whose are opposite to the soft one. [5]

A contemporary tendency is to replace the Pb in the PZT composition, such as $BaTiO_3$. The main reason for this replacement in the original recipe is due to the PbO , which is volatile and poisonous especially in the industrial process as the temperature is high. Unfortunately there is still a large scope of applications where classical PZT remain irreplaceable.

There is a tendency that replace the PZT — base with no Pb , such as $BaTiO_3$. The reason is $PZT(Pb(Zr,Ti)O_3)$'s main composition is PbO (up to 60% to 70%), who is volatile and poisonous especially in the process of high temperature sintering. But the PZT — based ferroelectric materials still has a large scope of use with its irreplaceable. [6]

Figure 1.3: $PZT(Pb(Zr,Ti)O_3)$ crystal structure [3]

This is out of the scope of this thesis and we will don't talk much about it.

1.1.2 Piezoelectric materials

In crystallography, crystals can be classified as 32 crystal classes. [7] As the crystal structures are composed of electrically charged particles, hence the piezoelectric behaviour of such a material is predictable. By studying the symmetry conditions of the crystal structures, one can distinguish the materials with piezoelectric properties from the others. In order to have such a property, a centre of asymmetry structure is necessary. Among the 32 classes, 21 cases are asymmetric while the others who possess center-symmetric structure are called the Laue classes. The 21 asymmetric classes, will not produce dipoles as an external mechanical excitation is applied, which means that no piezoelectric effect would be observed. The other 11 classes have the ability to exhibit piezoelectric effect as a mechanical solicitation is enough to separate the positive and the negative charges from their center of gravity in the crystal lattice. The dipoles will appear and as a consequence a polarization on both sides of the material. Besides mechanical stress or electrical field, temperature change can also induce a flow of charge to and from the surface of the tested sample. A current can be measured in a close circuit. The induced polarization direction is called the polar axis. This phenomenon is called pyroelectricity. Out of these 11 classes, 10 are pyroelectric. [8]

Ferroelectricity is another class of material. All pyroelectric materials are ferroelectric. A ferroelectric material will exhibit an electric polarization (parallel to polar axis) after having been excited by an external electric field. The dielectric polarization through a ferroelectric material can simultaneously switch its orientation under inverse electric field of sufficient amplitude. This properties has led to the development of the ferroelectric random access memory FRAM commonly employed for the computer memories.

The 32 crystal classes and their specifications are displayed in Fig. 1.4.

If a piezoceramic temperature is increasing and reaches the boundary temperature, known as Curie temperature T_c , the ceramic crystalline structure becomes cubic. The

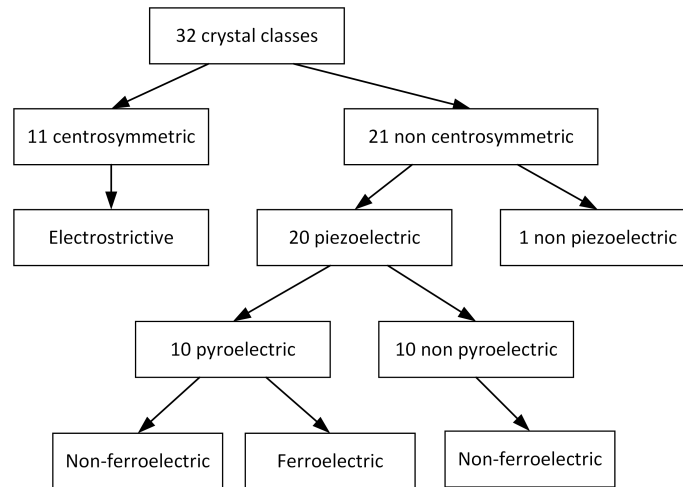


Figure 1.4: the 32 crystal classes denominations [8]

crystallographic axes exhibit the same length and the axes intersection angle reach 90° . Under these external conditions, the positive and the negative element remain stock in the charges center of gravity. The dielectric polarization effects disappear. After a period beyond T_c temperature and as the temperature is decreasing the crystalline structure loses its cubic shape; the axes length and the intersection angles are changing resulting by an imbalance of charge gravity and by the appearing of a dipole moment whose direction is along the polar axis. From a macroscopic viewpoint (at a grain level), the natural energy minimization give birth to various macroscopic domain characterized by own polarization direction. The ferroelectric domains are in a random state and the average dielectric polarization is in neutralization, showing zero as a whole. This state is known as non-polarized state (see Fig 1.5-a). If a sufficiently high electric field is applied to the ceramic in a non-polarized state, the ferroelectric domain polarization average orientation will rotate along with the electric field direction. Viewed from a microscopic viewpoint (at crystal lattice level), the positive charges and the negative ones will continue separate and are suffered from torque so the lattice shifts itself to the direction external electric field, aligning with its polar axis. Some lattices would change 90° while others would rotate 180° , as a result, the former case causes the piezoceramic dimension changes and the latter doesn't. This process is called dielectric polarization. (see Fig 1.5-b) Even if the electric field is eliminated, the positive and the negative charges will not return to their original positions and the domain average orientation will not rotate back. This dielectric state is called remnant polarization (see Fig 1.5-c); from an energy point of view, a non-polarized state is more stable than a polarized one. So after a long period of time, the remnant polarization level will slowly decrease and the tested ceramic will finally returns to a non-polarized state. [9] This behaviour is one of the reasons for ageing.

In this thesis study, we keep the focus on PZT materials (soft and hard ones, depending on our mechanical quality factor). A typical and widely used ceramic, type Navy 2-P188 from St-Gobain, has been employed first. This material is a “soft” piezoceramic known

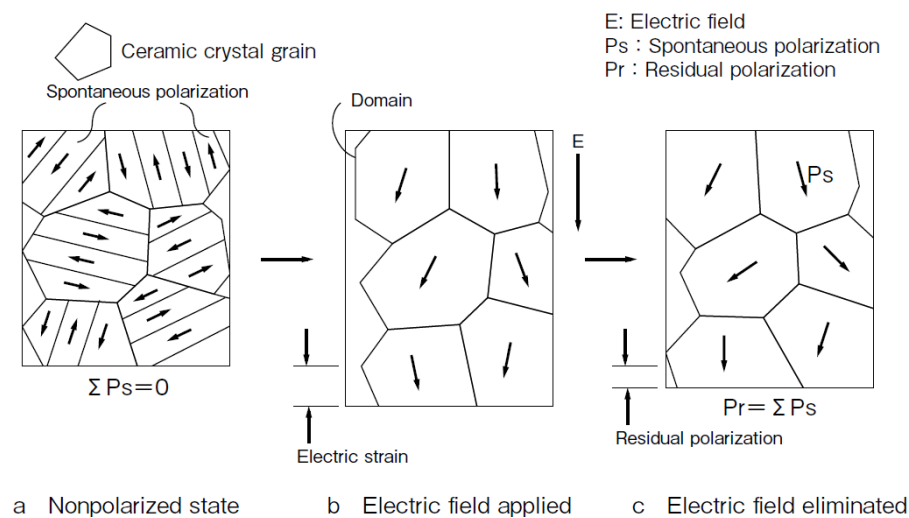
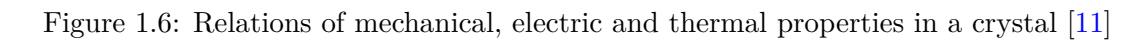


Figure 1.5: Crystal grain with respect to electric field [9]

for its high piezoelectric coefficient, and its low mechanical quality factor. After validation with this first material, others ceramics of changing compositions and characteristics have been taken into consideration. We have tested consecutively the PZT5A from Morgan Electro Ceramics, the FUJI-C2, C23, C202, C213 from Fuji Ceramics Corporation. Their manufacture technical data are shown in the following Table 1-1. 1.1 in the next page.

Table 1.1: Material technic data [10]

	Symbol	Unit	P188	P189	PZT5A (3195HD)	FUJI-C2	FUJI-C23	FUJI-C202	FUJI-C213
Electrical Properties									
Relative Free Dielectric Constant (1kHz)	K_{33}^T		1850	1150	1900	1460	800	1600	1470
Dielectric dissipation factor (1kHz)	$\tan\delta$	%	2	0.3	1.8	0.25	0.27	0.20	0.30
Curie Temperature	T_C	$^{\circ}C$	340	320	350	300	290	290	315
Electromechanical Properties									
Coupling factor	k_p k_t k_{31} k_{33}		0.65 0.49 -0.37 0.74	0.51 0.46 -0.32 0.65	0.65 0.72 0.36 0.72	0.63 0.53 0.37 0.76	0.59 0.54 0.35 0.73	0.56 0.47 0.32 0.69	0.58 0.48 0.34 0.70
Piezoelectric charge coefficients	$-d_{31}$ d_{33} d_{15}	$10^{-12}C/N$ or (m/V)	185 425 400	108 240 280	190 390	158 367 692	100 270 690	130 315 540	135 310 510
Piezoelectric Voltage coefficients	g_{11} g_{33}	$-10^{-3}Vm/N$ or (m^2/C)	11 26	-11 23	24	29.2	32.8	22.3	23.4
Frequency constant	N_p N_t N_{31} N_{33}	m/s	1970 2020 1450 1890	2350 2150 1750 2060	211	2100 2020 1550 1410	2210 2040 1650 1480	2240 2120 1620 1550	2230 2090 1620 1540
Mechanical Properties									
Density	ρ	kg/m^3	7700	7650	7800	7600	7630	7850	7800
Mechanical quality factor	$Q_{m,t}^E$		80	>1000	80	1200	1400	1200	2500



1.2 Piezoelectric, dielectric and mechanical properties of ferroelectric materials

Piezoelectricity means interactions between electrical and mechanical properties. The piezoelectric equations relay these interactions, including external and internal conditions. Relationships between the applied forces and the piezoceramic responses will depend of:

the piezoelectric properties of the ceramic;

the size and the shape of tested sample;

the direction of the electrical and (or) the mechanical excitation.

To identify directions in a piezoceramic elements, the three dimensional coordinates are necessary. Three axes, 1, 2 and 3, are analogous to X, Y and Z in the classical three dimension orthogonal set of axes. 4, 5, and 6 represent shear of the responding axes. These are schematically illustrated in the Fig. 1.7

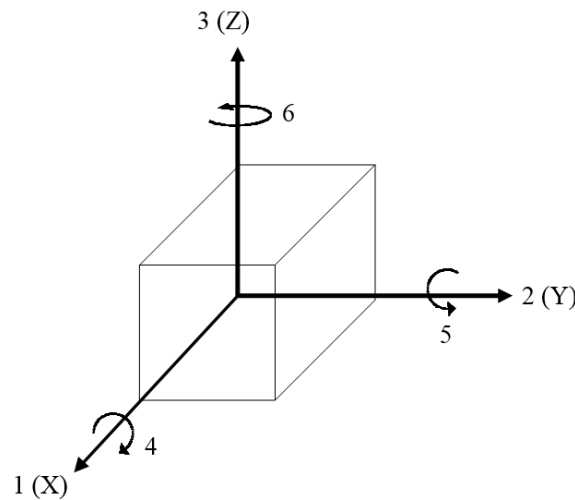


Figure 1.7: Coordinate system in the piezoceramic analysis [12]

1.2.1 Electrical boundary conditions:

The piezoceramic can be considered as short circuited, when the resistance of the external circuit connected to the two piezoceramic electrodes is much smaller than the resistance of the piezoceramic. The charges on the electrodes are then neutralized via the external circuit; the electric field remains constant equal to zero.

The piezoceramic can be considered in open circuit, when the resistance of the external circuit is much higher than the internal one. As the piezoceramic is excited by an external mechanical load, charges will join the electrodes and consequently an electric field is appearing.

1.2.2 Mechanical boundary conditions:

The piezoceramic can be considered as free, when the tested sample is clamped in the direction of no-deformation. The clamp force will not affect the movement and the deformation of the piezoceramic; it just behaves as a holding force. The piezoceramic can be considered as clamped, when the tested sample is clamped on both sides of the deformation direction, the mechanical strain in the clamped direction remains equal to zero. In experimental special conditions a clamped state can be imposed on just one size of the ceramic in order to increase coupling performances (known as cantilever beam).

1.2.3 Piezoelectric coefficients

The piezoelectric coefficients linked electrical and mechanical quantities. They are always associated to two subscripts. The first subscript gives the direction of the electrical field imposed or measured along the tested sample electrodes. The second subscript gives the direction of the mechanical stress or strain induced or applied. Furthermore, a superscripts will precise if the proposed coefficient has been determinate under constant or not electrical conditions (D, E) and reciprocally under constant or not mechanical conditions (S, T). Table 1.2 is dedicated to the piezoelectric coefficients superscripts indications; Table 1.3 gives the information for the subscripts ones.

Symbol	Parameter	Condition
T	Constant Stress	Mechanically Free
E	Constant Electric Field	Short Circuit
D	Constant Electrical Displacement	Open Circuit
S	Constant Strain	Mechanically Clamped

Table 1.2: Constant boundary condition [12]

By combination of electrical and mechanical boundary conditions, 4 forms of constitutive equations can be given. In the case of industrial applications including piezoceramic, other environmental conditions must be taken into consideration. According to this environment, internal parameters of the piezoceramic will be particularly affected, by instant:

The material's curie temperature

The crystal structure of a material will change as the thermal elevation of the tested sample will reach its Curie temperature, T_c . The material state will switch from piezoelectric (non-symmetrical crystallographic structure) to non-piezoelectric (symmetrical crystallographic structure). At this temperature, the material exhibits its maximum dielectric constant value and above this temperature its piezoelectric capacity will rapidly disappear.

The material's dielectric constant

The relative dielectric constant is defined as the ratio, between the material permittivity (ϵ_r) and the vacuum permittivity (ϵ_0), in a mechanical free condition.

$$K^T = \epsilon_r^T = \frac{\epsilon^T}{\epsilon_0}$$

K_3^S	K : Relative dielectric constant(ϵ_3^S/ϵ_0)	3: Electrodes are perpendicular to 3 axis	3: S	S : All strain in the material are constant or mechanical deformation is blocked in any direction
k_{23}	k : Electromechanical coupling factor	2: Electrodes are perpendicular to 2 axis	3: Stress or strain is in 3 axis	
d_{13}	d : Piezoelectric charge coefficient	1: Electrodes are perpendicular to 1 axis	3: Applied stress, or piezoelectricity induced strain is in 3 direction	
g_{23}	g : Piezoelectric voltage coefficient	2: Electrodes are perpendicular to 2 axis	3: Applied stress, or the piezoelectrically induced strain is in 3 direction	
s_{16}^E	s : Elastic compliance	1: Strain or stress is in 3 direction	6: Stress or strain is shear around 3 direction	E : Compliance is measured with closed circuit

Table 1.3: Subscript corresponding to the electrical and mechanical indication [12]

The dielectric constant is derived from the static capacitance measurement, usually close to 1 kHz, far from the resonant frequency. The capacitance is dependent on the material nature and dimension. However, the relative permittivity is purely a material property. The capacitance is given by the product of the relative dielectric constant, the vacuum permittivity, the electrode area and divided by the thickness of the material.

$$C = \frac{\epsilon_r \epsilon_0 A}{Th}$$

The dielectric loss factor

The dielectric loss factor is defined as the tangent of the loss angle ($\tan\delta$). The loss factor represents the ratio of conductance to susceptance in the parallel equivalent circuit of a piezoceramic element. It can be measured directly using an impedance analyzer. The

dielectric loss factor is related to the real and imaginary part of the dielectric permittivity:

$$\tan\delta = \frac{\epsilon''}{\epsilon'}$$

The mechanical quality factor

In physic science or engineering domain, the quality factor, Q , is a no dimension measure describing the resonance quality of a vibrator or a resonator (amplitude and selectivity of the resonant peak). It is a scalar coefficient describing the frequency bandwidth of the resonator around its resonance frequencies. It is also related to the sharpness of the resonance frequency. The mechanical quality factor can be determined using impedance meter analyzer, via the well-known -3 decibel method:

$$Q_m = \frac{f_r}{f_1 - f_2}$$

Here, f_r is the resonant frequency, f_1 and f_2 will respectively be calculated by substrate first -3 db to the resonant frequency gain and by the identification next of the frequencies (higher and lower than the resonant frequency) associated to this new gain. [12]

Another technique allows reaching this coefficient using the electrical equivalent circuit (Fig.1.8) of the piezoceramic. The mechanical quality factor is then given by the following relation:

$$Q_m = \frac{1}{R} \cdot \sqrt{\frac{L}{C_a}}$$

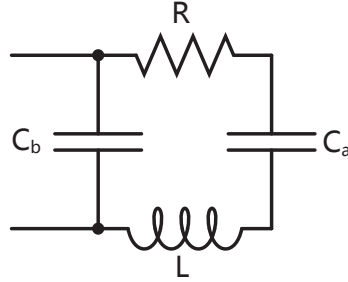


Figure 1.8: Equivalent electrical circuit of a piezoceramic.

Where C_b is the blocked capacity, C_a is the active capacity linked to the material compliance, L is the dynamic mass and R is the damping coefficient. [13]

Q is also related to the energy of an energy supplier, like a generator, per cycle, as the signal amplitude is constant.

$$Q_m = 2\pi \times \frac{\text{Energy stored}}{\text{Energy dissipated per cycle}} = 2\pi f_r \times \frac{\text{Energy stored}}{\text{Power loss}} \quad (1.1)$$

In this expression (1.1) [14], the stored energy is the total energy stored through the system, including potential and kinetic energies. The loss power is the energy lost during one experimental cycle to keep the magnitude constant.

A high Q indicates a lower rate of energy loss relatively to the stored energy of the resonator; the oscillations will die out more slowly. A vibrating beam oscillating in the air and bearing a lower damp, will get a high Q . On the contrary, a beam immersed in oil will exhibit a low Q .

The piezoelectric coupling coefficient

If we admit two successive energy piezoceramic conversions: first conversion will transform mechanical energy to an electrical one, second conversion will transform the electrical energy previously obtained to mechanical one. If these two conversions have been performed using same piezoceramic, the piezoelectric coupling coefficient of this sample will be given by the ratio between the two mechanical energy levels of these transformations. [15] The coupling coefficient (electromechanical coupling coefficient) is then also defined as the ratio of the electrical energy accumulated in response to a mechanical input or vice versa:

$$k = \sqrt{\frac{\text{Electrical energy stored}}{\text{Mechanical energy applied}}}$$
$$k = \sqrt{\frac{\text{Mechanical energy stored}}{\text{Electrical energy supplied}}}$$

Electromechanical coupling coefficient can be described as a numerical measure of the conversion efficiency between electrical and acoustic energy in a piezoelectric materials. [16] k values quoted in ceramic suppliers' specifications typically are theoretical maximum values. At low input frequencies, a typical piezoelectric ceramic can convert 30 - 75% of the energy delivered to it in one form into the other form, depending on the formulation of the ceramic and the directions of the forces involved. A high k usually is desirable for efficient energy conversion, but k does not account for dielectric losses or mechanical losses, nor for recovery of unconverted energy. The accurate measure of efficiency is the ratio of converted, useable energy delivered by the piezoelectric element to the total energy taken up by the element. By this measure, piezoelectric ceramic elements in well designed systems can exhibit efficiencies that exceed 90%. [17]

Elastic compliances

The Young's modulus describes the mechanical stiffness properties and is expressed as the ration of stress to strain. In a piezoceramic, a mechanical stress produces an electrical response in this opposite direction to the resulting strain. The value of the Young's modulus depends on the direction of the stress and of the strain. It also depends on the electrical conditions. The inverse of the Young's modulus, Y , is the elastic compliance, s , it is a piezoceramic major parameters and it can be calculated as follows:

$$s = \frac{1}{Y} = \frac{\text{Strain}}{\text{Stress}}$$

1.2.4 Hysteresis in a piezoceramic

Hysteresis is a nonlinear delay phenomenon between the input and the output signal of a system. This delay is mostly due to the memory effect. It means that the current output is not only dependent of the present input but also its history. Hysteresis plots are observable for electrical or mechanical conversions; hysteresis constitutes a characteristic of the tested material. Hysteresis loops can be plot for the characterization of magnetic or ferroelectric materials. In a piezoceramic a $P(E)$ dielectric hysteresis loop is obtained as we plot the evolution of the dielectric polarization P through a piezoceramic versus the electric field E . In an ideal capacitor the evolution of the polarization versus the electric field is a straight line with a gradient equal to the dielectric permittivity. Indeed in a perfect capacitor the temporal variation of the current is 90 degree ahead of the imposed voltage. As the polarization is equal to the temporal integration of the current, the voltage and the polarization exhibit same phase (see Fig. 1.9-(a)). By opposition for a perfect resistor, the current and the voltage are in phase. In the P-E plan, polarization versus electric field is a circle (see Fig. 1.9-(b)). Even if the manufactured capacitance exhibit behaviour close to the perfect one a parallel resistance must be taken into account as the frequency increase. Both effects will combine in a real capacitance as illustrated Fig. 1.9-(c). The slope of the loop is related to the permittivity and the loop area is associated to the well known losses angle of the capacitance. Finally Fig. 1.9-(d) shows the $P(E)$ loop of a real ferroelectric material, including hysteresis and saturation [18].

When a piezoceramic is submitted to a sinus low frequency, high amplitude electric field, the plot of the polarization field variations versus the electric field exhibit a hysteresis-type loop (as illustrated Fig. 1.10). Here, P_{sat} is the saturation polarization, P_r the is remnant polarization, and E_c is the coercive electric field. More details are available in [19].

Piezoceramic acts as an actuator since it offers nanometer resolution, high stiffness and fast response when subjected to a varying electric field. However, as the external excitation increases, hysteresis will affect its accuracy. This aspect is particularly annoying as piezoceramic are employed as sensors or positioning controllers. Indeed, in an open loop control system, hysteresis can cause inaccuracy and can generate amplitude-dependent phase shifts and harmonic distortions that reduce highly the efficiency of the feedback controls [20].

1.3 Piezoceramic applications and justification of a non linear model

During the last 30 years, the improvement of the piezoelectric performances of piezoceramics has permitted the manufacturing of a lot of new applications in the field of sensors, and actuators (see Table 1.4). Piezoceramic actuators as an example can be employed in MEMs machining, hard disk drive positioner, or probe of scanning tunnelling microscope. The advantages of such actuators are:

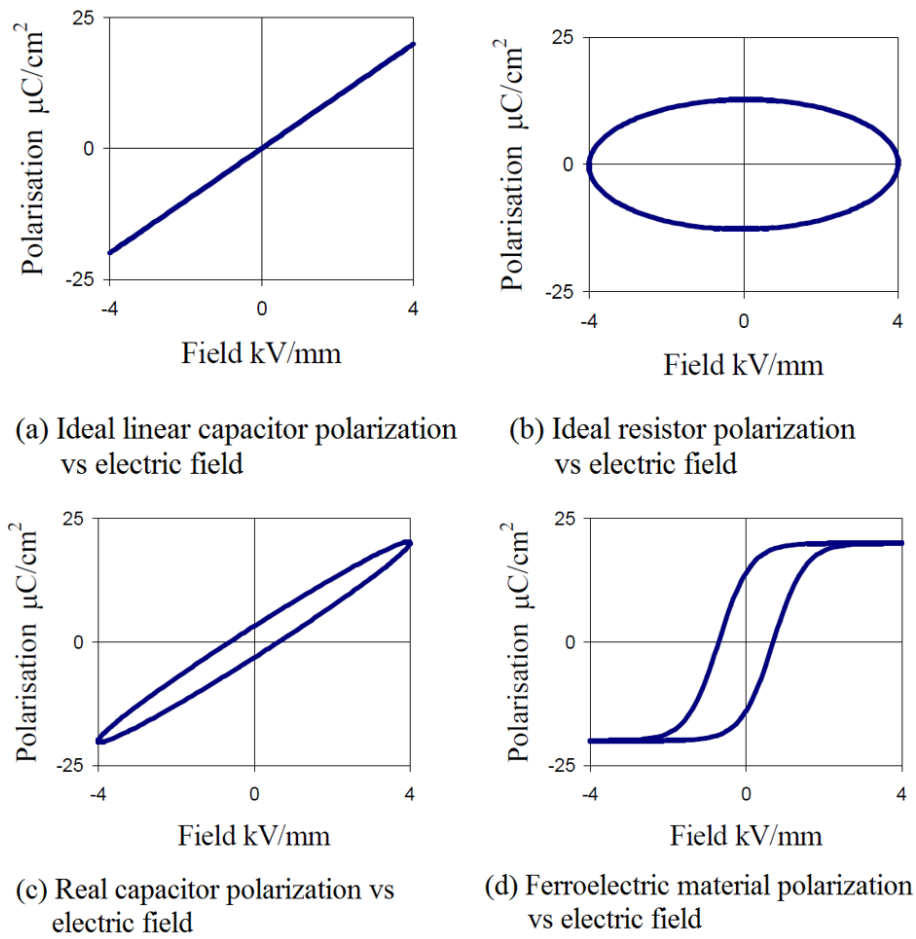


Figure 1.9: Illustration of different electric element polarization under electric field

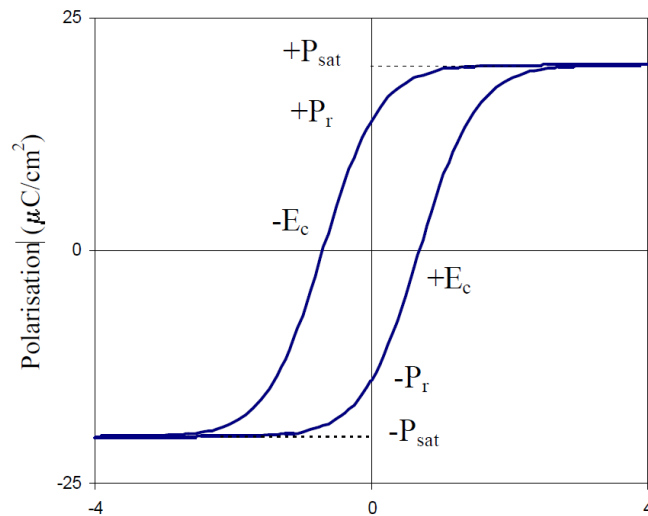


Figure 1.10: P-E hysteresis loop for a ferroelectric piezoceramic [18]

A quick response,
A high accuracy,

A great versatility,
The small level of vibration induced,
The capability to work under high level of external load.

One major limitation to the piezoceramic expansion is its intrinsic non-linear behaviour as we plot the output signal versus the input excitation. Consequently traditional control and feedback method are no longer useful and especially dedicated model and technics are required to correctly deal with such materials.

Applications based on direct piezoelectricity	Applications based on converse piezoelectricity	Applications based on two effects
Microphone	Loudspeaker	Ultrasonic echo sounder
Hydrophone	Buzzer	Ultrasonic testing
Shock sensor	Sonar transducer	Proximity sensor
Push button	Ultrasonic cleaning	Gyroscope
Force sensor	Relay	Ultrasonic buffer rods probes
	Micro positioner	
	Laser adjustment	
	Ink jet	
	Piezoelectric pump	
	Piezoelectric scalpel	

Table 1.4: Typical ferroelectric material applications [21]

1.4 Energy Harvesting Technology

The so-called “energy harvesting” is the process that convert the environment energy (such as thermal energy, vibration, light, wind energy, etc.) into electricity. This energy can be stored or employed as supplier to low-power small devices (wearable gadgets, control remotes and so on). Due to the limitation of the batteries capacity and even if the power consumption of processors is weak, a continuous usage of such apparatus is impossible without an external electric grid support. With the evolution of the contemporary life, the demand for portable devices of long term usage has been highly multiplied. To satisfy this demand, manufacturers are always looking for new solutions, energy harvesting offer a good compromise, it represents an alternative solution for the energy supply of all these portable devices. In the last 20 years, the development of the electronic and particularly the reduction of the component consumptions enable the employment of such techniques and the independence of the whole system to an external electric grid support. To illustrate

this evolution, let's take the example of modern computers. With modern industrial design and new performances of electronic components, where a usual battery provided a supplying time close to 5 hours 10 years ago, the same battery will give an amount of energy sufficient for an operating time close to 10 hours, taking the laptop for an example. The reduction of energy consumption, has also allowed the increase of the microprocessor (CPU) speed, for example, in Fig. 1.11, the progression of a typical CPU speed has been 250% between 2001 and 2005, and such performances have been obtained for a power consumption evolution of just 40%.

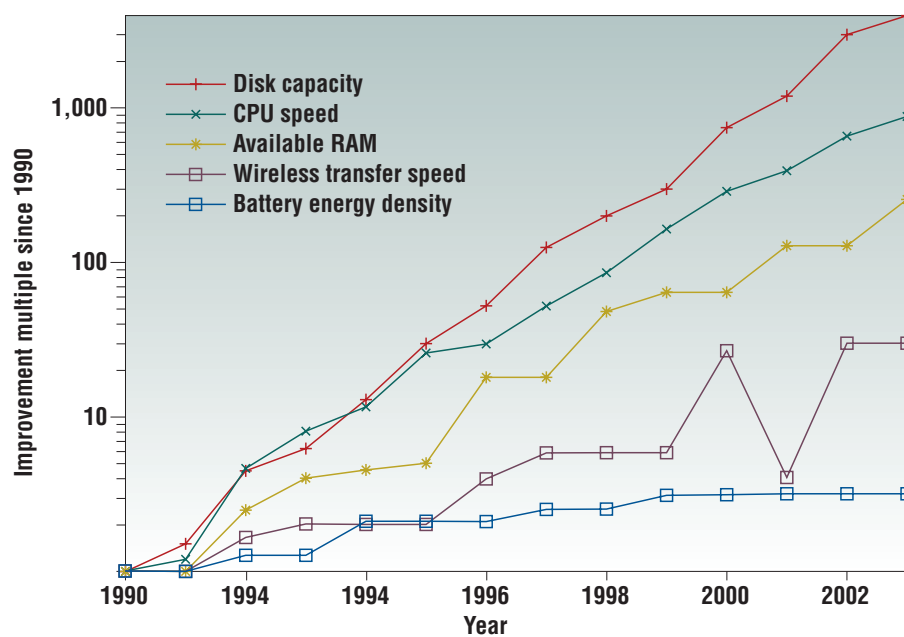


Figure 1.11: Development of disk capacity, CPU speed, available RAM, wireless transfer speed, battery energy density from 1990 to 2002 [22]

With power optimization and low power-consumption chips, the electronic devices could work for long time. The battery energy density increase is still too weak and means a real limitation for the operating time of such apparatus. An energy harvesting system could scavenge ambient energy to supply these low-powered devices or prolong battery life time. As the development of processing technique implies reduction for the power consumption, see Fig. 1.12, energy harvesting efficiency is increasing year by year. Soon, the balance state between the level of energy harvested from ambient energy and the level of energy required will be reached providing the energetic independence of all portable electronic gadgets.

Beside these first usages, other fields of applications for our energy harvesting systems can be investigating:

The remote areas

As illustrated by the recent Camel Fridge project in Africa (see Fig. 1.13), energy harvesting systems give a new alternative to provide electrical energy to isolated geographic

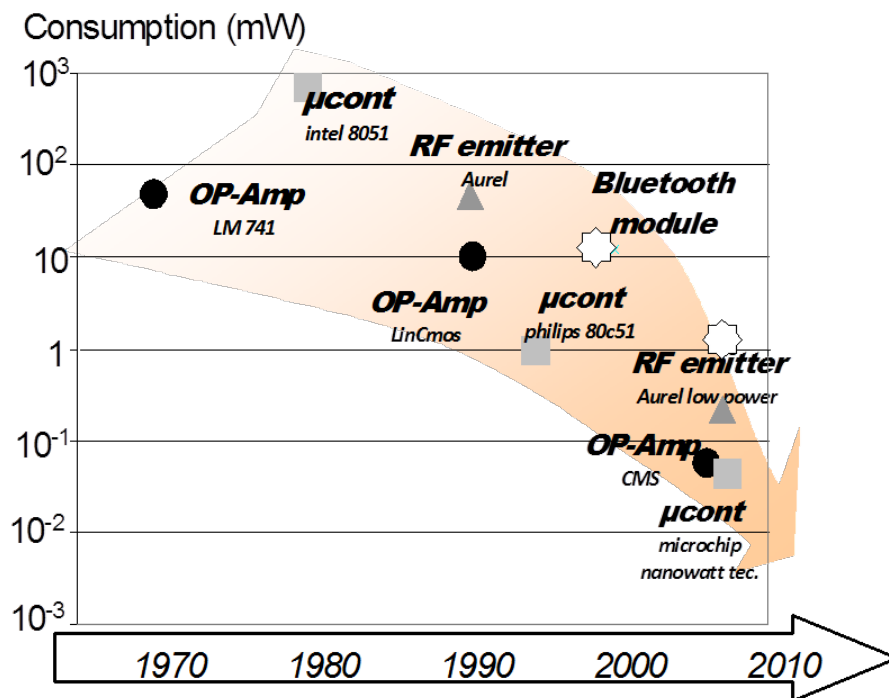


Figure 1.12: Progress of some chips' energy consumption standard [23]

areas. In this project, the protagonist use solar-powered fridge lay on camel's back to send chilled medicines and vaccines to remote and rural areas where roads and vehicles are missing. The mini fridge is put into a bamboo saddle which is light in weight and could be carried for miles in rough terrains and the solar panels put on the fridge provide powers both for the camel clinic and illumination. This Eco-friendly and cost-effective method provides medicine to thousands of people geographically isolated.

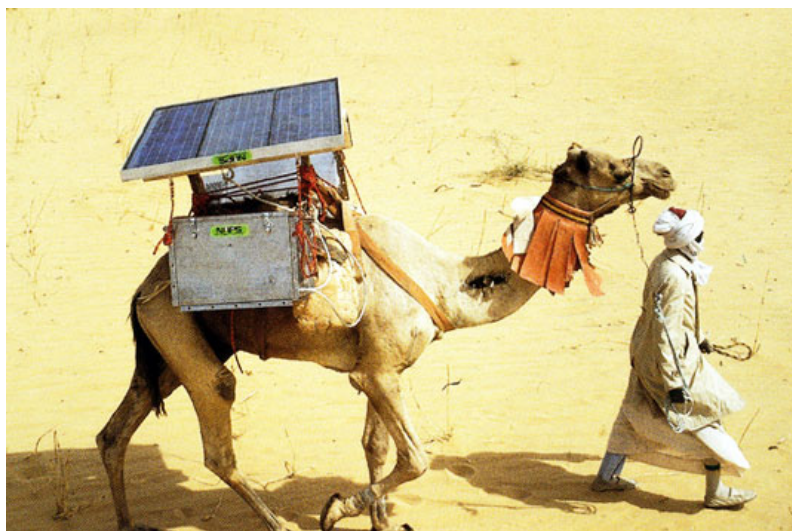


Figure 1.13: The Camel Fridge project to deliver medicines to the remote villages in Africa (Photo from <http://inhabitat.com/>)

The extreme environment

In the extreme environment, under high humidity, high temperature, corrosive, or radiated conditions, to provide correct information sensors require a stable electric supply. Usually in such environments, electric grids are not covered. In this condition, a battery is usually the first choice for the power supply. Due to the lifespan of the battery, long time detections are not possible. Sudden attack of mud-rock flow gives an example of such environment, scientist supervisors put lots of detectors in the field where electric grid is obviously not covered. Due to these unstable locations, the maintenance and the batteries changing are hazardous; a solution with energy harvesting seems particularly adapted. Other places like an aircraft engine, an oil drill, or a space shuttle, could make use of their vibration, thermal and light energy to self-power the sensors.

The wireless devices

In this section, we will talk about wireless devices and gadgets surrounding us daily like mobile-phone, mp3, GPS, devices used in medical field implanted in the human body or military communication devices ... Currently, to maintain a long period of operating time, the battery volume can reach half the size of the device. To replace a medical implant, like a pacemaker, a surgery is needed when the battery runs out. For military manoeuvres, to keep the radios, computers, range finders, TWS (Thermal Weapon Sight) running, soldiers can wear up to 13 kg backpack full of batteries. Conventional AA piles are just one dollar while the one used by military private can reach more than 30 dollars. Bionic Power company from Canada invents a Bionic energy harvester adjust to knees to scavenge energy from walking. According to their report, one user walking at a comfortable speed generates an average of 12 watts of electricity which is sufficient to fully charge 4 phones during a little over an hour of walking.

1.5 Natural energy sources and harvesting technology

Our surrounding environment is filled by natural energies of varying origins and natures. Among all these energies available, the most dedicated to be harvested seems to be the solar energy, the mechanical energy associated to the natural vibrations, and the thermal energy. Photovoltaic cells, wind turbines, piezoelectric devices, thermoelectric generators and so on have been developed and optimized to perform and harvest energy whatever the nature of the source [24], see table. 1.5.

Harvesting method	Power Density
Solar cells	$15mW/cm^3$
Piezoelectric	$330\mu W/cm^3$
Vibration	$116\mu W/cm^3$
Thermoelectric	$40\mu W/cm^3$

Table 1.5: Energy harvesting sources [24]

Before opting for the right energy harvesting method, one can check first the conversion

efficiencies, and the power densities. Other factors like electrical properties (voltage or current sources), physical properties (size, shape and weight), environmental properties (water resistance, operating temperature range) and maintenance properties must be also taken into account.

In our case and as piezoceramic is the main substance of this thesis, we focus on energy harvesting systems dedicated to surrounding natural vibrations. Compared to other resources (thermal, solar or wind), vibrations are everywhere. This property offers an important potential for future specific usages as for the civil infrastructure, where embedded sensors self-supplied can monitored and send real time information to supervisors. Track device for the wild animals is another specific application requiring such kind of energy source. To develop and improve performances of such apparatus requires to be able to reproduce in laboratory all the common vibration situations. As is illustrated in Fig. 1.14, the level of natural mechanical vibration in a laboratory is high and to obtain good experimental results it is necessary to consider the acoustic spectrum in this environment.

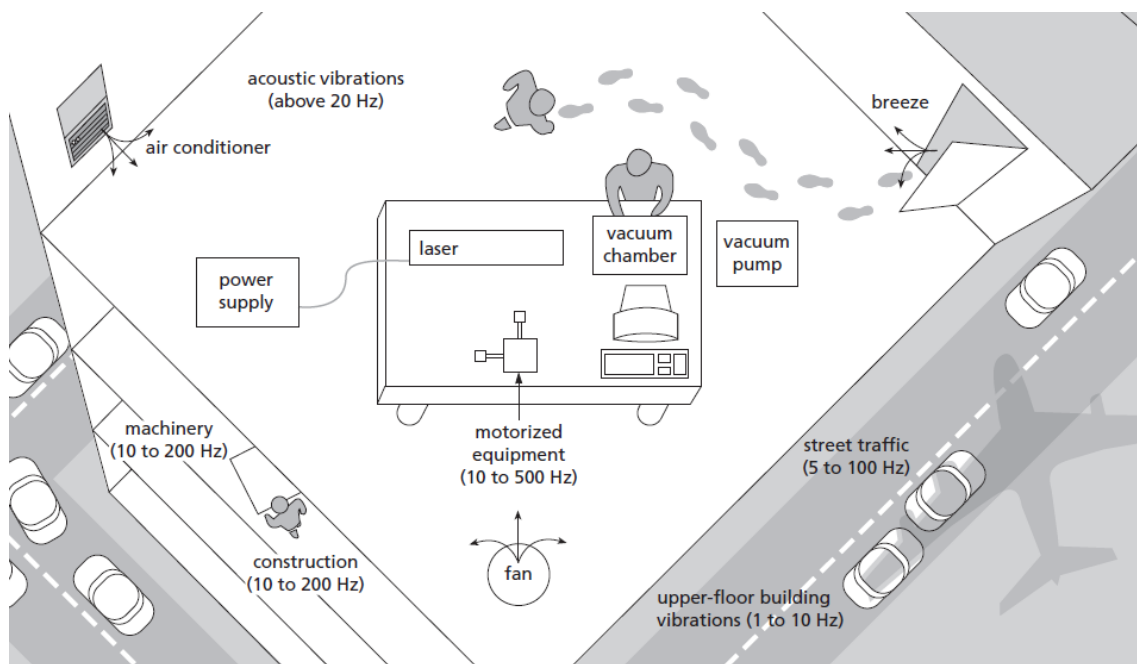


Figure 1.14: Common vibration in a laboratory, [25]

Among all the laboratory surrounding natural vibrations, many of them due to their weak amplitudes or weak frequencies are difficult to be treated. Table. 1.6 Classify these vibrations by their usability, these frequencies vary from 4 Hz to 100 Hz, and the peak is around 40 Hz.

Other situations such as in a populated area (railway station, school, hospital, ...) or a car-rich area (highway ...), is also rich of natural vibrations of frequency range close to the laboratory's one. In these two situations, vibrations are available permanently giving a promising field to the energy harvesting techniques. Unfortunately, natural vibrations are never monochromatic and one of the future challenges for scientific teams will be to

Type	Frequency(Hz)	Amplitude
Air Compressors	4 - 20	$10^{-4}m$
Handling Equipment	5 - 40	$10^{-5}m$
Pumps (Vacuum, comp or non-comp fluids)	5 - 25	$10^{-5}m$
Building Services	7 - 40	$10^{-6}m$
Foot Traffic	0.5 - 6	$10^{-7}m$
Acoustics (B)	100 - 10000	10^{-4} to $10^{-6}m$
Punch Presses	Up to 20	10^{-4} to $10^{-7}m$
Transformers	50 - 400	10^{-6} to $10^{-7}m$
Elevators	Up to 40	10^{-5} to $10^{-7}m$
Building Motion	46/Height in meters, Horizontal	$10^{-3}m$
Building Pressure Waves	1 - 5	$10^{-7}m$
Railroad*	5 - 20	$\pm 0.15g$
Highway Traffic*	5 - 100	$\pm 0.001g$

*Amplitude is reported in dB using the acceleration due to gravity as the reference acceleration.

Table 1.6: Vibration frequency and amplitude in a laboratory and daily life, [25]

maximize the frequency bandwidth of their systems, to reach correct amount of energy harvested.

1.6 Conclusion

This chapter gives a brief introduction to the knowledge of piezoelectricity and its applications as energy harvesting technology. It begins with the definition of piezoelectricity, then the ferroelectric material classification is introduced, and the electrical-mechanical-thermal interactions are exposed. The ferroelectric constitutive equations are explained and special effort has been done to explain each coupling coefficients. Special ferroelectric properties like hysteresis are also treated. Then, energy harvesting and the potential energy sources associated were described. One part of this thesis work will concentrate on energy harvesting applications using piezoelectric conversion. As previously exposed, piezoceramic materials are naturally efficient to convert mechanical vibration to electricity. But a precise modeling including all piezoceramic nonlinearities such as hysteresis, mechanical creep or ageing is still missing. In this thesis for a lack of time we have focused our attention on the frequency dependence of the dielectric hysteresis $f > 1\text{Hz}$, but future work are planned to validate the behavior under very weak dynamic excitation, as it the case for ageing or creep. Different models for the hysteresis ferroelectric materials have already been proposed, such as Rayleigh model, Preisach model and so on, but each one is quickly restricted, as the frequency or the amplitude of the excitation are changing.

The hysteresis knowledge and control is a fundamental issue as we need precise position or displacement control. This is the case for energy harvesting systems or nano-positioning

probes. In this thesis, large efforts have been realized to propose a hysteresis precise model including all the dynamic considerations. Fractional operators have been used to extend highly hysteresis model bandwidth. The final objective is to develop a model that should be applicable for different nature of excitation (electrical and mechanical), whatever the frequency and the amplitude. By instant, an accurate simulated relation of dielectric density with mechanical excitation is required both for a precise positioning control and to manage the energy harvesting amount of dedicated system.

Fractional derivative operators allow to highly ameliorating the precision of piezoceramic dielectric behaviour consideration. Non entire operators give a practical way to extend the excitation model bandwidth and overpass usual hysteresis model restricted to operational frequency close to the quasi-static behaviour. In the case of energy harvesting systems, it helps to determinate the exact amount of energy harvested.

Dielectric hysteresis model

2.1 Modeling of the Piezoceramic

Most applications on energy harvesting systems based on piezoceramic conversion operate under levels of excitation sufficiently low to consider linearity for the conversion processes and the physical behaviors. At such weak excitation levels, a piezoceramic is characterized by the tensor coefficients: permittivity, elastic compliance and piezoelectric coefficient. Four coupled equations [13] are related to the piezoceramic electrical behavior and four others for the mechanical behavior.

$$S_{ij} = s_{ijkl}^E T_{kl} + d_{kij} E_k$$

$$D_i = d_{ikl} T_{kl} - \epsilon_{ik}^T E_k$$

$$S_{ij} = s_{ijkl}^D T_{kl} + g_{kij} D_k$$

$$E_i = -g_{ikl} T_{kl} - \beta_{ik}^T D_k$$

$$T_{ij} = c_{ijkl}^E S_{kl} - e_{kij} E_k$$

$$D_i = e_{ikl} S_{kl} + \epsilon_{ij}^S E_k$$

$$T_{ij} = c_{ijkl}^D S_{kl} - h_{kij} D_k$$

$$E_i = -h_{ikl} S_{kl} - \beta_{ik}^S D_k$$

These equations are usually adequate at static and moderate conditions without special

accuracy requirements. As we reach higher excitation contributions, including high frequency and high amplitudes of mechanical or electrical excitations, nonlinearities appear and linear description is rapidly inaccurate. In usual application situations, the piezoelectric actuators can easily reach relatively high electric field (about 500V/mm) to get an effective use. Their behaviors exhibit large differences compared with usual data measured under low electric field levels. Disparity of strain between the theoretical calculation with linear and static equations and experimental results on soft PZT ceramic can easily reach a 100% difference [26]. These nonlinearities are obviously also observable in the strain/electric field plot $S(E)$ as illustrated Fig. 2.1.

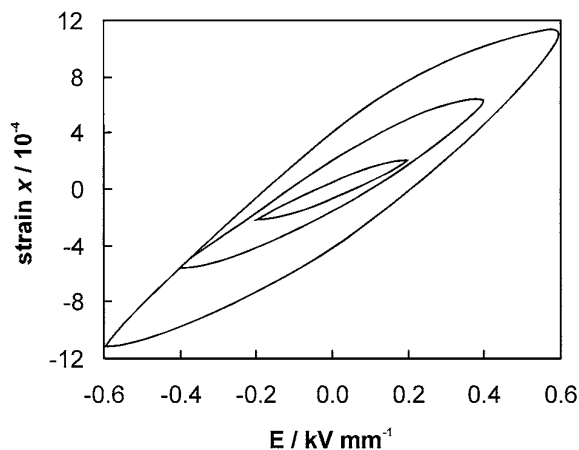


Figure 2.1: $S(E)$ curve of a piezoceramic. [26]

One of this thesis study tasks is to develop an efficiency energy harvesting complete model for piezo-systems working under high electric and mechanical excitations. In this situation, nonlinearity plays an important role and can affect a lot the final amount of energy harvesting. The nonlinearity taken into account is especially important in high precision travel-control, precision positioning, wide bandwidth energy harvesting, etc. Consequently, linear material relations are unfortunately no longer suitable for the material behavior, not to mention they are taken into account in a whole system where more sophisticated and coordinated interrelations are needed. A more complicated model including saturation and hysteresis is then necessary to obtain numerical results close to the experimental ones. A fully applicable model useful for complex excitations is a valuable tool to understand the physical relation and the physical behavior of the piezoceramic.

Based on experimental considerations, we have developed a high-precision piezoceramic dielectric hysteresis model $P(E)$ suitable both for high-frequency bandwidth excitation and high amplitude excitations, which provides good accuracy regardless of the excitation nature (electrical or mechanical, with variations in amplitude and frequency) [27–29].

The nature of current hysteresis model for ferroelectric materials can be roughly categorized as follows: (1) macroscopic theories based upon phenomenological principles, (2) microscopic theories based on quantum mechanics, classical elasticity and electromagnetic relations, or thermodynamic laws, or (3) semi-macroscopic theories which are derived using

a combination of approaches. [30]

The first category concentrates on the phenomenon and empirical results so the mathematical characterization comes first regardless of the intrinsic microscopic mechanism. For example, in the frequency regime, a second-order development of the piezoelectric equation makes it possible to partially describe the non-linear effect observed on power transducers in resonant mode [31, 32]. Unfortunately, this model is only suitable close to the experimental conditions, for other conditions bad comparison simulation/measure are obtained. Large number of information is required to precisely describe the complex mechanism of nonlinearity of ferroelectric materials.

The localization of a phenomenological model restricts itself to evolve into a general and theoretical model. By using a micro-mechanism model to study the elements in a piezoceramic, studies are starting from microscopic domain. Lots of investigations, separately at molecular or crystal levels, have already been done and plenty of experience could be used in modeling. Compared to the first approach, the present method start with a set of equations describing micro-mechanism domain and then extended to the macroscopic point of view. However, in a ferroelectric material, combination and interaction of these quantum mechanisms remains uncertain. A model includes all the grain boundary attributions or inter-granular stresses cannot be established, indeed the taken into account of so numerous data and parameters will rendered it too difficult. Polarization behavior is a complex process and a model including all these precise variables and interactions is unfortunately not possible. To simplify this, we can establish a model with physical foundation in addition to phenomenology method. The main mechanisms are described with physical equations and lead to a precise description, the extension to phenomenology method helps to compensate the deviation that could occurred and could has been neglected with physical equations. Model like this give precise simulation results and can go further in prediction even beyond experimental limitations [30].

In our case electric and mechanical excitation are both considered and combined in the model. It not only provides a high precision for the description of the macroscopic phenomenon, but also offers a better understanding for the physical constitution mechanisms. The predictive capability of the model is particularly interesting it allows providing results beyond the experimental limitations.

The model described in this thesis is developed from a combination of consideration of the domain wall theory (microscopic level) and the phenomenological mechanical and electrical behavior of the materials at macroscopic level. The original model has been first built in 2007 restrained to the dielectric behavior $P(E)$ (polarization under electric field excitation). Then, it has been extended to the mechanical stress influence on the dielectric polarization.

The model has historically first been set to a soft ceramic P188 navy-type material (see experimental chapter for details) good results were obtained, but the model also works properly with other piezoceramic of changing nature (such as FUJI-C2, PZT5A and so on). In the extended model, mechanical stress and electric field excitations are simultaneously

taken into consideration when most investigations are concentrated on either pure electric or pure mechanical one (respectively corresponding to direct and reverse piezoelectricity). It leads to further complexity but more applicable in real world employment because in most cases piezoelectric element acts against external load of multi-physical nature.

After a large description of the quasi-static contribution of our model, short description and comparison with the classic hysteresis Preisach model will be done in order to give us an overall view of the diversity and interdependence of the quasi-static dielectric hysteresis models. Then we will discuss the dynamic contribution and will expose the limit of the usual dynamic contribution considerations. Our solution, including fractional operators will be explained and special attention will be given to establish the improvement of such operators and in particular the considerable extension of the model frequency bandwidth. Finally, after this large report of the direct dielectric model $P(E)$, inverse model $E(P)$, $E(S)$ and $T(P)$, will be introduced and a description of each one will be done.

2.2 Quasi-Static dielectric hysteresis model

It is well known that hysteresis phenomenon of a ferroelectric material are mainly due to the macroscopic domain wall movements. Different theories and definitions for these domain wall movements have already been published by various researchers. These movements give a great contribution in dielectric polarization. The domain walls separate the ferroelectric domains characterized by different polarization orientation such as 90° and 180° . The impurities and inclusions (defects) through the material act as pinning points on the surface of the domain wall and restrain the domain size variation; they affect the domain wall motions according to Miller and Savage [33]. Electric field is analogous to a mechanical force applied on the domain wall. The domains require different potential energy to move depending on the pinning effect or their origin viscosity. If the analogous mechanical force is sufficient to drive the domain, they would exhibit a sudden jump, which lead to a small changing of the average polarization, if not, the low potential domain wall would lightly change while high ones will remain constant. Different types of domain wall movements have been reported: domain wall vibration, domain wall translation and domain switching. Domain wall vibration are considered as a reversible movement around the equilibrium position (appearing for electric fields as low as 10 V/mm). At weak electric field level, the dielectric property was mostly attributed to this kind of vibration movement. Domain wall translation and switching phenomenon need relatively high electric field amplitude to be observable and to contribute depending on the property of the piezoceramic. From a modeling point of view all these movements were considered to have the same origin, i.e. electric forces applied on the domain wall. Whatever the reversible and non-reversible ones, they had their own contribution with respect to field and the superposition with higher or lower excitations. At low frequencies ($f \ll 1\text{Hz}$) and for high electric field excitation amplitudes, hysteresis loop-like are observed when plotting the induced polarization P , versus the electrical field E . At such frequency levels, wall

movements are assumed to undergo a mechanical-like dry friction, see Fig.2.2.

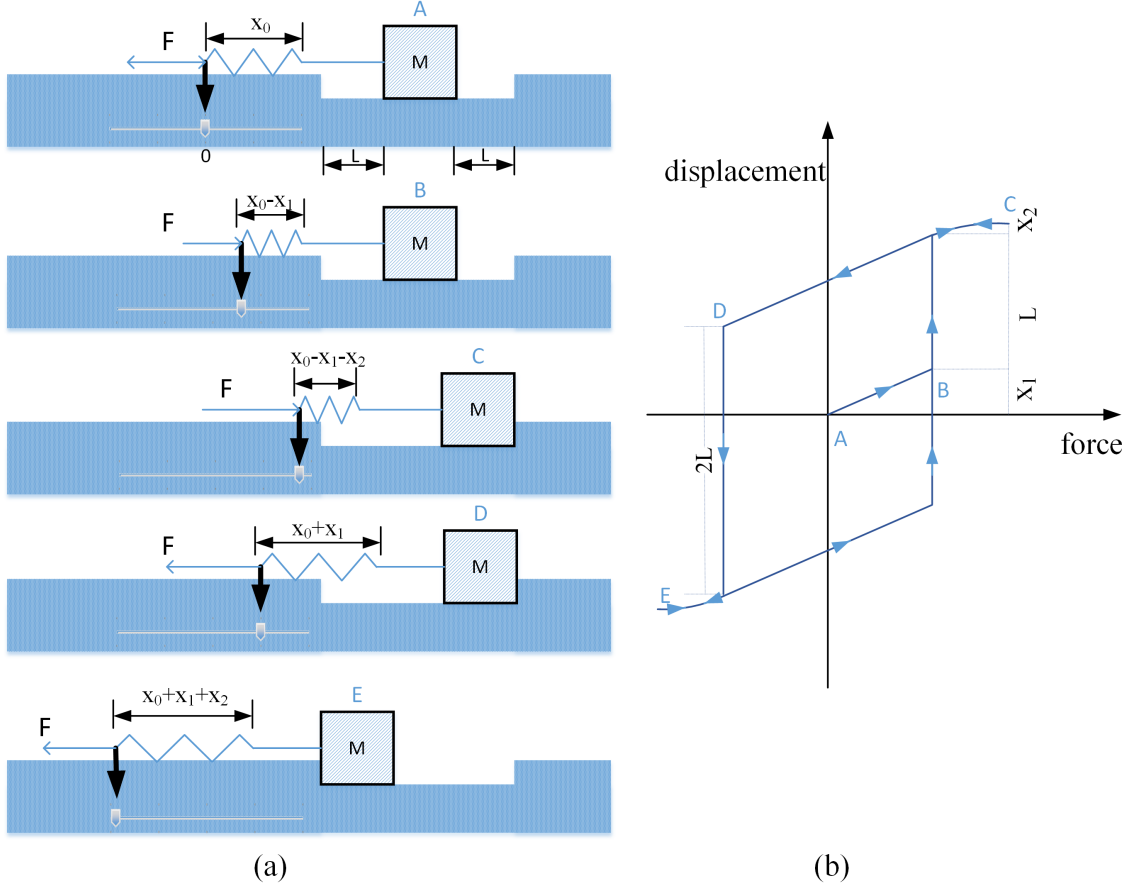


Figure 2.2: Illustration of the quasi-static analog mechanical dry friction.

For a better understanding an analog mechanical consideration can be explained: if we suppose a mass place in a groove, sealed to a spring on its right side (characterized by a stiffness k). The spring whose natural length is X_0 , at position A, working within its elastic limit whatever the situation even for a deformation of $X_1 + X_2$. When the spring deformation exceeds X_1 (B), the applied force overcomes the dry friction and the mass begins to move until it reaches the edge of the groove. The applied force is altered until a deformation of $X_1 + X_2$ (C). After this first step, the applied force changes its direction and the spring starts to expand to the other direction until reach $X_0 + X_1$ (D), when the dry friction is overcome, the mass starts to move until reaches the distance of $2L$ to the other edge. The force continues to increase until the spring deformation reaches $X_1 + X_2$ (E). Afterward, the force changes its direction and a new cycle is beginning. In the comparison mass-spring movement/domain wall, the mechanical force acts as the electrical force and the pointer displacement is analog to the polarization field. To be sure to obtain a full material polarized state, the electric field must be much higher than the coercive electric field and wait for minutes to assure the polarized effect. The two displacement limits are analog to a total polarized state (saturation state), which mean that even under the

application of a higher electric field, the polarization will remain the same.

A static (frequency-independent) equation based on its mechanical dry-friction counterpart has been established in order to account for this property. A good approximation of a major $P(E)$ hysteresis loop is obtained by translating an anhysteretic curve (the translation is equal to $\pm Ec$, depending on the sign of the time derivative of the polarization), see Eq.2.1 and Fig 2.3.

$$P(t) = f(E(t) - Ec \cdot \text{sign}(\frac{dP(t)}{dt})) \quad (2.1)$$

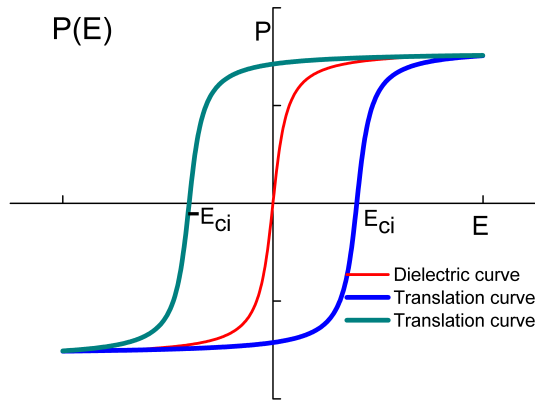


Figure 2.3: Illustration of the anhysteretic curve translation.

A pure non-linear dielectric curve (red curve in Fig. 2.3) describing polarization against electric field can be mathematically defined as an arctangent function (Eq. 2.1). This anhysteretic polarization curve describes the energy state of a piezoceramic under electric field; it represents the minimal energy state without consideration of defects (oxygen vacancies, dopant, acceptor or donor) and impurities of the crystal. As illustrated in Fig. 2.3, on the dielectric curve, the variation of the polarization will remain high until the rotation of the dipoles (as the electric field is increasing), when the polarization reaches saturation states, no more changing are observable [34].

$$f(E) = \sigma \cdot \tan^{-1}\left(\frac{E}{\gamma}\right) \quad f^{-1}(P) = \gamma \cdot \tan\left(\frac{P}{\sigma}\right) \quad (2.2)$$

$f(E)$ (reciprocally $f^{-1}(P)$) represents the behavior of a non-linear dielectric (without hysteresis). The parameters γ , σ are determined by comparison between simulation and measurements. Special program using Matlab toolbox curve fitting has been developed in order to get success in this operation. To obtain the anhysteretic curve, we first needed a complete major hysteresis loop obtain by measurement; then for a given polarization the corresponding electric field was calculated with the average value of the increasing and decreasing electric field of hysteresis loop $E_{anh} = (E_{inc} + E_{dec})/2$. Eq. 2.1 gives a model where polarization remains constant until the electric field E reached the coercive field Ec , and as soon as E exceeds Ec , an electrical displacement occurs. After E_{max} was

reached and the field was reversed, the polarization remained constant until E dropped below $E_{max} - 2Ec$ and so on. This behaviour was as had already explained very similar to a mechanical static dry friction.

Eq. 2.1 gives a correct description of the major hysteresis loops observed during steady state of the ceramic and under a high-amplitude electrical field ($E_0 > E_c$). Unfortunately, this equation is ineffective for hysteresis loops observed under asymmetrical excitation field waveforms (e.g. first polarization curve, minor loops, etc.). This limitation can be overcome by introducing a distribution of a basic element (spectrum), characterized by its own coercive fields in addition to its own weight.

$$\sum_{i=1}^k Spectrum(i) \cdot P_i = P \quad (2.3)$$

Every ferroelectric domain through the piezoceramic obeyed to the principles of a pure dielectric polarization. The difference between each domain is their pinning potential energy; each domain will vibrate and switch under different electrical excitation levels. Considering this property, the polarization loop is actually the superposition of different pure dielectric curves, each one affected by its own weight and characterized by its own pinning potential energy. Fig. 2.4 shows how from the anhysteretic curve, we can get by translation the corresponding dielectric polarization curve of domain wall characterized by different energy potential (i.e. different switching electric field levels, E_{ci}).

Every shifted anhysteretic dielectric polarization curve $P(E)$ has its own contribution in the final sample polarization. The final macroscopic polarization result is affected by each contribution characterized by its own weight and by its own electric field switching level as illustrated Fig. 2.5. Special attention must be given to the definition of the $Spectrum(E_{ci})$ function.

In Eq.2.3, the function $Spectrum(i)$ represents the distribution of elementary loops. A specific protocol has been established to obtain this distribution. This protocol, involved first the determination of the sample anhysteretic curve. The spectrum distribution was then obtained through deconvolution of the material first polarization curve (experimentally measured in Fig.2.6-(a)) by the previously obtained anhysteretic curve. Based on this process, it has been possible to systematically establish the static parameters of the material. The spectrum illustrated Fig.2.6-(b) has been calculated around a distribution of 50 shifted anhysteretic curves. This number was enough to precisely describe all hysteretic behaviour of the tested sample, including asymmetrical loops such as first polarization curve (as illustrated Fig. 2.6-(a)). Numerous results as well as further information concerning the quasi-static dielectric direct model $P_{stat}(E)$ were available elsewhere [35].

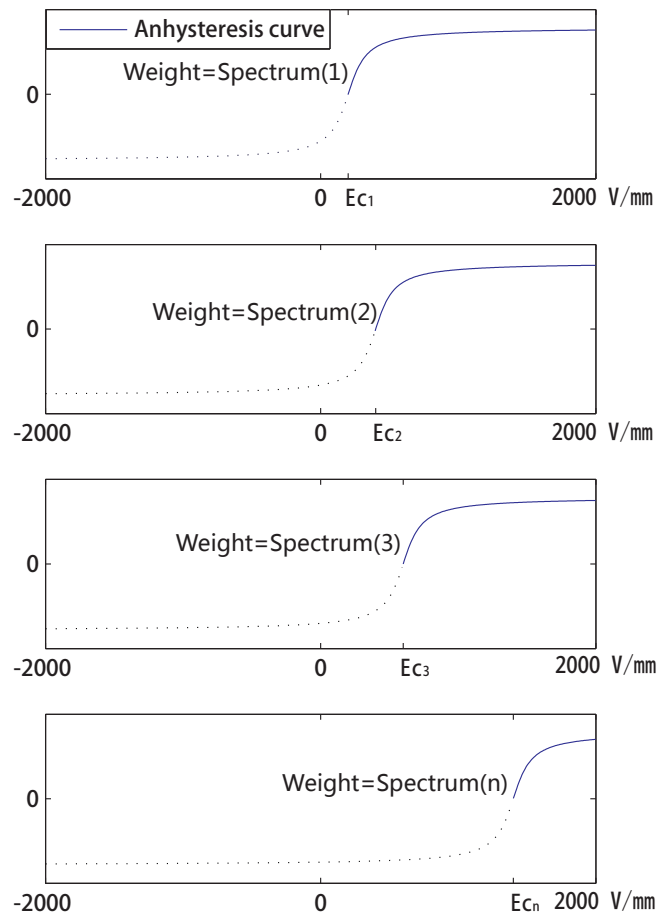


Figure 2.4: Translation of the E_{cn} value of the anhyseretic curve corresponding to different ferroelectric domains.

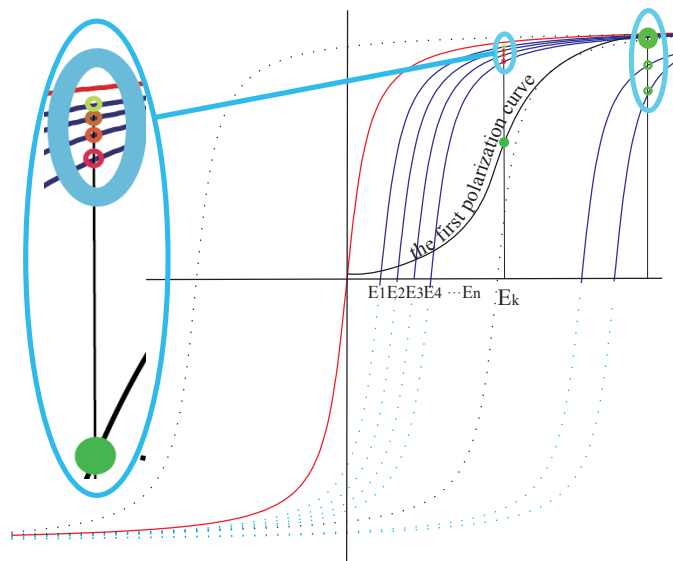


Figure 2.5: Translation of the anhyseretic curve.

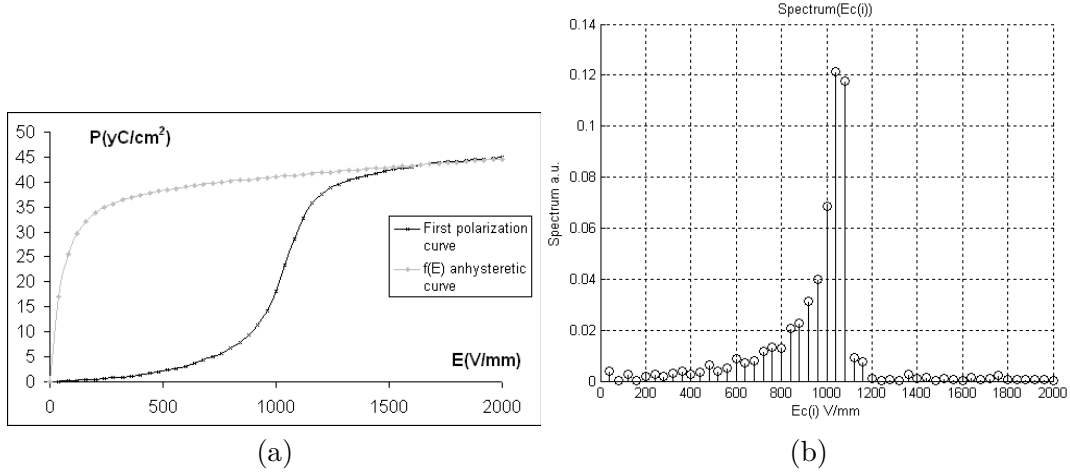


Figure 2.6: (a) First polarization curve (Black), perfect dielectric curve (Grey), for a P188 sample, (b) Distribution (Spectrum) of elementary loops.

Finally, a precise quasi-static hysteresis model can be written as:

$$\begin{cases} P(t)_i = f(E(t) - E_{ci} \cdot \text{sign}(\frac{dP(t)_i}{dt})) \\ \sum_{i=1}^k \text{Spectrum}(i) \cdot P_i = P \end{cases} \quad (2.4)$$

Where P_i is a local elementary polarization field, read on an elementary dielectric shifted anhysteretic curve characterized by its own coercive field E_{ci} and P is the global polarization field through the material [36].

The model is experimentally validated at 2 mHz (at this frequency level we assume that the piezoceramic reaches its quasi-static state; the dynamic contribution is insignificant, furthermore this is also the lowest frequency available with our experimental bench, see the previous chapter), comparison simulation/experimental results of hysteresis loop of PZT piezoelectric ceramic, are displayed on Fig. 2.7-(a). Fig.2.7-(b) shows same comparisons for first-order reversal curves excitation-type, obtained using triangular waveform electric excitation with a constant maximum electric field and a decreasing minimum ones. Good simulation results obtained in both cases give the validation of our model [35]. More comparisons between experimental results and simulation will be given in the experimental bench description chapter.

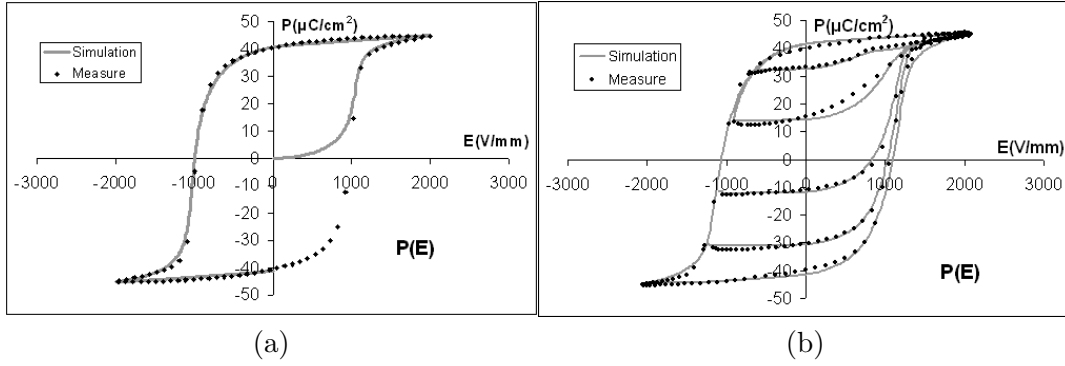


Figure 2.7: (a). Comparison measure/simulation for quasi-static hysteresis loop. (b). Comparison simulation/measurement at 2mHz for reversal curves.

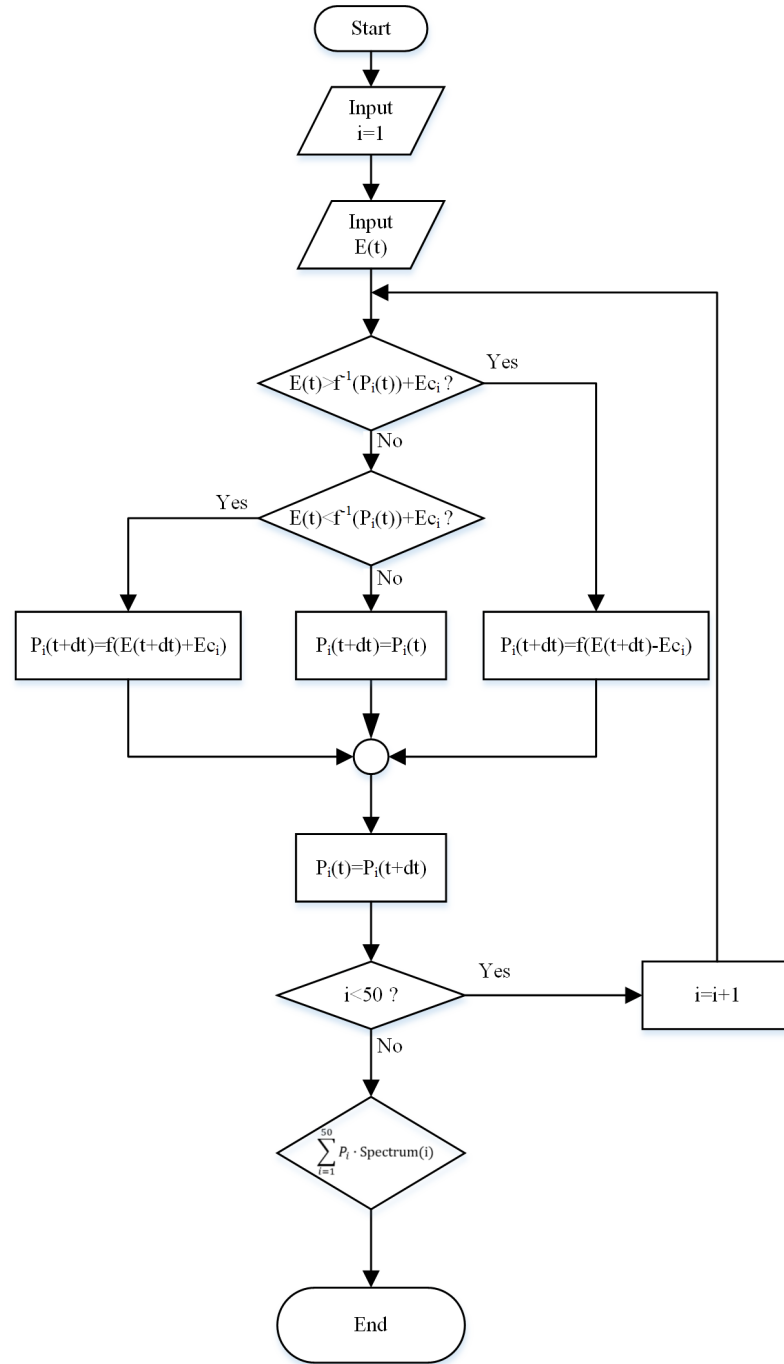
Fig. 2.8 shows as an illustration and for a better understanding, the equivalent algorithm of the proposed quasi-static model. The quasi-static model we developed in this study could be commonly described as using the density of different microscopic contributions affecting the final polarization. Concerning this conception, another well-known model has been proposed using this kind of thought: the Preisach model. In this thesis, authors have decided to limit the comparison of the quasi-static hysteresis dry-friction model to the Preisach model because since its first suggested, Preisach model has always been widely accepted by the scientist community, and in the field of ferroelectricity it is the hysteresis model connected to the highest number of article related. Other popular models such as Bouc-Wen, Jiles-Atherton model, the reader can refer to [37, 38]. To illustrate the advantages and the inconvenient of our model, we propose to realize a brief introduction and give some explanation and comparison with this classic model. In describing hysteretic magnetization property, Preisach model has been employed in a large variety of industrial application models. Besides magnetic physical domain, Preisach quasi-static hysteresis model can also be used with success for the description of ferroelectric material hysteretic behavior. When the Preisach model is used for the modeling of hysteresis in piezoceramic, the expression relating the piezoceramic expansion $f(t)$ to the excitation voltage $u(t)$ is:

$$f(t) = \iint_{\alpha \geq \beta} \mu(\alpha, \beta) \gamma_{\alpha\beta}[u(t)] d\alpha d\beta \quad (2.5)$$

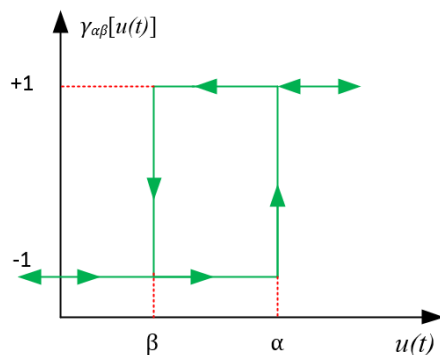
Where $\gamma_{\alpha\beta}[\cdot]$ are elementary hysteresis operators with switching values α and β and whose values are determined by the input voltage signal $u(t)$ (see Fig.2.9). The function $\mu(\alpha, \beta)$ is a weighting function estimated from measured data and also known as the Preisach function.

More details and explanation on Preisach model are available in the literature [20, 39–42].

To get good simulation results using Preisach model, it is necessary to precisely define the Preisach distribution function, $\mu(\alpha, \beta)$. Different ways lead to the achievement of

Figure 2.8: Algorithm of the quasi-static direct $P(E)$ model.

this function. First way is to assume that the distribution function has a particular form (Lorentzian, Gaussian) and to determinate the parameters of the chosen function leading to a correct average hysteretic behavior. The second way is to discrete the distribution function in a finite set of values. This method required a large number of experimental data to give a correct distribution. Another technique determines the discrete distribution function with state independent reversible polarization and plays with the symmetrical


 Figure 2.9: Hysteresis operator $\gamma_{\alpha\beta}[u(t)]$

	Our model	Preisach model
Experimental information	😊	😞
Memory management	😊	😞
Extention to dynamic contribution	😊	😞

Table 2.1: Comparison of our model with Preisach model

properties of the distribution function to fill the remaining part of the Preisach triangles. Compared with the first two techniques, the third one needs experimental informations easily obtained and a typical calculation time reduced. But unfortunately the average precision which is directly linked to the level of initial information is usually reduced too [43].

After implementation and comparison between our quasi-static model and Preisach model, the following conclusions have been proposed: The dry friction model seems briefer in calculation even if we admit that our implementation of Preisach model can be optimized in term of calculation time. The material memory administration is limited to a one dimension spectrum for the dry-friction model, whereas for the Preisach model the material memory requires the management of the 2 dimensions Preisach triangle. For the dry-friction model the spectrum function is obtained using deconvolution between first polarization curve and anhysteretic one. This means that the level of experimental informations required for the configuration of our model is relatively low. In the case of Preisach model as previously explained various techniques exist to get the Preisach triangle. The precision level of the model is directly linked to the number of experimental informations required to the construction of the triangle.

Finally, we can conclude that our model seems to be a good compromise to Preisach model. Indeed, even if the precision is usually lower for very special excitation type (as reversal curves or minor loops, . . .), the management memory is interesting, its implementation in Matlab software has been very easy and its extension to dynamic contribution is direct.

2.3 Dynamic model

Beyond the quasi-static limit, ferroelectric materials exhibit hysteresis loops that are strongly dependent on the frequency. These states of dependence were clearly considered in literature, indeed numerous theoretical studies have described the scaling law of the hysteresis area as a function of f and E_0 , i.e., $\langle A \rangle \propto f^\alpha E_0^\beta$ (where α and β are real parameters depending on the geometry and the nature of the system). As reported in others papers [35,36], the dynamical effect is usually considered as an equivalent dissipative field derived from an Ohm's resistivity, ρ . The dynamical effect is then introduced by adding the product of a resistive term ρ and the derivative polarization to the static contribution (as illustrated on the extension of the Eq. 2.6).

$$E = E_c \cdot \text{sign}\left(\frac{dP}{dt}\right) + \rho \cdot \frac{dP}{dt} = f^{-1}(P) \quad (2.6)$$

But as explained in [44] and illustrated in Fig. 2.10, this dynamical modelling remains unfortunately accurate for a very restrained frequency bandwidth. The identification of the parameter ρ that perfectly fit the low frequency part of the $\langle A \rangle (freq)$ curve led to an over-contribution of the dynamical term $\rho \cdot dP/dt$ for the high frequency part of the curve. Reciprocally, by adjusting the parameter ρ on the high frequency component of the curve, one can at low frequencies observe large differences between simulated and measured results.

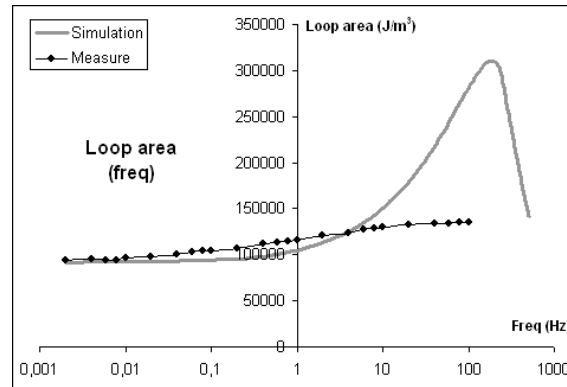


Figure 2.10: Comparison measure/simulation for hysteresis loop area (frequency)

To overcome this problem, we better need an operator that balances the low frequency and the high frequency component in a different way than a straight time derivative. Such operators exist in the framework of fractional calculus; there are the so-called non-entire derivative or fractional derivatives.

2.3.1 Fractional derivative

Fractional calculus is a branch of the calculus that extended the integer differential operator to real number powers or complex number powers. In the field of power function,

it is easy to understand that $a = b^3$ means a is equal to 3 times of b . Then, how to describe a number $a_1 = b^{2.25}$ by making use of the traditional power function explanation, it is not possible to explain by double b multiplying with another $1/4$ times of b physically. In calculation, it can be achieved with the help of calculator or computer. In the field of power function they have one definite value with any operator, no matter it is integer, fraction or complex number power. In the same case with the differential D^n , n is usually an integer while people seldom think it about when it's a fraction. We will give a quick look at the fractional derivative in this section. The usual definition of an entire derivation is given by:

$$D^1 f(x) = \lim_{h \rightarrow 0} \frac{f(x+h) - f(x)}{h} \quad (2.7)$$

To get higher order derivatives, n^{th} derivative means to iterate $n - 1$ times Eq. 2.7. So, for any natural number, the general derivative function is

$$D^n f(x) = \lim_{h \rightarrow 0} h^{-n} \sum_{k=0}^n (-1)^k \binom{n}{k} f(x + (n-k)h) \quad (2.8)$$

where

$$\binom{n}{k} = \frac{n!}{k!(n-k)!} \quad (2.9)$$

In (2.9), n and k are usually non-negative integer. The factorial function can be generalized with gamma function, where its argument is shifted down by 1 and expanded to real number and complex number. when n is a positive integer,

$$\Gamma(n) = (n-1)!$$

The gamma function works with all the complex number field except zero and negative integer where it has some poles. With a complex number with its real part is positive, gamma function is defined as,

$$\Gamma(z) = \int_0^\infty t^{z-1} e^{-t} dt$$

The Gamma function values along in the real axis is depicted in Fig 2.11

Consequently for a factorial function, it can be rewritten by using the gamma function,

$$\binom{n}{k} = \frac{n!}{k!(n-k)!} = \frac{\Gamma(n+1)}{\Gamma(k+1)\Gamma(n-k+1)} \quad (2.10)$$

The definition of binomial coefficients is able to be extended to fraction, real and complex

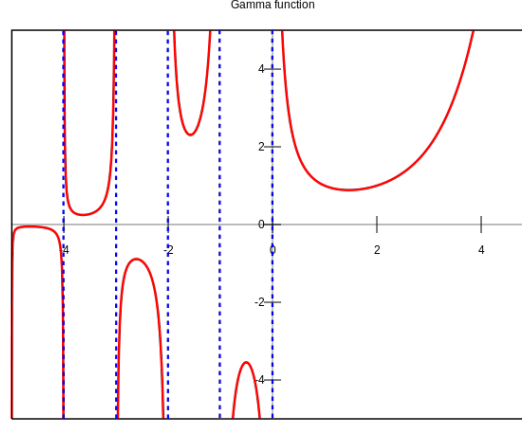


Figure 2.11: Gamma function in real axis

number by replacing n with an arbitrary number α .

$$\binom{\alpha}{k} = \frac{\alpha(\alpha-1)(\alpha-2)\cdots(\alpha-k+1)}{k(k-1)(k-2)\cdots 1} \quad (2.11)$$

for $k \in \mathbf{N}$, α is a arbitrary number the binomial in (2.8) can be also opened up as

$$(a+b)^n = \sum_{k=0}^n \binom{n}{k} a^{n-k} b^k \quad (2.12)$$

combined with (2.10) and (2.12), the generalization from integer to fraction of the function is,

$$(a+b)^\alpha = \sum_{n=0}^{\infty} \frac{\Gamma(\alpha+1)}{n!\Gamma(\alpha-n+1)} a^{\alpha-n} b^n \quad (2.13)$$

As we know, the derivative of an exponential function is simple and basic where we can start from and it give us some clues for the expansions.

$$\begin{aligned} D^\alpha e^{ax} &= \lim_{h \rightarrow 0} h^{-\alpha} \sum_{k=0}^{\alpha} (-1)^k \binom{\alpha}{k} e^{a(x+(\alpha-k)h)} \\ &= e^{ax} \lim_{h \rightarrow 0} h^{-\alpha} \sum_{k=0}^{\alpha} (-1)^k \binom{\alpha}{k} (e^{ah})^{\alpha-k} \\ &= e^{ax} \lim_{h \rightarrow 0} h^{-\alpha} (e^{ah} - 1)^\alpha \\ &= a^\alpha e^{ax} \end{aligned} \quad (2.14)$$

in Eq.2.14, α is applicable for any complex number. So, we can use it with the trigonometric function,

$$\begin{aligned} D^\alpha \cos(x) + i D^\alpha \sin(x) &= D^\alpha e^{ix} = i^\alpha e^{ix} = e^{\frac{\alpha\pi i}{2}} e^{ix} \\ &= e^{ix(x+\frac{\alpha\pi}{2})} = \cos\left(x + \frac{\alpha\pi}{2}\right) + i \sin\left(x + \frac{\alpha\pi}{2}\right) \end{aligned} \quad (2.15)$$

The above equations demonstrate the analytical fractional derivative calculation of simplest trigonometric function, *sin* or *cos*.

To take advantage of derivative fractional, the most difficult part is its complicated calculation because it concerns lots of integral. By transferring it into an analysis method as (Eq.2.15), the computational work is greatly reduced. And we will introduce this method into section 2.3.2, which precisely describes the dynamic behavior.

From a spectral point of view, fractional derivative means that the frequency spectrum $f(\omega)$ of $f(t)$ will be simply multiplied by $(j\omega)^n$ in place of $j\omega$ for a first order derivation. The fractional derivative term can be explained and modelled using constant phase element. The admittance of the usual constant phase element (CPE) is $Y = a \cdot (j\omega)^n$ ($0 < n < 1$). When n is close to 1, the CPE resembles a capacitor, and the angle phase is constant and close to 90° . If n is close to 0 the CPE react as a resistor. In the analogy between an electrical circuit and our hysteresis model the current will be not equal to the polarization but to its derivative value, then a constant phase element is not correct to interpret the fractional term. The true admittance of the non-entire term is $Y = \rho \cdot (j\omega)^{1-n}$ (Fig. 2.12). This specific component is characterized by an opposed behaviour of classical CPE element, i.e. when n is close to 0 the component react as a capacitor and when n is close to 1 it has a resistor behaviour. [36]

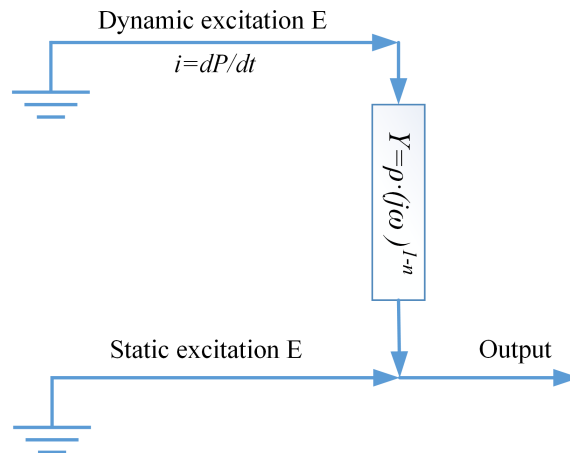


Figure 2.12: Constant Phase Element in the analogy electrical circuit [36]

2.3.2 Dynamic model

As the excitation frequency is increasing and exceeds the quasi-static limit ($f > 1Hz$), the piezoceramic hysteresis loop area is also increasing. Loop area variations give the evidence that hysteresis losses (linked to the hysteresis loop area) are strongly dependent on the frequency, see Fig. 2.13. The hysteresis losses can be separated into two contributions:

$$\text{Hysteresis loop area} = \text{static losses} + \text{dynamic losses}$$

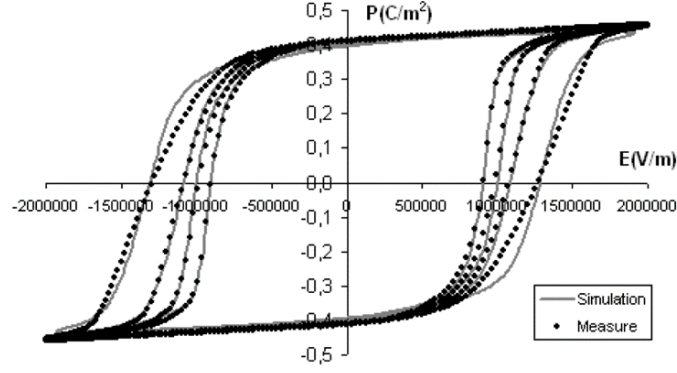


Figure 2.13: Comparison measure/simulation for hysteresis loop area as the frequency is increasing.

The quasi-static model provides the static contribution. Large details of this contribution have been detailed in the previous section and reported in various papers. As explained previously the usual dynamic consideration (including entire derivation) is quickly limited as the frequency is increasing [36, 44, 45].

Indeed, these losses taken into account can work precisely with the low-frequency excitation, but in the high-frequency case, it will overestimate the frequency influence. To reach a correct behavior, a new mathematical tool is introduced to correctly balance the frequency performances. Fractional derivative exposed in the previous part will constitute the perfect mathematical operator required. Fractional derivative operator is the extension of derivative dimension to real or complex numbers. In our model, an equivalent electric field will be introduced as the product of the fractional derivation of the polarization with a coefficient ρ , property of the material:

$$E_{dyn} = \rho \frac{d^n P}{dt^n} \quad (2.16)$$

After inclusion of the dynamic contribution in Eq. 2.16, the model equation becomes:

$$\begin{aligned} & \text{if } E(t) > f^{-1}(P_i(t)) + E_{ci} + \rho_1 \cdot \frac{d^n P_i(t)}{dt^n} \\ & P_i(t + dt) = f(E(t + dt) - E_{ci} - \rho_1 \cdot \frac{d^n P_i(t)}{dt^n}) \\ & \text{if } E(t) < f^{-1}(P_i(t)) - E_{ci} - \rho_1 \cdot \frac{d^n P_i(t)}{dt^n} \\ & P_i(t + dt) = f(E(t + dt) + E_{ci} + \rho_1 \cdot \frac{d^n P_i(t)}{dt^n}) \\ & \text{if } f^{-1}(P_i(t)) - E_{ci} - \rho_1 \cdot \frac{d^n P_i(t)}{dt^n} < E(t) < f^{-1}(P_i(t)) + E_{ci} + \rho_1 \cdot \frac{d^n P_i(t)}{dt^n} \\ & P_i(t + dt) = P_i(t) \\ & \sum_{i=1}^k \text{Spectrum}(i) \cdot P_i = P \end{aligned} \quad (2.17)$$

Various definitions of fractional derivative exist and usually exhibit similar properties. Among these, the Grunwald derivative is well suited for numerical implementation, and will be used for this study. The Grunwald derivative is given by:

$$D^n f(t) = \lim_{h \rightarrow 0} \frac{1}{h^n} \sum_{k=0}^{\infty} (-1)^k \binom{n}{k} f(t - kh) \binom{n}{k} = \frac{n(n-1)(n-2) \cdots (n-k+1)}{k!} \quad (2.18)$$

Where h is the sampling time period and n is the fractional derivative order. The introduction of Grunwald operator into Eq. 2.4 leads to:

$$\rho \cdot \left(\frac{1}{h^n} \sum_{k=0}^{k=t/h} (-1)^k \binom{n}{k} P(t - kh) \right) = E - [f^{-1}(P) + E_c \cdot \text{sign}(\frac{dP}{dt})] \quad (2.19)$$

On next Fig. 2.14, dynamic contributions provided by entire and fractional derivatives are compared with measurements. Hysteresis loops are varying from 2 mHz to 1 Hz. Fractional derivative contribution exhibits great advantage as the frequency is increasing. This is particularly readable on Fig. 2.15 which compared for same configuration the hysteresis loops area variation versus the frequency.

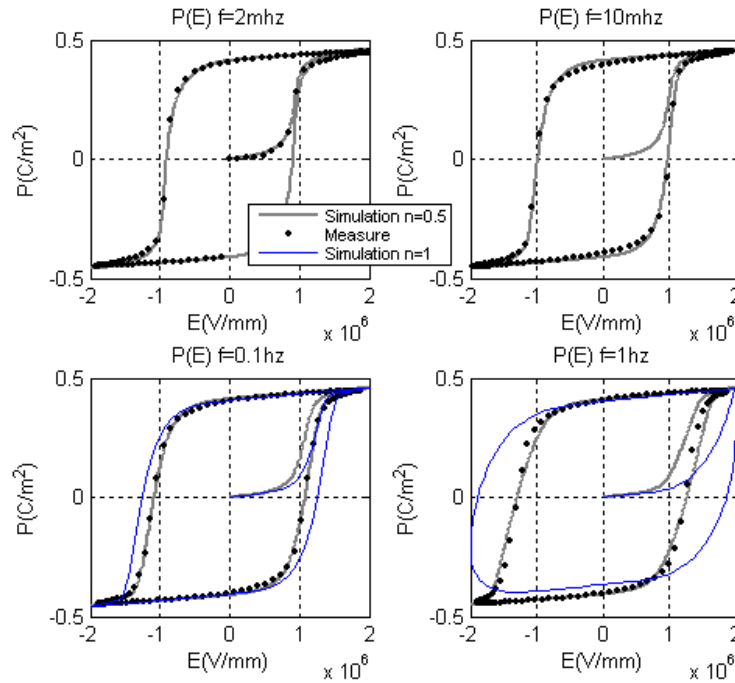


Figure 2.14: Comparison measure/simulation for hysteresis loop area as the frequency is increasing.

A dedicated protocol has been established in order to obtain the fractional model parameters couple ρ and n . This protocol involved, firstly, to obtain three major experimental hysteresis curves ($E_{max} \gg E_c$), to get the best accuracy each experimental curve

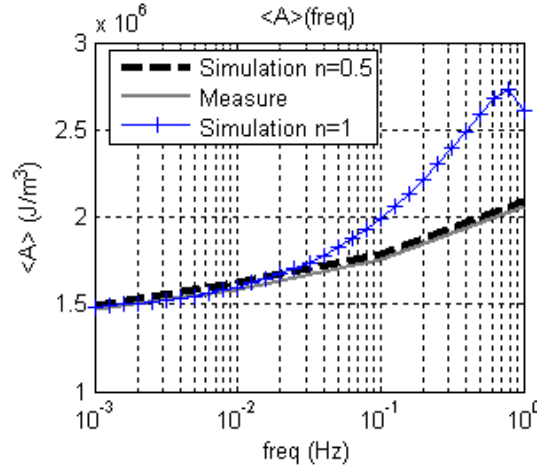


Figure 2.15: Hysteresis loop area versus the frequency $A\langle f \rangle$.

must be obtained for three different decades of frequency. The parameters ρ and n are obtained when the simulated hysteresis loop perfectly matched the experimental one. To improve these parameters setting a new investigation work has been done. We have established the relation between the high amplitude, low frequency dielectric hysteresis model (considering fractional operators) and the weak excitation stress level but high frequency bandwidth well known dielectric permittivity fractional Cole-Cole model [46–48]. Good comparison simulation/measure in both cases, allow attributing same physical origin of the dielectric losses taken into account (the dielectric relaxation). The physical relation between these two behaviour obtained for two very distinctive excitations is particularly interesting because it allows limiting the piezoceramic characterization to the impedance analyzer (where all the model parameters can be set) and to anticipate the high electrical amplitude stress behaviour in simulation.

2.4 Inverse Model

In the previous section, piezoceramic dielectric hysteresis has been study and modelled. We mainly focus on the direct hysteresis behaviour $P(E, T)$ through the piezoceramic sample. In this PhD labour, one of the main objectives is to monitor or to predict the material properties under working situation (such as energy harvesting installation, piezoactuator, micropositioning, \dots). Piezoactuators are employed in a large variety of applications such as noise and vibration control, nanopositioning and aerospace positioning systems. In particular, the high precision positioning capability of piezoactuators has been exploited in industrial applications, such as scanning probe microscopy (SPM), to move sensor probes over micro-sample surfaces while collecting nano-level surface property information. However, this high precision can be considerably reduced due to nonlinear hysteresis effects when piezoactuators are employed over large operating ranges. [49] Other nonlinear effects, such as creep effects, cause a loss in precision and become particularly significant when

a high precision is required over extended periods of time [50, 51]. A high precision can be achieved over large operating ranges by using a hysteresis control system, and non-linear hysteresis effects can be corrected through charge control. Furthermore, capacitor-insertion methods can be employed to improve the linearity of the actuator [52]. Induced vibrations are also a current limitation of the positioning bandwidth. Post-correction techniques [53] have been developed to remove creep, hysteresis and vibration effects, but such techniques cannot be used when real-time compensation is required. Recent investigations in high precision actuators and sensors have led to a feedback-based control method, which is the most effective method when dealing with nano-positioning. [54] The feedback control uses model based inversion approaches, and these techniques make it possible to correct nonlinear hysteresis effects and, thereby, to improve the positioning performances of the sensor. An inverse model must satisfy competing objectives; it must be sufficiently accurate to predict the nonlinear material dynamics under varying operating conditions and it must be efficient enough to allow a real-time implementation. This section discusses the development of a methodology for constructing a new accurate hysteresis inverse model based on experimental results, for a large frequency bandwidth using fractional derivatives. As previously exposed for the direct model, the proposed inverse model comprised two important terms: an inverse static contribution $E_{stat}(P_{stat})$, and a time-dependent loss term, made up of the product of a material constant, ρ , and a fractional polarization derivative term, $d^n P/dt^n$ ($n \in R$).

2.4.1 Quasi-static inverse contribution

The previous relations exposed in the quasi-static direct model section can be utilized to construct inverse models specifying the field that is necessary to achieve a given polarization waveform (amplitude, \dots). If we limit our work to steady states; transient phases and unsymmetrical loops are then excluded. This restriction allows the use of a model consisting of a single basic element (mechanical dry friction). The inverse model requires the knowledge of the derivation polarization sign, and this information can be calculated from the imposed polarization excitation. If $dP/dt > 0$, the model describes the increasing part of the hysteresis loop, whereas if $dP/dt < 0$, the decreasing part is described. The inverse model can be resumed in the following equation system:

$$\text{if: } dP/dt > 0, P_i(t + dt) = f(E(t + dt) - E_{ci})$$

$$\text{if: } dP/dt < 0, P_i(t + dt) = f(E(t + dt) + E_{ci})$$

As illustrated in Fig. 2.16, this new inverse formulation leads to accurate results. In this case, a sinus-type polarization waveform was imposed.

In the case of industrial application including transient states, previous inverse relation is not allowed. Like E and P are not one-to-one nonlinear mapping, one can't inverse it directly. So a feedback control solution can be employed. Due to the high nonlinear

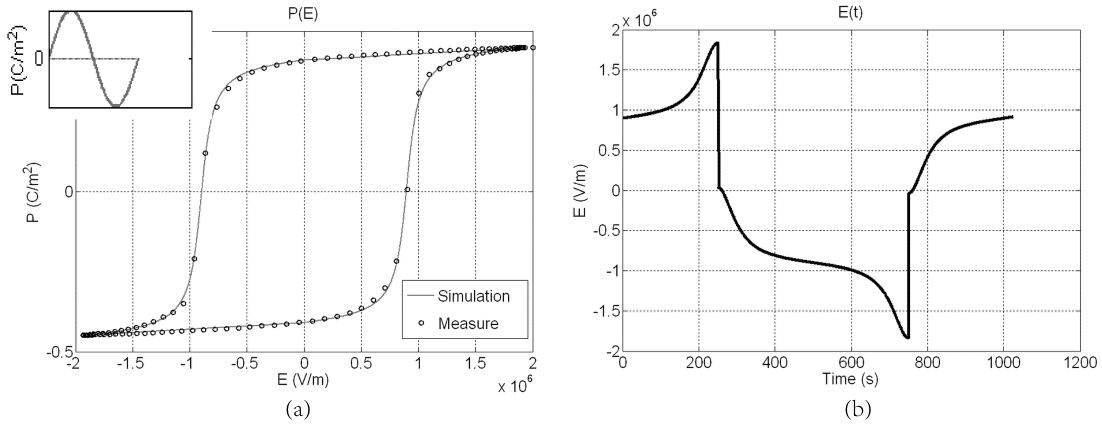


Figure 2.16: (a) A comparison of measured data/simulation on a quasi-static major hysteresis loop, using the quasi-static inverse model 1.(b) The associated electric field.

behaviour of the piezoceramic, a just proportional corrector is not enough to reach good simulation results which is something done by employing a well-adjusted proportional integrator corrector as illustrated in the following Fig. 2.17:

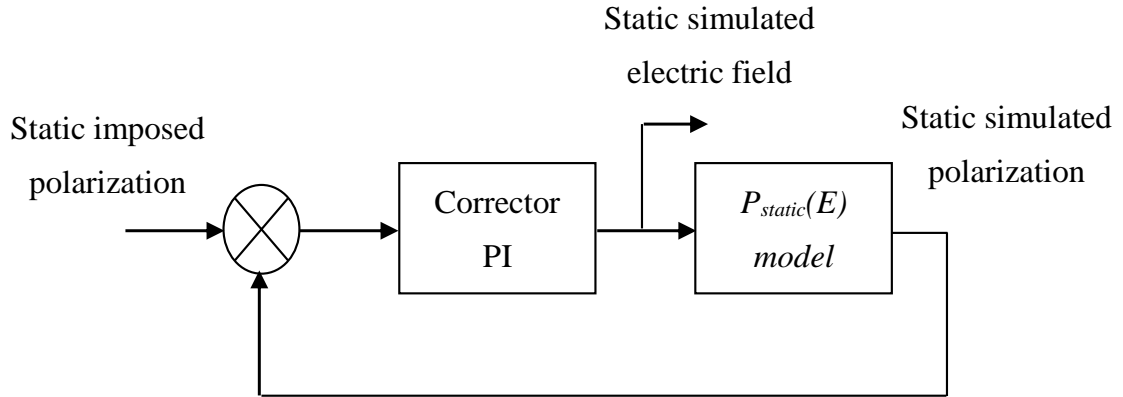


Figure 2.17: $E_{static}(P)$ inverse model

2.4.2 Dynamic inverse contribution

In the inverse model, the dynamic polarization is imposed. The dynamic electric field is obtained by adding the dynamical fractional equivalent electric field (i.e. the product of a constant ρ and the fractional derivative of the polarization) to the quasi-static electric field contribution:

$$E = E_{static}(P) + \rho \cdot d^n P / dt^n \quad (2.20)$$

The quasi-static electric field is computed using the quasi-static inverse model as explained in section 2.4.1. The fractional term $\rho \cdot d^n P / dt^n$ is calculated either analytically when possible (sinusoidal-type polarization waveform) or numerically using the numerical implementation of the fractional derivative Grunwald definition, as explain in the dynamic

consideration part of this chapter.

2.4.3 Polarization control

The objective of the polarization control is to impose the waveform (amplitude, frequency, etc.) of the polarization field of the ferroelectric sample. We assume here electrical field excitation, two contributions (static and dynamic) are then necessary as explain previously. The parameters of the model, i.e. static parameters γ , σ , spectrum and dynamic ones ρ , n must be set on the direct model for the testing material. The corresponding electric field and voltage are computed first in simulation and will give the excitation field for our experimental validation.

2.4.4 Strain control

To control piezoceramic strain using the previous model, a relation between the mechanical strain (S) and the polarization field is necessary. In the literature [32, 35], authors get simulation success with a proposed simple mathematical relation between these parameters: S has been described as a linear function of P^2 :

$$S(t) = \beta \cdot P^2(t) \rightarrow P(t) = (S(t)/\beta)^{0.5} \quad (2.21)$$

Here, β is a material characteristic independent of the sample geometry and determined by comparisons between measurement and simulation. Experimental tests show that this relation [44] can be particularly well adapted independently of the frequency. In the inverse model $E(S)$, the strain waveform is imposed. The first step consists in computing the polarization field associated with the imposed strain. For this, equation is employed. Subsequently, the dynamical inverse model $E(P)$ is used to determinate the electrical field waveform necessary:

$$S_{imposed}(t) \rightarrow (X(t)/\beta)^2 \rightarrow P(t) \rightarrow E(P) \rightarrow E(t) \quad (2.22)$$

2.4.5 Polarization contrl under mechanical-type excitation

In the previous part, piezoceramic dielectric hysteresis direct and inverse model $P(E)$, $E(P)$, has been study and modeled. We have talk about polarization and strain control under electrical excitation. In this part we will talk about polarization control under mechanical excitation, which can be very useful for energy harvesting applications. If we are able to control the polarization, one can imagine a magnificence of the amount of harvested energy by placing our system close to the best conditions. The scaling relation introduce previously between the electric field, E , and the mechanical stress, T , is used to take into account the electromechanical coupling. This scaling law links our three ferroelectric materials dimensions in a simple function: the polarization, P , the electrical field, E , and the mechanical stress, T . The scaling law expresses the product of the

mechanical stress, T , the polarization P and a parameter α as an equivalent electric field.

$$E_{eq}(t) = \alpha \cdot T(t) \cdot P(t) \quad (2.23)$$

α is a material characteristic, independent of the sample geometry and determined by comparisons between measurements and simulations. This scaling relation has already been used with success in previous articles [32, 35, 55, 56], in these article more details are also provided. Fig.2.18 shows the $T(P)$ model with dynamic consideration, using the Eq. 2.23.

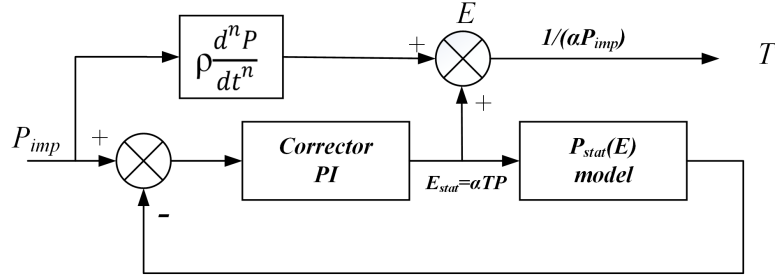


Figure 2.18: Inverse model $T(P)$

2.5 Conclusion

This chapter gives a detailed description of the modeling of piezoceramic under electrical and mechanical excitation. A further developed inverse model, $T(P)$ is also included and depicted in detail. The foundation for the modeling quasi-static contribution is based on the domain wall movements. With the consideration of the fractional derivative operator in modeling dynamic behavior, the model will give an accurate calculation of dielectric polarization whatever the property of excitation. A calculation of the fractional method has been presented in order to give a better understanding. Both in the electrical model and mechanical model, we use the same fractional derivative operator and characterized parameter. In the following chapters, good results will be presented. By using the electrical model in this chapter, we characterized new piezoceramics for further study of this model and use them in the mechanical model. To validate the mechanical model, special measuring bench has been developed.

Piezoceramic characterization – Experimental measuring bench

3.1 Introduction

Due to their natures and compositions, piezoceramic exhibits different amplitudes and shapes as plotting the dielectric polarization curve versus pure mechanical stress, pure electrical field or a combination of both excitations. It is necessary to well understand these mutual relationships and interactions as we want to make fully use of their high coupling potentials. [26] In the second chapter of this thesis, we have exposed different techniques for the modeling of the dielectric and mechanical behavior of such materials, in this part some experimental results has already been displayed. Indeed a first series of experimental results is necessary to set the model parameters and another is required to determinate its validation domain boundaries. Furthermore, experimental results are obviously required as we want to explore extreme ferroelectric material properties and try to reach its working limits.

The last chapter of this thesis will talk about industrial applications such as energy harvesting, nano-positioning and sensors. To validate such applications and reproduce experimentally such working conditions, various kinds of mechanical and electrical excitations must be taken into account by our measuring bench.

In this thesis, various behaviors of a piezoceramic are studied, we particularly insist on the nonlinear ones such as the dynamic dielectric hysteresis. To validate and give an experimental orientation of this thesis, three specific thematic requiring experimental

point of view are highlight:

- The fractional contribution of the piezoceramic polarization under electrical field and mechanical stress excitation.
- The validation of the inverse modeling of the piezoceramic polarization under electric field or mechanical excitation for a wide frequency bandwidth with consideration of fractional derivative operators.
- The piezoceramic behavior under a combination of both excitation mechanical stress and electric field. The objective here is to reproduce the industrial conditions of energy harvesting systems and try to get the exact amount of energy available.

In order to set up all these experimental situations and start to get our first results different specific measuring benches and experimental methods have been developed. Before describing all these experimental situations, we will first give a short description of the tested sample and will also explain in detail the treatments required to give to the piezoceramic its piezoelectric ability.

3.2 Material processing

First of all, all the selected piezoceramic tested for this study exhibit relatively high piezoelectric coefficient, high coupling coefficient and are easy to machine. There are already considered as mature commercial products, and are employed in various already existed industrial applications. The tested piezoceramics come from major international producer such as FUJI, Morgan Advanced Materials, Saint-Gobain and so on.

Piezoceramics are commonly divided into two categories; we distinguish “soft” and “hard” ones depending on the mobility of the dipoles and the domains. These movements are directly linked to the polarization and the depolarization behavior. Hard piezoceramic can be exposed to high electrical and mechanical stresses. The stability of their properties makes them ideal for high-power applications. For such applications low loss materials are privilege, indeed low dielectric and mechanical losses ($\tan\delta$, Q_m) combined with high piezoelectric charge constant (d_{33}) make them suitable for high-performance ultrasonic applications. Other hard ceramics characterized by good frequency and ageing stability can be exposed to high repetitive quasi-static and dynamic loads for ignition applications. Soft piezoceramics are distinguished by a comparatively high domain mobility and a relatively easy polarization. These materials are characterized by high relative permittivity, large electromechanical coupling factors, large piezoelectric constants and low mechanical quality factors. These materials are particularly suitable for sensing applications, receivers, actuators and low power transducers. [57, 58]

To highlight non-linear behavior, we have decided to start our study with a soft piezoceramic characterized by a moderate angle losses $\tan\delta$. P188 from Quartz & Silice (France)

has been selected, this ceramic is a Navy type II ceramic. This material is appropriate for our experiment; indeed nonlinear behaviors are easily reachable even for relatively weak external excitations. Tab. 3.1 gives the main characteristics of this ceramic as they appear in the manufacturer data-sheet.

Table 3.1: Main characteristics of standard P188 ceramic given by the manufacturer [29]

Parameters	Symbol	Units	Typical values
Density	ρ	10^3 kg.m^{-3}	7.7
Poisson's constant	σ		0.3
Curie point	T_c	$^{\circ}\text{C}$	340
Dielectric permittivity	$\varepsilon_{33}^T/\varepsilon_0$		1850
Piezoelectric coefficient	d_{33}	pC/N	425

Depending on the final objectives of the measuring session, sometimes before exploitation the piezoceramics need to be polarized. To get this polarized state, a specific procedure is required; this procedure is illustrated in Fig. 3.1.

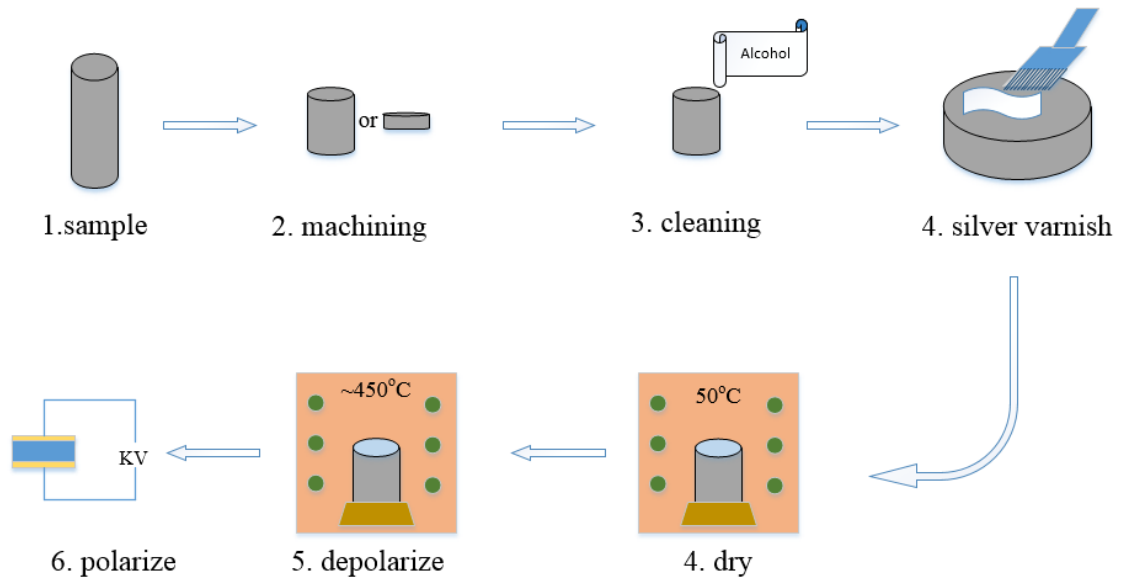


Figure 3.1: Illustration of the procedure for the conditionings of the piezoceramic samples.

Cylindrical specimens ($\phi = 6.3\text{mm}$) coming from manufacturer are first painted with silver conductive varnish (Electro-Science Laboratories, Inc. Cermet Silver Conductor 590-G) on both cross sections and put in the oven (50°C for 30 min) to be dried. It will constitute the electrode required to establish the electrical contacts.

After this first treatment, our samples are deposited in an oven where temperature is slowly increasing and decreasing (maximum temperature 450°C , increase and decrease temperature speed was $3^{\circ}\text{C}/\text{min}$). The tested samples are wrapped through an aluminum

paper in order to short circuit the electrodes and dissipated the remaining charges. This cure insure a perfect depolarization and remove all the mechanical stress induced by sintering and machining.

The specimens are subsequently poled at room temperature under an electrical field of 2 kV/mm during 1 min in a silicone oil bath, Fig. 3.2. Constant temperature conditions and free mechanical properties of the sample are assumed.

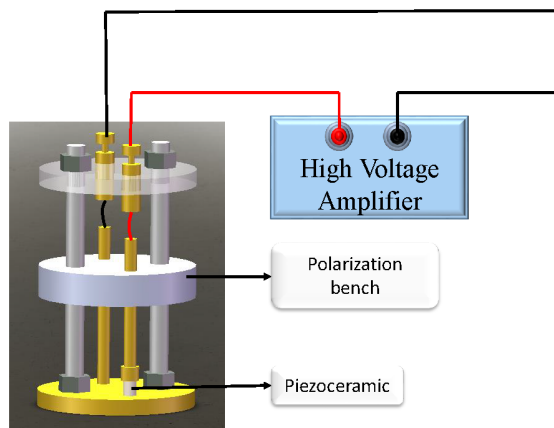


Figure 3.2: Polarizing bench under high voltage electric field.

After this polarization procedure, a remnant dielectric polarization is obtained through the piezoceramic. All the ferroelectric dipoles inside the piezoceramic are almost oriented in the same direction; the piezoceramic exhibits a high coupling coefficient and a piezoelectric ability. During polarization step, two conductive tapes can be paste on both sides of the electrodes to monitor the poling current though the tested sample and check if the polarized state has been reached correctly. After all these conditioning steps, the ceramic samples are ready to be carried out.

Independently of the excitation nature (electric/mechanical or a combination of the two), the setting procedures of the tested samples follows the same steps described and illustrated above, Fig. 3.2. However, the composition of the sample and its dimensions have an influence on the process condition in turn; by instant the depolarization temperature (linked to the Curie temperature) and the polarization electric field amplitude (linked to the thickness and material composition) can modified the procedure parameters.

For the dielectric dynamic hysteresis curve verification experiment, under electric field excitation in direct $P(E)$ and inverse conditions $E(P)$, our cylinder specimens were cut into $\phi 6.3 \times 1\text{mm}$; for the mechanical inverse model, $T(P)$, $\phi 6.3 \times 6\text{mm}$ were chosen and for the Ericsson loop energy harvesting experiment, to make sure the high voltage was applied in a relative safe range, specimens of dimension of $\phi 6.3 \times 5\text{mm}$ were chosen.

To test the portability of our models and our experimental measuring benches, various piezoceramics have been tested. We have in particular decided to experiment one soft piezoceramic of each major material manufacturers. P188 soft ceramic from Saint-Gobain has already been presented, the second sample tested is a PZT-5A which is a soft

piezoceramic recommended for hydrophones or instrument applications because of its high resistivity at elevated temperatures, high sensitivity, and high time stability. Tab. 3.2 gives the main characteristics of this ceramic as they appear in the manufacturer data-sheet.

Table 3.2: Main characteristics of standard PZT5A ceramic given by the manufacturer [10]

Parameters	Symbol	Units	Typical values
Density	ρ	10^3 kg.m^{-3}	7.75
Poisson's constant	σ		0.3
Curie point	T_c	$^{\circ}\text{C}$	365
Dielectric permittivity	$\varepsilon_{33}^T/\varepsilon_0$		1700
Piezoelectric coefficient	d_{33}	pC/N	374

The last sample tested is a C2 from Fuji manufacturer. This is a hard piezoceramic well distributed and recommended for gas lighter and cleaner applications. Tab. 3.3 gives the main characteristics of this ceramic as they appear in the manufacturer data-sheet.

Table 3.3: Main characteristics of standard C2 ceramic given by the manufacturer [59]

Parameters	Symbol	Units	Typical values
Density	ρ	10^3 kg.m^{-3}	7.6
Poisson's constant	σ		0.3
Curie point	T_c	$^{\circ}\text{C}$	300
Dielectric permittivity	$\varepsilon_{33}^T/\varepsilon_0$		1460
Piezoelectric coefficient	d_{33}	pC/N	367

Specific measuring benches offering and sensing high mechanical and electrical excitation were developed to reproduce all the situations previously described. First measuring bench will be used under electrical field exclusively to validate the proposed dielectric model fractional contribution and the inverse model, second measuring bench has been developed to provide measure under pure mechanical excitations. Finally, in order to give experimental validations for energy harvesting “Ericsson loop” technique, last measuring bench including excitation combination has been established. In next part, all these measuring benches are described in detail.

3.3 Experimental design

3.3.1 Measuring bench for the pure electrical excitation situation

As illustrated in the second chapter of this thesis the dielectric behavior of a piezoceramic is highly nonlinear, it is frequency dependent and exhibit hysteresis and saturation

as the external excitation level is high. A good characterization and knowledge of these behaviors is of major interest as we want to envisage an industrial employment of such materials. For the first measuring bench proposed in this study, we focus on the acquisition of dielectric polarization and mechanical strain information as the ceramic is submitted to an external electric field. This measuring bench can be used to get material information under imposed electric field, and provide information and validations for direct dielectric model $P(E)$. Furthermore, added to a waveform pre-calculation via inverse dielectric model $E(P)$, the same measuring bench can be employed for the validation of the dielectric inverse model $P(E)$ and for the imposed strain model $S(E)$.

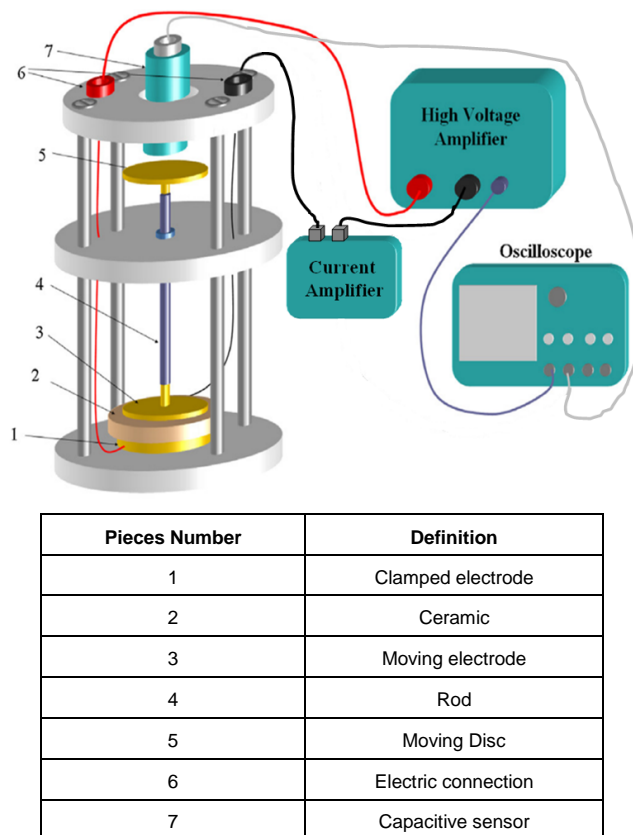


Figure 3.3: Schematic diagram of capacitive displacement sensor and polarization current amplifier used to measure the electromechanical activities and dielectric polarization of a piezoceramic.

Fig. 3.3 shows the dedicated test bench realized to measure the dielectric polarization and the mechanical strain versus an electric field excitation; Fig. 3.4 is the equipments connections in the laboratory. The strain is measured with the help of a non-contact capacitive measurement sensor (FOGALE MC 940) with a precision on the order of 10 nm. The tested samples are placed on a horizontal stainless steel disks (20 mm in diameter) in order to avoid measuring a parasitic flexure motion, and a second brass disk positioned on the top of the film rendered it possible to apply the bipolar electric field. The total weight of pieces 3, 4 and 5 shown in Fig. 3.3 is 5 g (equivalent to 156 Pa) which is a suitable

small stress, in order to avoid clamping of the sample. We assume constant temperature conditions and free mechanical properties of the sample. The ceramic is subjected to an electric field with the help of a waveform generator (Agilent 33220A) for which the output was amplified through a high voltage amplifier (model 10/10, TrekInc.), the strain is deduced by divided the displacement by the initial thickness. The sample is subjected to a varying electric field with maximum amplitudes higher than $1.5 \text{ kV} \cdot \text{mm}^{-1}$ in order to exceed the coercive field of the material. To avoid dielectric breaking, specimens are electrically insulated with silicon grease. Electric displacement is calculated by charge measurements (with a Keithley amplifier 5011). The polarization field is computed by integration of the current. Lecroy wave surfer 44XS oscilloscope is configured to monitor simultaneously an image divided by one thousand of the imposed electric field, the outputs of the current amplifier and of the capacitive measurement sensor.

For the imposed polarization and imposed strain models, a corresponding electric field waveform is pre-calculated in simulation using inverse model $E(P)$ and $S(P)$. The waveform is then stored as an arbitrary waveform in the Agilent 33220A arbitrary waveform generator. This waveform is used as a driver of the high amplitude Optilas Trek 10-kV voltage supply. Dielectric polarization and mechanical strain are obtained in measure via same protocol and comparison between respectively imposed and measured polarization and strain can be done.

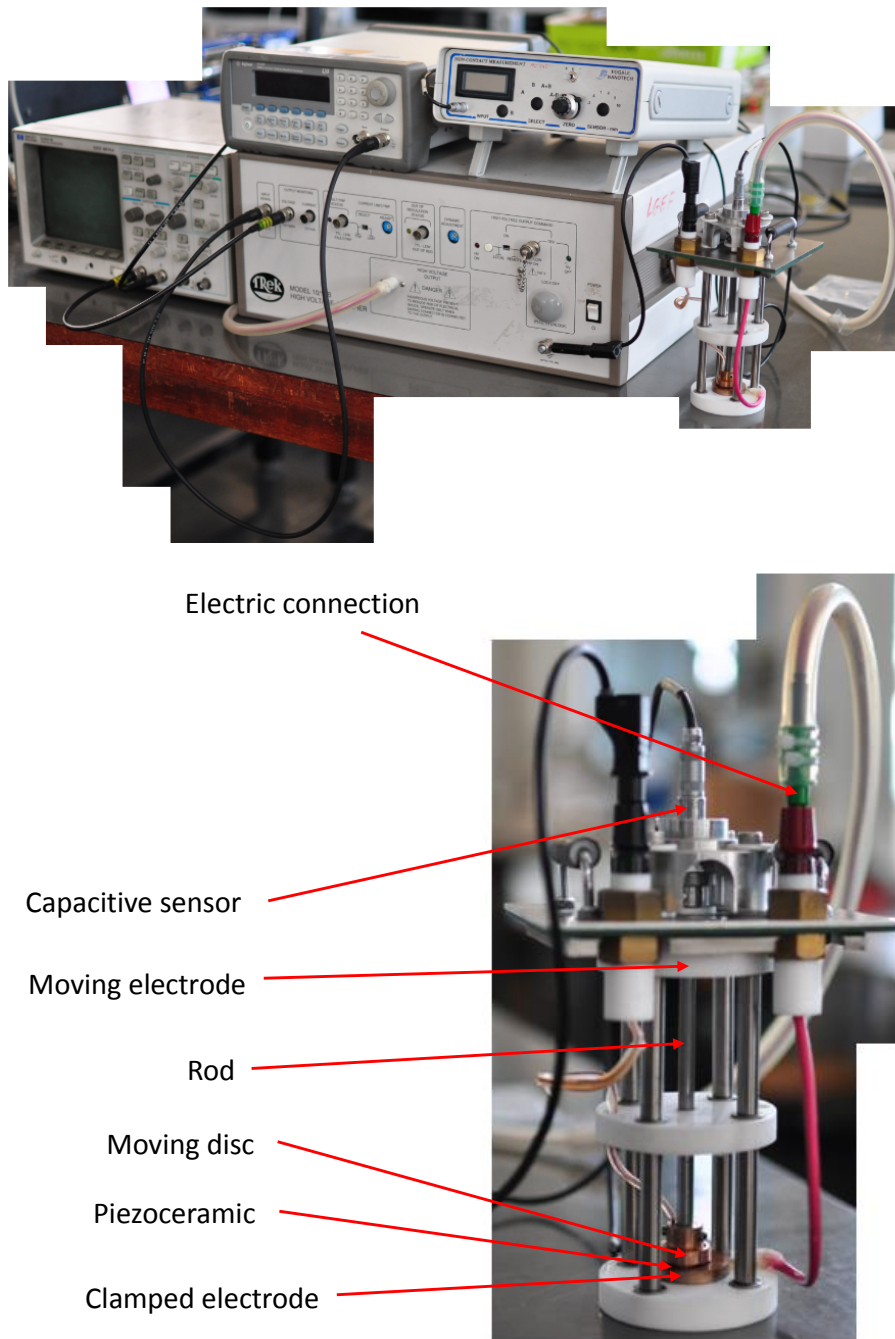


Figure 3.4: Photo of capacitive displacement sensor and polarization current amplifier used to measure the electromechanical activities and dielectric polarization of a piezoceramic.

3.3.2 Measuring bench for the pure mechanical excitation situation

When a polarized piezoceramic is pressed along its polarization axis, the variation of the polarization state will give birth to an electric current through the ceramic. This current can be monitored via the electrodes of the tested sample and a current amplifier; by integrating this current with time, polarization-stress $P(T)$ plot is achieved. In this kind of experiments, mechanical stress parameters (frequency, amplitudes and waveform)

must be controlled by a waveform generator and a force sensor is necessary to check the mechanical stress. Under external excitation (electrical field or mechanical stress) a frequency increase has direct consequences on the output signal, it means an increase of the dielectric losses through a piezoceramic readable on the hysteresis loops $P(E)$ or $P(T)$. In the second chapter of this thesis, we have described a dynamic dielectric polarization model using fractional derivative operators to fit with this property. The measuring bench presented in this section has been developed to check the validity of this model under mechanical stress conditions. This bench can be used in direct $P(T)$ (dielectric polarization versus mechanical excitation) or in inverse $T(P)$ depending on the final objective of the study. It must relate ceramic behavior under mechanical stress of different waveforms (sinus, triangular, ...) of amplitude and of frequency bandwidth as large as possible. The measuring bench used in these experiments is schematically shown in Fig. 3.5

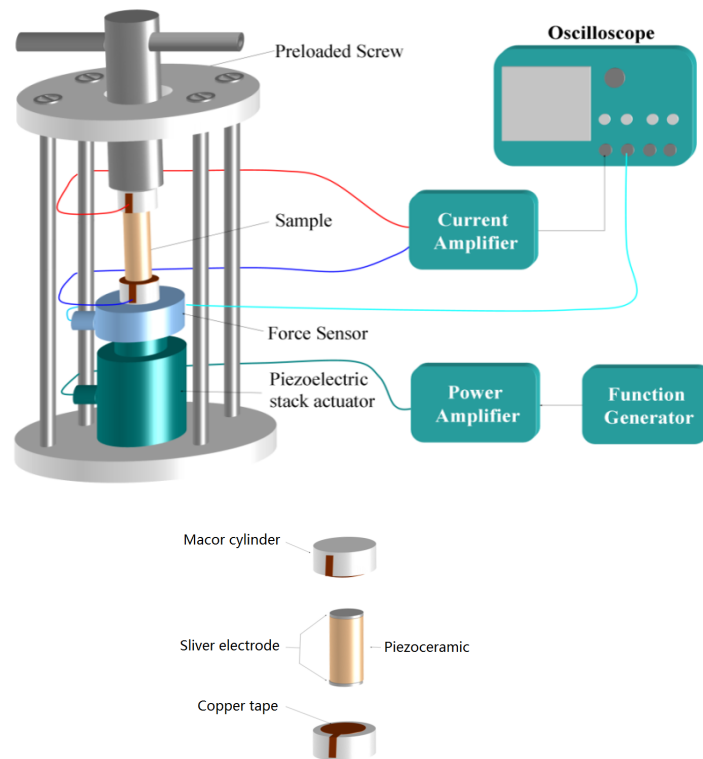


Figure 3.5: Schematic diagram measure of electric polarization behavior under mechanical excitation of a piezoceramic.

In this measuring bench, a piezoceramic stack (P-246 supplied by PI Ceramic Company (Germany)) controlled by a function generator (Agilent, 33220A), and supplied by a power amplifier (HVPZT power amplifier from PI Ceramic Company (Germany)) generated the dynamic excitation. For each new measurement, the function generator is programmed to provide a burst of ten periods of sine wave excitation. The piezoceramic stack is characterized by an extremely high stiffness, pushing forces up to 30 kN and a travel range up to 120 μm . The stress sensor is a XFC200R from FGP Sensors and Instrumentation Company. It

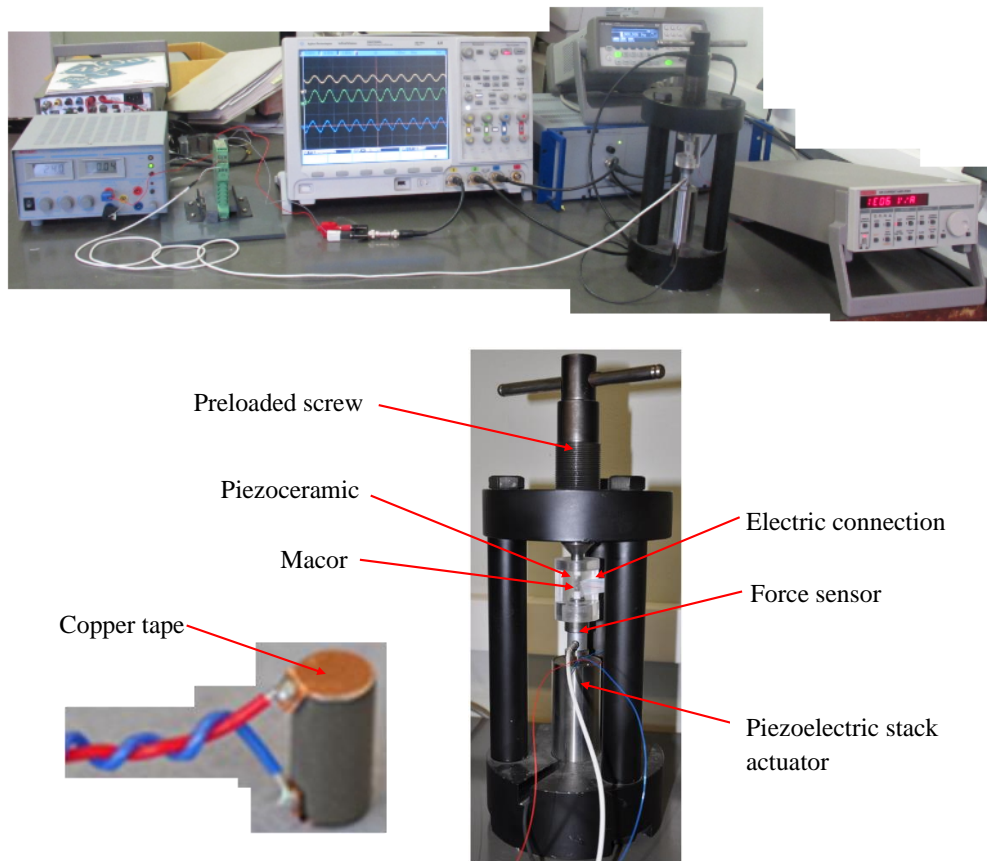


Figure 3.6: Photo of the measure of electric polarization behavior under mechanical excitation of a piezoceramic.

is distinguished by a full scale range $0 \rightarrow 2$ to $0 \rightarrow 10$ kN, with a high stiffness. The stress sensor is driven by an ARD154 DIN rail mountable amplifier from the same company. Two macor ceramic disks ($\phi 6 \times 3$ mm) guaranteed the electrical insulation. Conductive tape has been used to measure the poling current through the tested ceramic. The polarization variations is recorded by short-circuit current measurements using a Keithley current amplifier model 428. The polarization is obtained by time integration of the current. The structure is pre-stressed in order to increase the mechanical strength of the piezoceramic elements and to maintain mechanical contact up to high frequency levels. As illustrated in Fig. 3.5, the applied stress has an uniaxial direction (3 directions). Up to 170 MPa mechanical pressure can be reach on the piezoceramic with this experimental dispositive, which is effective to observe the nonlinearity phenomenon in a usual piezoceramic. [27]

3.3.3 Measuring bench for the hybrid situation, combination of simultaneous mechanical & electrical excitation

The possibility of recycling ambient energies with electric generators instead of using batteries with limited life spans has stimulated important research efforts over the last past years. The integration of such generators into mainly autonomous low-power systems, for

various industrial or domestic applications is envisioned. In particular, in this thesis we focus on energy harvesting from natural surrounding mechanical vibrations. Where direct piezoelectric energy harvesting (short circuiting at maximum mechanical stress level on capacitance storage, for example) leads to relatively weak energy levels, insufficient for an industrial development. By coupling electric field and mechanical stress excitation on Ericsson-based cycles, the amplitude of the harvested energy can be highly increased, and can reach a maximum close to 100 times its initial value. Unfortunately to reach such high gains, high electrical field amplitude levels are required and linear considerations of the material are no more suitable. To get material information and behavior under such conditions a hybrid measuring bench, coupling electric field and mechanical stress excitation is proposed in this section. Fig.3.7 shows the experimental setup used in the present work.

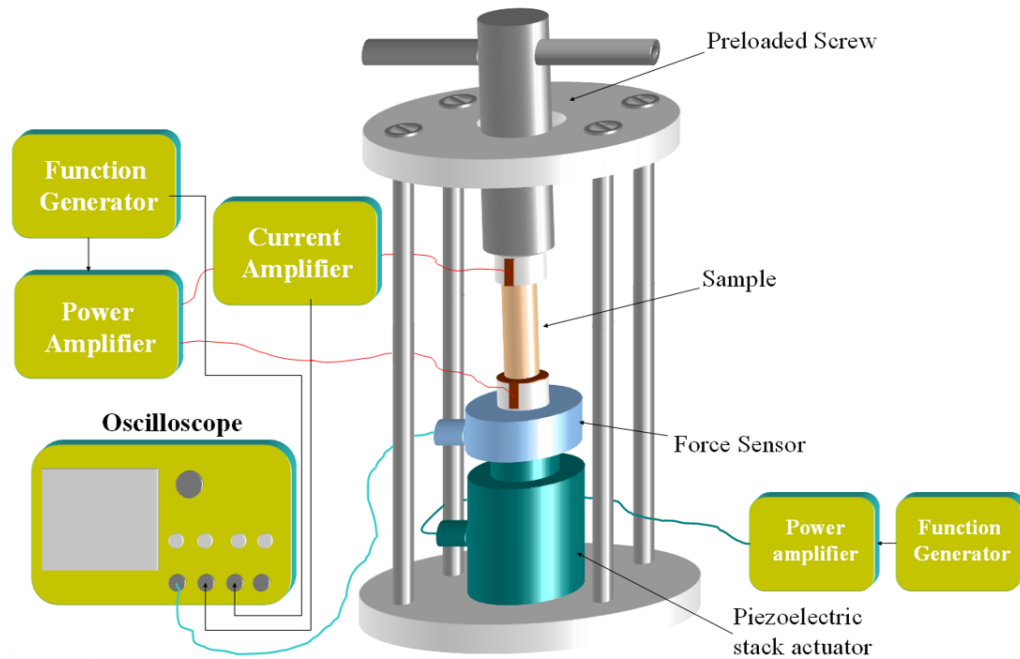


Figure 3.7: Schematic diagram of hybrid measuring bench, simultaneous control of the external electrical and mechanical excitation.

This new experimental bench is actually an extension of the previously described “under mechanical stress condition” measuring bench. In this measuring bench, two synchronized function/arbitrary waveform generator (Agilent, 33220A) are used to control the mechanical excitation and electric field respectively. First one is connected to the piezo-ceramic stack, and is supplied by a power amplifier (HVPZT power-amplifier), this stack generate the mechanical dynamic excitation. Another same function generator controlled the high-voltage amplifier necessary for the imposed electric field, see Fig. 3.8.

To reproduce Ericsson-based cycles conditions, the two waveform generators must be synchronized. The temporal variations of the mechanical and electrical excitations are

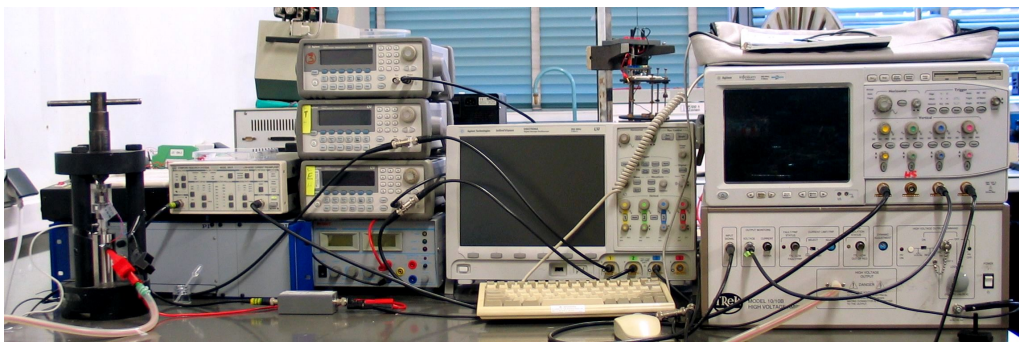


Figure 3.8: Photo of hybrid measuring bench, simultaneous control of the external electrical and mechanical excitation.

displayed in Figure 3.9. The waveform are stored as an arbitrary waveform and for each new measurement, the function generator is programmed to provide a 4-period burst excitation. [28]

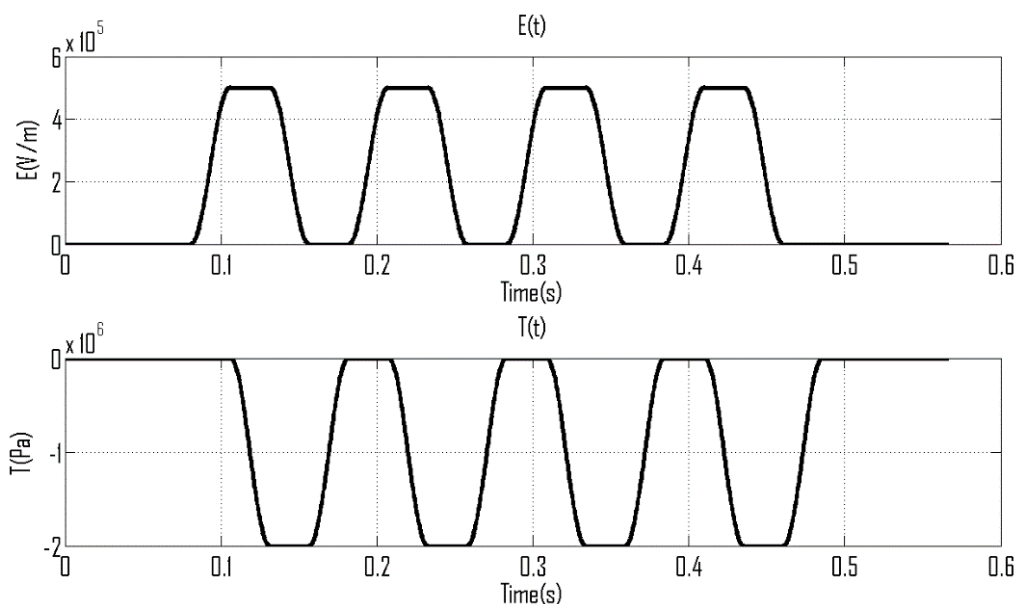


Figure 3.9: Temporal variation of electrical and mechanical excitation in order to reproduce Ericsson-based cycles conditions.

3.4 Experiment initialization & parameter validation

In this section, the first experimental results will be proposed. We distinguish in particular experimental results obtained under electric field excitation, experimental results obtained under mechanical stress contribution, and experimental results under both contributions. These measurements help to fit constants in the modeling & simulation and provide a detailed behavior of the piezoceramic under various excitations situation as well. The result comparison and explanation of each part will be elaborated in the Chapter 4.

3.4.1 Under electrical field excitation

To illustrate the good behavior of our experimental bench and our fractional dielectric $P(E)$ model, a set of comparisons between experimental and simulated dielectric hysteretic loops are proposed as the first result. The three tested samples (see Fig. 3.10, Fig. 3.11, Fig. 3.12) have been submitted to a high amplitude electric field of frequency varying from 10mHz to 10Hz.

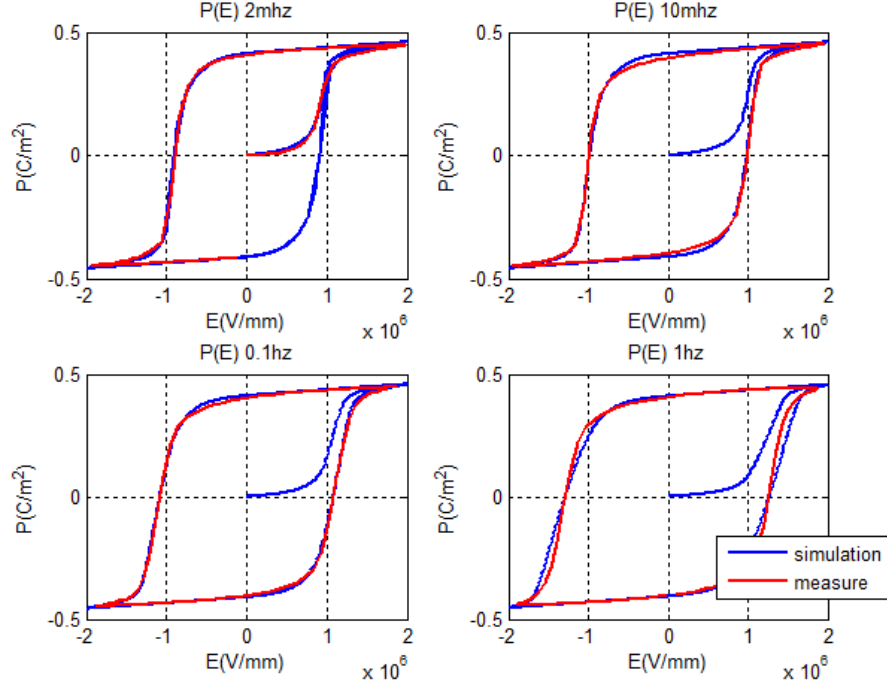


Figure 3.10: Comparison measure/simulation, for 3 decades of frequency on P188 piezoceramic

To obtain such simulation performances, the model parameters have been set previously by the comparison the experiment and simulation results, Tab. 3.4 gives a resume of the simulation parameters for our three tested samples. In this table, n is the order of the fractional operator, we can note in particular that whatever the tested sample, this coefficient remains close to 0.5. Though this fractional operator have been achieved from the electrical excitation, it will be used in the mechanical excitation condition modelling to validate its universality.

3.4.2 Under mechanical stress excitation

To illustrate the good behavior of the “under mechanical excitation” measuring bench a set of comparison simulation/measure is displayed in Fig. 3.13. In this figure experimental measurements are compared with simulated counterparts for varying frequencies ($0.02 \rightarrow 1$ Hz) and for two fractional coefficients ($n = 1$ and $n = 0.5$). When $n = 1$, the mechanical losses could be assimilated to viscous losses. The absolute value of the

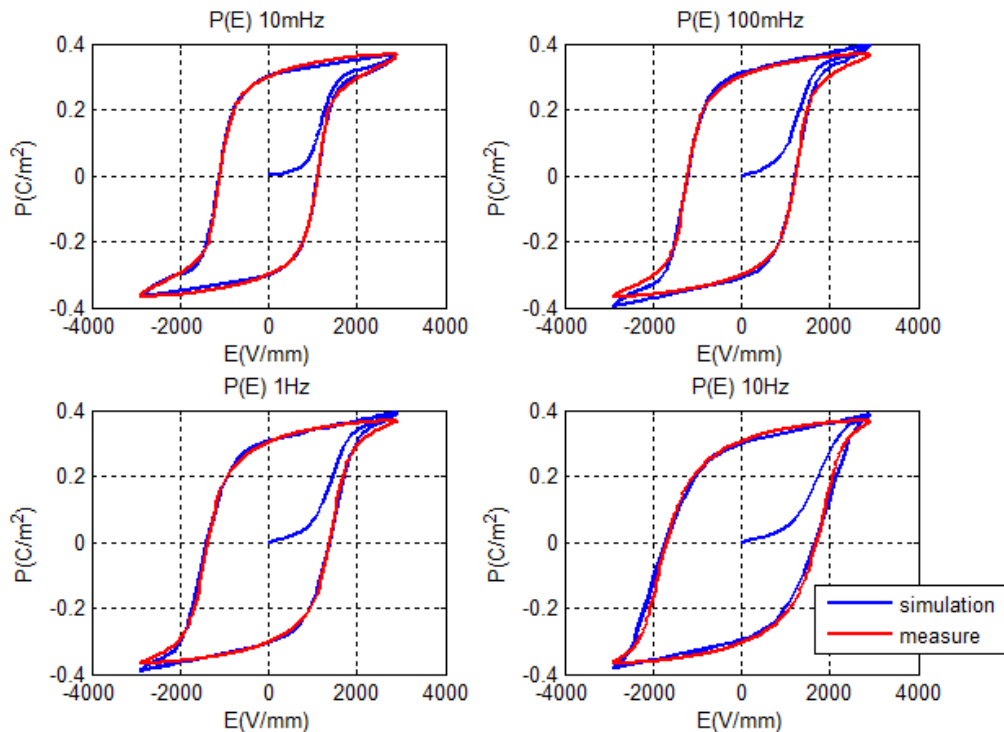


Figure 3.11: Comparison measure/simulation, for 3 decades of frequency on PZT 5A piezoceramic

maximum mechanical stress excitation should be constant and close to 170 MPa, and the static stress was fixed at 80 MPa. Just P188 has been tested here, and the model parameters have been conserved identically to those previously exposed in Tab. 3.4. All results exposed in this section are steady state results, our experimental measuring bench and our model are able to provide transient phases.

The good simulation results displayed in Fig. 3.13 lead to the confirmation that whatever the nature of the external excitation the frequency parameter is correctly taken into account by the fractional model. In the second set of experimental results, the tests have been performed for two constant frequency levels, with 3 maximum excitation stress amplitudes, Fig.3.14. The two constant frequencies tested are 50 mHz and 500 mHz. The idea here is to verify the accuracy of the model for different excitation levels.

As previously found (Fig. 3.14), the measurements agreed well with the simulations ($n = 0.5$), regardless of the excitation level.

3.4.3 Under a combination of electrical field and mechanical stress

To illustrate the good behavior of our hybrid measuring bench, we have decided to present a comparison simulation/measurement for a dielectric Ericsson loops $P(E)$. The excitation conditions involved: an electric field of amplitude 3×10^5 V/m, a frequency of 0.1 Hz, and a mechanical stress of amplitude of 50 Mpa. The temporal variations of the mechanical excitation and of the electrical field excitation are displayed on Fig. 3.9.

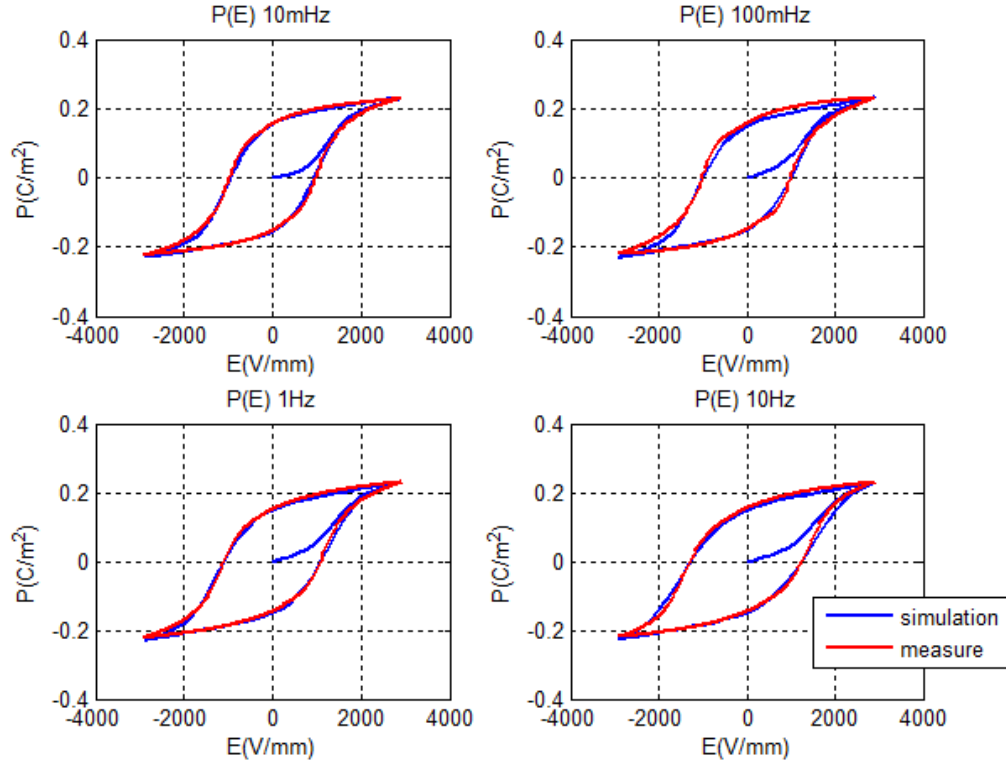


Figure 3.12: Comparison measure/simulation, for 3 decades of frequency on C2 piezoceramic

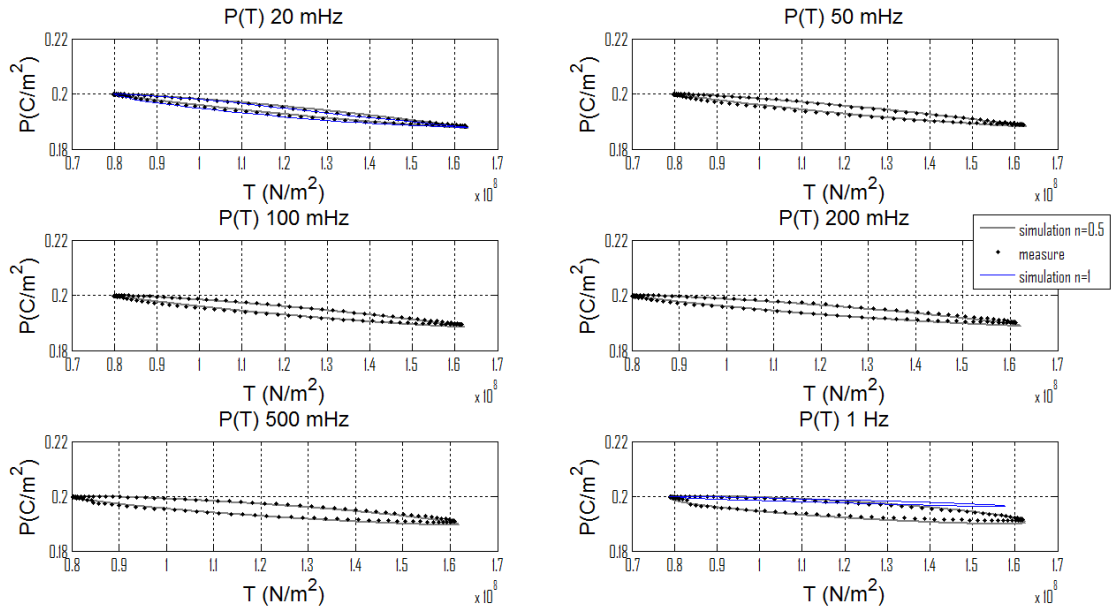
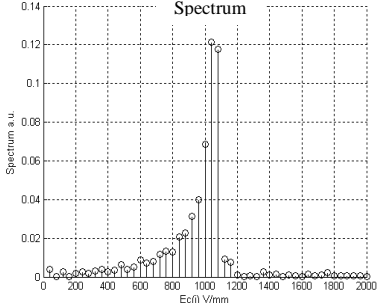
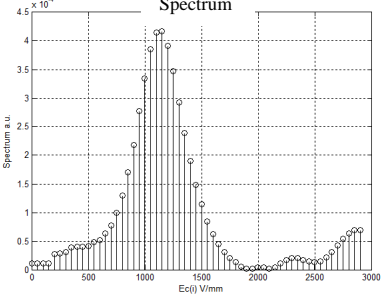
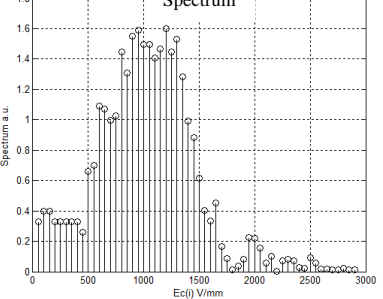


Figure 3.13: Comparisons between measurements and simulations for $0.02 < f < 1$ Hz under the sum of a constant mechanical static stress and a sinus dynamical mechanical stress of constant maximum value.

Table 3.4: Simulation optimum parameters, for the P(E) dielectric model

	Static coefficient: $\gamma = 40;$ $\sigma = 39;$ Dynamic coefficient: $n = 0.48;$	P188
	Static coefficient: $\gamma = 100;$ $\sigma = 37;$ Dynamic coefficient: $n = 0.46;$	PZT5A
	Static coefficient: $\gamma = 180;$ $\sigma = 36;$ Dynamic coefficient: $n = 0.42;$	C2

In this hysteresis dielectric virtuous circle, the loop area $\langle A \rangle$ represents the maximum amount of energy harvested.

This Fig. 3.15 has been displayed in order to validate the good temporal correlation between the simulated and the measured Ericsson loops under high-amplitude excitations. More details on Ericsson loop energy harvested technique will be given in next chapter. Indeed, in this chapter, we will focus on the employment of the piezoceramic studied in this thesis through industrial applications (such as energy harvesting technique).

3.5 Conclusion

From the procedures to prepare the sample to the simulation parameters establishment, this chapter has given a comprehensive description of the measuring bench we have employed in these experiments. Every objective in the work has been carefully studied with consideration of the industrial application. The specific measuring bench for each experiment and the model validation associate closely with each other. Different kinds

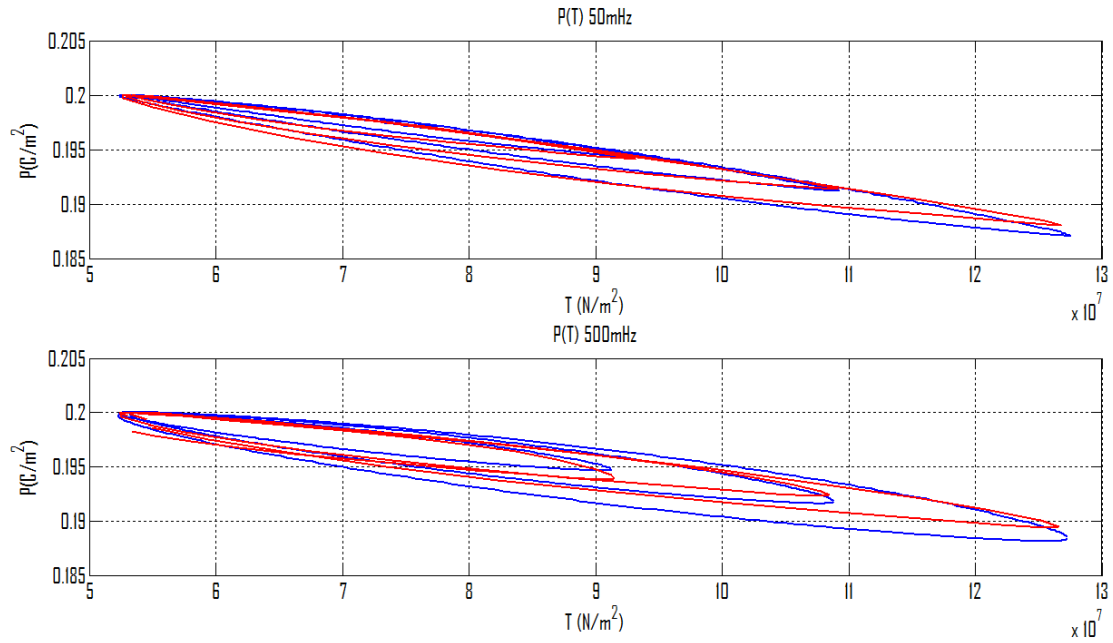


Figure 3.14: Comparisons between measurements and simulations for $f = 50$ mHz and $f = 500$ mHz under a constant mechanical static stress for 3 maximum dynamical mechanical stress values.

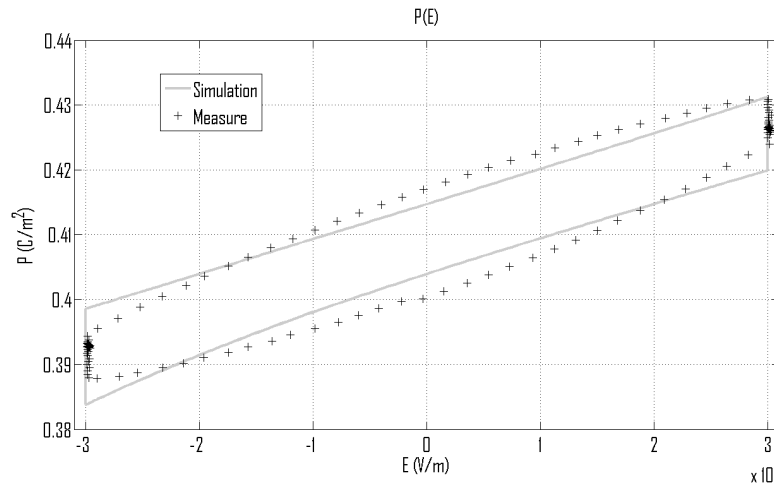


Figure 3.15: Comparison between simulations and measurements for Ericsson loops.

of stimulations on the piezoceramic are precisely modeled with consideration of the fractional derivative. Based on the measurements, it helps to gradually ameliorate the fitting accuracy. No matter what the excitations are, the present model by use of the basic characteristic data of the piezoceramic can give a accurate output to the extrinsic stimuli.

This chapter also confirm the fractional operator for the piezoceramic and in the next chapter, we will use the model including the operator to make more precise comparison with experiment measurement.

Results and Discussion

4.1 Introduction

Recent scientific developments have permitted the manufacturing of new ferroelectric materials with magnificent coupling properties. These new properties render possible the industrial development of various new piezoceramic applications (actuators, sensors, energy harvesters and so on). A precise model including material non-linearities (saturation, hysteresis) is highly required as we want to define precisely control laws and sensor behaviors. [60] To reach correct amount of energy harvested, an external excitation of huge amplitude is necessary. Usually, this amplitude is so high that the material non-linear state is reached. Unfortunately, this non-linear behavior affects a lot the system precision and leads to a degradation of the conversion performances. The piezoceramic behavior under both combination of external excitation, electrical field and mechanical stress has been relatively weakly studied by researchers. Even if this simultaneous combination is frequently present on industrial applications (energy harvesting processes,...) and exhibits high impacts on piezoceramic, few studies existed where both excitations are taken into account simultaneously. [26] A full understanding of the interaction mechanism of the piezoceramic under electrical and mechanical excitation will give precious information, and the rule to follow as we want to precisely control power actuators and control energy harvesting systems in complex situation and highly increase their efficiencies.

In this chapter, we mainly concentrate on the piezoceramic dynamic behavior under common life or industrial applications. In the first part, we focus on the behavior under external mechanical excitation as it the case in passive energy harvesting processes. In the second part hybrid situation have been studied. As illustrated in the first part of

this thesis, natural surrounding vibrations are everywhere. To harvest energy from these unlimited resources gives interesting perspectives. To reach high performances, the energy harvester must be highly excited, and unfortunately exhibited non-linear behaviors. Duffing oscillators with loaded mass magnified mechanical stress in such systems and even if natural vibrations are weak, the increasing of the mechanical stress due to the mechanical oscillator is sufficient to reach non-linear behavior through the material.

Electrical and mechanical external excitations are highly connected. As it is explained in chapter 2, when the frequency of the external excitation is weak ($f \ll 1Hz$), the piezoceramic exhibits a quasi-static behavior. In such conditions, the static contribution (frequency independent) takes a leading role in the dielectric polarization or mechanical displacement induced through the sample. When the frequency exceeds the quasi-static threshold, dynamic contribution will come into play.

In the first part of this last section, we focus on the behavior (characterization and model) of the piezoceramic under external mechanical stress. We particularly insist on illustrate how starting from dielectric consideration (chapter two), the model has been extended to mechanical ones. Scaling relation between electric field and mechanical stress has been employed to get success in this operation. A well understanding of such conditions is particularly interesting, it allows configuring the best external excitation leading to efficient energy harvester systems.

In the second section of this chapter, we will talk about coupling effect (electric field, mechanical stress), and how via a synchronized external excitation (electric field, mechanical stress) also called “Ericsson loops” it is possible to highly increase the rate of semi-passive energy harvesting piezoelectric technique.

4.2 Model for the dielectric polarization variation under external mechanical stress excitation $P(T)$

4.2.1 Description

The piezoceramic polarization is highly dependant of the mechanical external excitation properties (frequency, amplitude). The relation between the ceramic dielectric property and the mechanical force can be considered as linear only if the amplitude is weak. This nonlinearity is especially apparent at high frequency. In chapter two, to increase the frequency bandwidth of our dielectric model $P(E)$, we have employed fractional derivative operators. In this section we will check that same operators can be employed with success under mechanical excitation.

To extend dielectric model $P(E)$ to external mechanical stress excitation, a scaling relation between electric field and mechanical stress has been employed. This scaling relation has been firstly proposed and successfully used in [32, 35, 55, 56]; it is based on the following considerations:

Experimental measures on PZT ferroelectric ceramics show that the polarization falls

under compressive stress. This polarization decrease induces variations and degradations of the piezoelectric properties (Ferroelectric-ferroelastic domain rearrangement is one reason). In the experimental part of this thesis, we have noticed that electric field excitations induce ΔP variations independents of the polarization sign. By opposition, mechanical stress induces ΔP variations opposed to the polarization sign. For physical symmetry reasons mechanical stress T can be introduced in the model as an equivalent electric field ($F = \text{applied force} = E = h(P) \cdot T$). Where $h(P)$ is a specific function which allows to translate the symmetry described above. $h(P)$ must be an odd function, $H(P) = \alpha P$ can be used, α value is fitting on experimental measures [32]. The dielectric dynamic model $P(E)$ exposed in Chapter 2 gives good results whatever the excitation waveform, it will constitute the basic model of more general ones, including mechanical stress excitation. In the final version of the model the product polarization field, mechanical stress is introduced as an equivalent electric field.

$$E_{equ} = \alpha \cdot T \cdot P$$

Here, α is a material characteristic, independent of the sample geometry and determined by comparisons between measure and simulation. This scaling relation between electric parameters and mechanical ones renders it possible to consider the ceramic behavior regardless of the nature of the excitation stress. Finally, the full model including electrical, mechanical stress and dynamic consideration is given by the following system:

$$\begin{aligned}
 & \text{if } : E(t) + \alpha \cdot T(t) \cdot P(t) \geq f^{-1}(P_i(t)) + E_{ci} + \rho_1 \cdot \frac{d^n P_i(t)}{dt^\alpha} \\
 & \rho_1 \cdot \frac{d^\alpha P_i(t)}{dt^n} + f^{-1}(P) = (E(t) + \alpha \cdot T(t) \cdot P(t)) - E_{ci} \\
 & \text{if } : E(t) \leq f^{-1}(P_i(t)) - E_{ci} - \rho_1 \cdot \frac{d^n P_i(t)}{dt^\alpha} \\
 & \rho_1 \cdot \frac{d^n P_i(t)}{dt^n} + f^{-1}(P) = (E(t) + \alpha \cdot T(t) \cdot P(t)) + E_{ci} \\
 & \text{if } : f^{-1}(P_i(t)) - E_{ci} - \rho_1 \cdot \frac{d^n P_i(t)}{dt^n} < E(t) < f^{-1}(P_i(t)) + E_{ci} + \rho_1 \cdot \frac{d^n P_i(t)}{dt^n} \\
 & P_i(t + dt) = P_i(t) \\
 & \sum_{i=1}^k \text{Spectrum}(i) \cdot P_i = P
 \end{aligned} \tag{4.1}$$

Finally, this general model can be employed under electric field $P(E)$ ($E = 0$), mechanical stress $P(T)$ ($T = 0$) or both external excitation $P(E, T)$.

4.2.2 Experimental results and analysis

The experiment has been carried out at high intensity of mechanical stress, up to 170 MPa, on a piezoceramic bulk of $\phi 6.3 \times 10$ mm of P188. The preload static stress has been set to 60 Mpa, at such level of mechanical stress, first nonlinear behaviours can be

observed. A precise description of the experimental bench has been done in the second chapter of this thesis. The hysteresis model parameters have been set under electric field external conditions and to get good simulation results α value is $0.02 \text{ C}^{-2}\text{m}^4$. Fig. 4.1 and 3.13 give an illustration of the importance of the order of the fractional operator by comparing measure and simulations for two different orders.

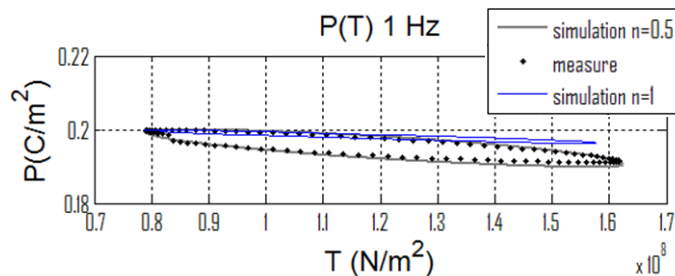


Figure 4.1: Comparisons between measurement and simulation for 1 Hz under the sum of a constant mechanical static stress and a sinus dynamical mechanical stress.

As it is the case under electric field excitation, comparisons simulation/measures under mechanical stress confirm that lower than 1 Hz, the static contribution plays a major role in the polarization state. At higher frequency ($f \gg 10 \text{ mHz}$) again in respect with the behaviour under electric field, compared with the conventional integer derivative ($n = 1$), the fractional one ($n = 0.5$) gives much more precise description of the dynamic behaviour. The integer value can only be used on a restrain frequency bandwidth or for the low frequency where the dynamic influence is weak.

The piezoceramic behavior under mechanical stress excitation of different intensity level has also been studied. Comparison measure/simulation for mechanical stress of frequency 50 mHz and 500 mHz and varying amplitude are displayed in Fig. 3.14; the simulation ($n = 0.5$) agreed well with the experiment and confirmed that the model including fractional operators worked well with the experiment regardless of the mechanical excitation property. It is particularly interesting to notice that even if simulations with different fractional orders are not displayed in the figures of the thesis, the best dynamic consideration has been obtained when n is close to 0.5. This is particularly remarkable since it led to the conclusion that dynamical phenomena through the piezoelectric materials were independent of the nature of excitation and could be modeled using the same fractional operator.

Finally, the last experimental result (Fig. 4.2) presents the variation of the hysteresis loop area versus the frequency for the measured and simulated results ($n = 1$ and $n = 0.5$). Fig. 4.2 shows loop $\langle A \rangle (freq)$ under an electric field excitation (of 2 kV/mm amplitude) and the same curves under mechanical stress excitation (of $10 \times 10^7 \text{ N/m}^2$).

Hysteresis loop areas were calculated for the high electrical field excitation (major loops) for the electrical case, and explained the large differences in absolute values of the areas between the two curves. We can observe that the loop rates of the simulation area ($n = 0.5$) related to the material dynamic were in both cases (electrical and mechanical)

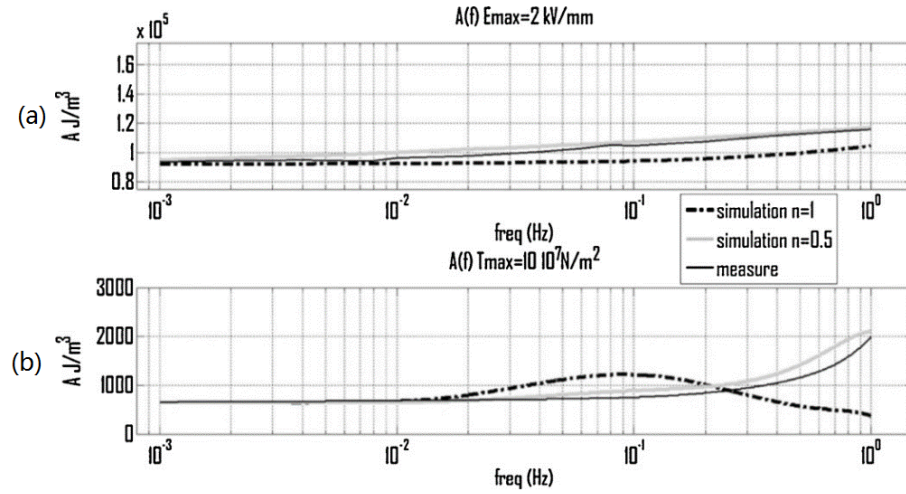


Figure 4.2: $\langle A \rangle (freq)$ curve under electric field stress (a). $\langle A \rangle (freq)$ curve under high mechanical stress (b).

very close to the experimental curve, thus confirming the above conclusions.

4.2.3 Discussion and conclusions

The objectives of the study exposed in this section were to develop a polarization model (physically linked to wall movements) able to take into account varying amplitudes and frequencies regardless of the nature of the excitation, including external mechanical stress. It has been previously demonstrated under electrical excitation that the usual considerations of dynamical variations ($\rho \cdot dP/dt$) can only be used with partial accuracy on a very narrow frequency bandwidth. The limitations of ‘viscous’ losses are however well known. The dielectric loss angle, for example, is known to vary slowly over 6–7 decades of frequency for most ferroelectric materials. [36, 44] By using the fractional derivative model, perfect fits of the loop $\langle A \rangle (freq)$ curves obtained from measurements and simulations were found on a frequency bandwidth higher than 4 decades. [36]

By modeling the dynamical variation under mechanical stress and under electrical excitation using identical fractional operators, it became possible to conclude a universality of ferroelectric dynamical behavior. It could be demonstrated that the reasonable accuracy on $P(E)$ cycles and $P(T)$ cycles could be explained with the common origin of the modeled phenomena. Actually the behavior of the domain wall was responsible for dielectric, hysteresis and nonlinear mechanical losses. A good understanding of dielectric behaviour under mechanical stress excitation gives interesting perspectives in the piezoceramic energy harvesting field. In fact, in simulation one can define the best profile of mechanical external excitation leading to an optimized efficiency of such systems.

In the energy harvesting process it is preferable to control the polarization, as a matter of fact, the polarization variation is directly linked to the amount of energy available. To obtain the best mechanical external waveforms, inverse model $T(P)$ is required. A solution

for such model is proposed in the section 4.3 of this chapter.

4.3 Inverse model $T(P)$ for dielectric polarization under mechanical stress excitation

4.3.1 Introduction and applications

The direct piezoelectric effect of a piezoceramic with consideration of its nonlinearity property at high intensity excitation has been investigated in the previous section of this chapter. The consideration of nonlinearity property enables us to precisely model the piezoceramic under various and complicated conditions. For industrial applications when a specific polarization is required, the inverse model version of the previous model needs to be developed. In this section, we mainly focus on introducing and illustrating this inverse model, $T(P)$.

In the energy harvesting domain, there are different ways to increase the conversion rates, the material properties, the mechanical structure, the excitation waveform (frequencies, amplitudes, ...). To get the best conversion properties it is clearly useful to work on simulation where optimal conditions of parameters can be obtained rapidly without long and expensive experimental tests. To maximize the simulation results it is necessary to correctly take into account the piezoelectric material properties. In the field of energy harvesting the usual solicitation has a mechanical origin (natural mechanical vibrations due to dynamic environment). An inverse model $P(T)$ is required to determinate the mechanical waveform giving the maximum conversion or to envisage in simulation the exact amount of energy harvested.

In this part, we discuss the development of a methodology for constructing a new accurate hysteresis inverse model of piezoceramics based on experimental results, for large frequency bandwidth based on fractional derivative operators and under mechanical stress.

A proposed theoretical inverse model for electric excitation has already been developed in the second chapter of this thesis, it is composed of two terms: an inverse static contribution $E_{stat}(P_{stat})$, and a time-dependent losses term, constituted of the product of a material constant, ρ , and a fractional polarization derivative term, $d^n P/dt^n$ ($n \in R$). Our model will derived from this inverse $P(E)$ model. The scaling relation $E = \alpha \cdot T \cdot P$ already used with success will be employed again to introduce the mechanical stress excitation in the model.

4.3.2 $T(P)$ inverse model

The complete mechanical inverse model including dynamic considerations is schematically displayed in Fig. 4.3.

As illustrated in this figure, two contributions are required in the $T(P)$ model. The first contribution is a frequency independent contribution derived from the quasi-static inverse

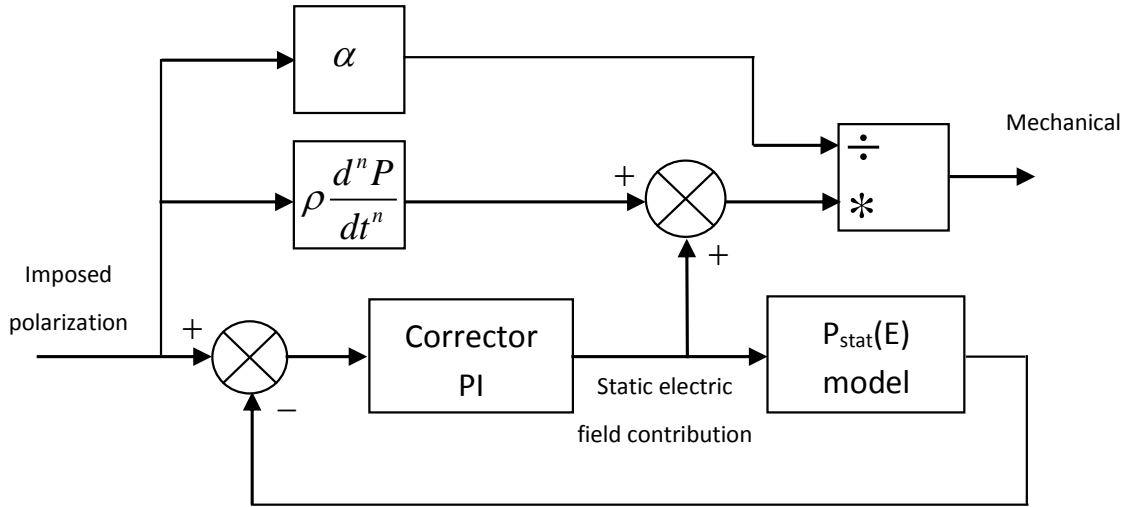


Figure 4.3: Block diagram of the inverse $T(P)$ model

model. The feedback control enables to obtain an equivalent static αTP regardless of the waveform (sinus, triangular and) of the imposed polarization. To this static contribution is added the fractional dynamic contribution, and the result is divided by αP in order to obtain the correct mechanical stress corresponding to the imposed polarization.

4.3.3 Experiment results

The parameters of the model, γ , σ and ρ have been set previously under direct mechanical and electrical conditions. Here γ is equal to 40 000, σ to 0.28 and ρ to 400 000, we are still testing P188 samples. The frequency dependence of the polarization is investigated in the frequency range from 0.1 Hz to 10 Hz. A constant amplitude polarization waveform is first imposed in order to study the frequency aspect in the inverse model. Fig. 4.4-(a) and (b) just show the case $n = 0.5$, because differences are weak between the imposed polarization for simulations with $n = 0.5$ and $n = 1$. As the frequency is going up, exceeding 1 Hz, the simulation differences begin to clearly appear.

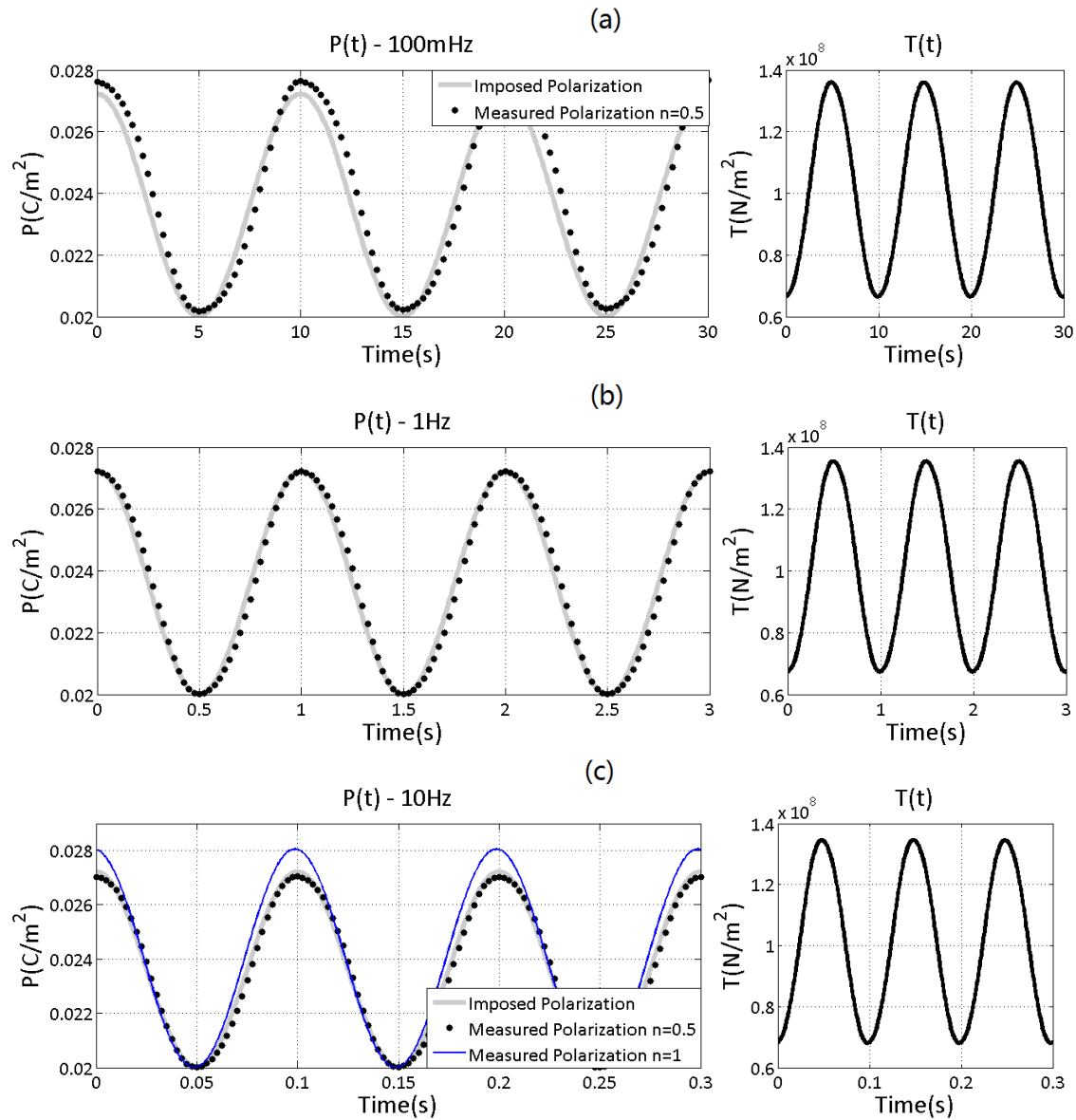


Figure 4.4: Comparisons between the imposed and the obtained polarization $P(T)$, and the corresponding mechanical excitations, $T(t)$, for increasing frequencies

From the above comparison between the experimental results and the simulations, it can be concluded that again in such external conditions the fractional derivative taken into account leads to a higher accuracy. Under high frequency conditions ($f > 10$ Hz) where dynamic behaviour comes into effect, the conventional dynamic counterpart, $\rho \cdot dP/dt$ gives an overestimation of the behaviour and the errors obtained rapidly reach values higher than 10%.

To illustrate the efficiency of the inverse model next figure exposed result obtained under non harmonics polarization conditions. The objective here is trying to obtain a triangular polarization waveform, Fig. 4.5.

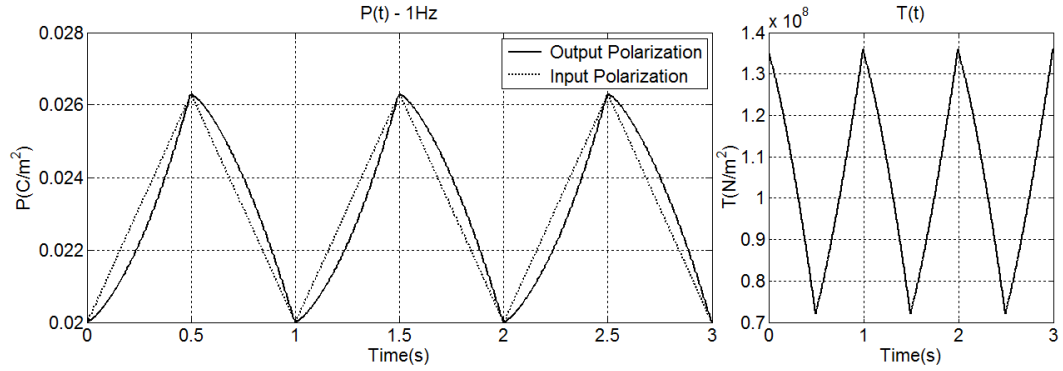


Figure 4.5: Comparisons between the imposed and the obtain Polarization $P(t)$, and the corresponding Mechanical excitations, $T(t)$, for triangular type waveform excitation.

Finally, the last set of figures (Fig. 4.6) show the polarization variations under conditions of constant excitation frequency but varying amplitudes. The idea here is to study the amplitude factor effect on the model accuracy. The frequency is set to 1 Hz and the three different maximum amplitudes imposed are 0.023, 0.025, 0.027 C/m².

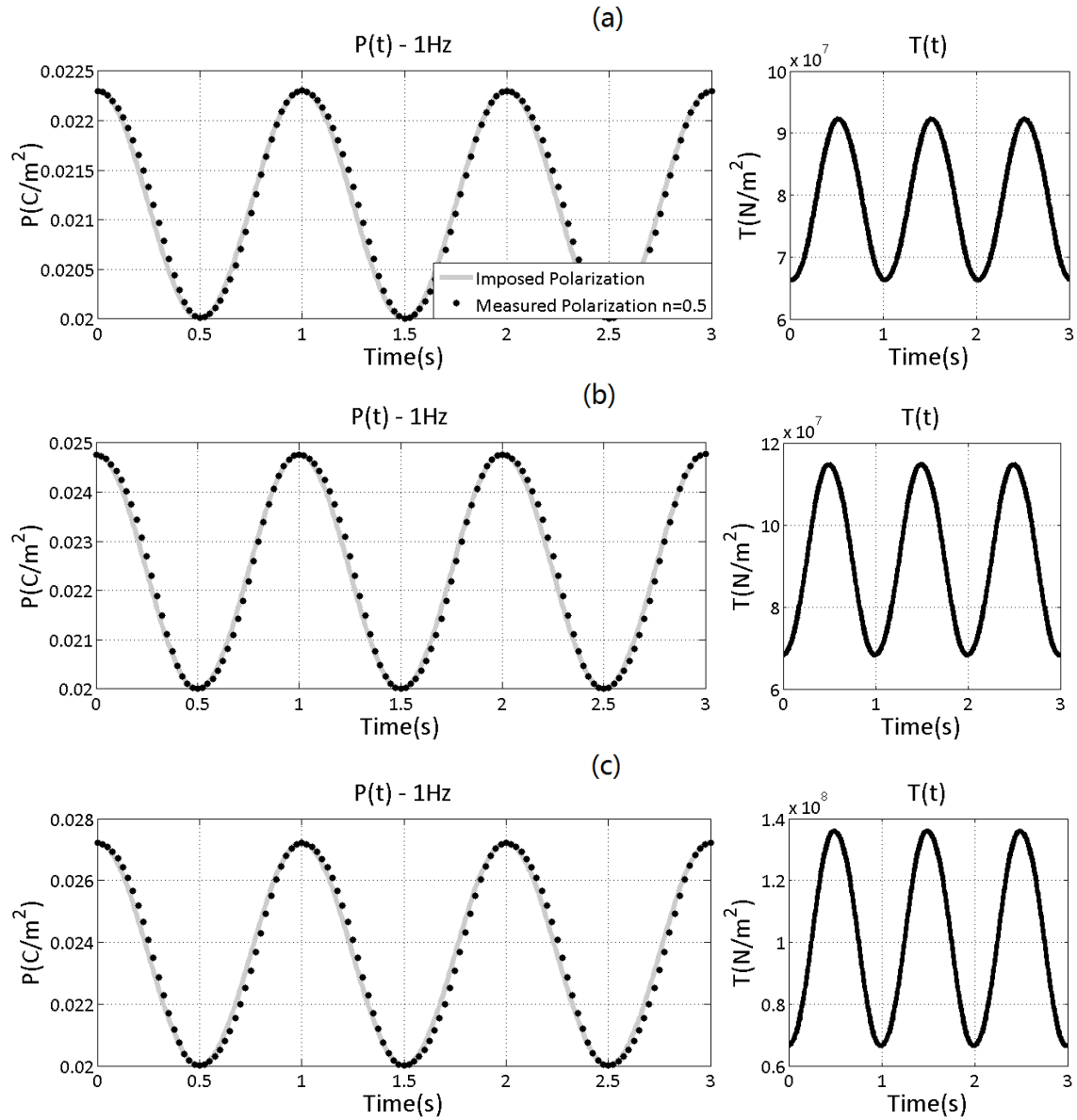


Figure 4.6: Comparisons between the imposed and the obtain polarization $P(T)$, and the corresponding mechanical excitations

After analysis of this result, we can conclude that the imposed polarization could be obtained using the inverse model regardless of its properties, such as its frequency and its amplitude. Here we get the confirmation that our model gives good results whatever the excitation conditions (electrical, mechanical or both together).

4.3.4 Conclusion and discussion

When the piezoelectric ceramic is submitted to a mechanical stress, variation of the dielectric polarization can be measured by integration of the electric current circulating through the ceramic; this information is required in various domain applications, such as energy harvesting. It helps us to determine and adjust the property of external mechanical

excitation leading to the maximum of energy harvesting efficiency. In this section an inverse model $P(T)$ has been proposed. This model is made of two contributions:

1. Quasi-static contribution, relates to the domain wall movements, exhibiting a behavior close to a mechanical dry friction.
2. Dynamic contribution, frequency dependent, constituted by the product of a constant and the fractional derivation of the polarization.

As it is already the case under electrical external conditions, the introduction of fractional derivative allows to accurately computing polarization field over more than 3 decades.

In the Section 4.4 of this chapter, we will expose a piezoceramic application where both external excitations are employed. The characterization bench and the dynamic hysteresis models previously introduced are required for such applications. It will constitute the perfect illustration for all the work already done in this thesis.

4.4 Energy harvesting based on Ericsson loop

4.4.1 Technique introduction and application

In the previous sections of this chapter, we have proposed a complete model (direct and inverse) for the evolution of a piezoceramic dielectric polarization under mechanical external excitation of varying amplitude and frequency. This model is actually an extension of the dielectric model exposed in the second chapter of this thesis. Industrial applications (sensors, actuators or energy harvester, ...) usually exhibit piezoelectric systems where both kind of external excitation are combined, in this section we will focus on such system. Indeed, in this section we will exposed a new technique based on a combination of mechanical stress and electric field leading to a magnificence of the energy harvesting system efficiency. We will define in particularly the best combination of electric field and mechanical force to apply on the piezoceramic to improve its polarization property. Using such kind of hybrid excitation will greatly increase the polarization level and consequently highly increase the rate of energy harvested compared to classical systems working under exclusive mechanical stress. [28, 29] Such systems are appropriate to the models developed in this thesis because the materials tested are highly excited and most of them reached their non-linear state. A well understanding and taken into account of the dielectric losses are of major interest here. The usage of the fractional derivative gives a correct description of the phenomena and exact rate of energy available are obtained.

4.4.2 Basic Harvesting technique

Basic harvesting technique under mechanical excitation requires switch control. The idea is to short circuit the piezoceramic as the mechanical stress is maximal. The dielectric

cycle through the tested sample follow a virtuous loop (clockwise) which area is equal to the maximum energy available. To illustrate such technique one can use piezoelectric road example, where the mechanical excitations are performed by the vehicle movements and where the tested samples are embedded through the road tar. Fig. 4.7 gives an illustration in four steps of such technique.

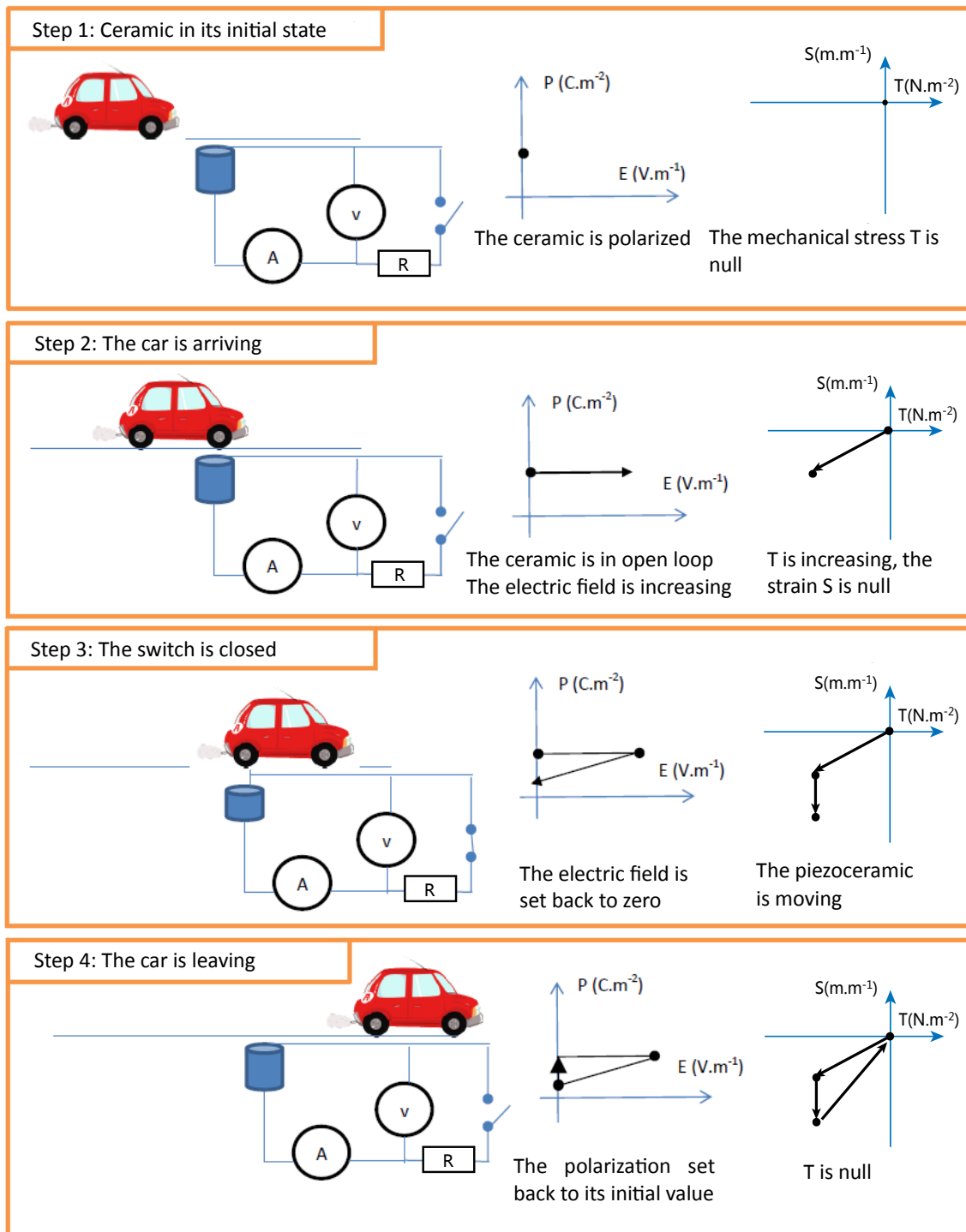


Figure 4.7: Harvesting basic technique, piezo road

4.4.3 Ericsson loops technique for the energy harvesting under synchronized electric field and mechanical stress

To improve the level of energy harvested, we proposed here a new technique coupling both external excitations, electrical and mechanical. The idea is to increase the area of the virtuous loop $P(E)$ presented in the previous sub-section, by adding synchronized with the mechanical stress an external electric field excitation.

Here, an analogy is realized between the thermodynamic well known Ericsson loops, where two transformations isobar and two transformations isotherm are realized, and our piezoceramic virtuous dielectric loop two transformations isostress and two transformation isofield are imposed. To complete our dielectric Ericsson loops, pre-polarized piezoceramic are required. The electric field and the mechanical stress are imposed respectively following the chronographs illustrated in Fig. 4.8. In the first step of the loop, the mechanical stress is null, the electric field is increasing until reach its maximum value. This maximum external electrical field excitation is maintained constant during all the second step, the mechanical is increasing. As the maximum mechanical stress is reached can start the third step, the mechanical stress remains to its maximum value and the electrical field is decreasing. The last step starts when the electrical field value is close to zero. This step corresponds to the decreasing of the mechanical stress. When the mechanical stress excitation has totally disappeared can start a new cycle.

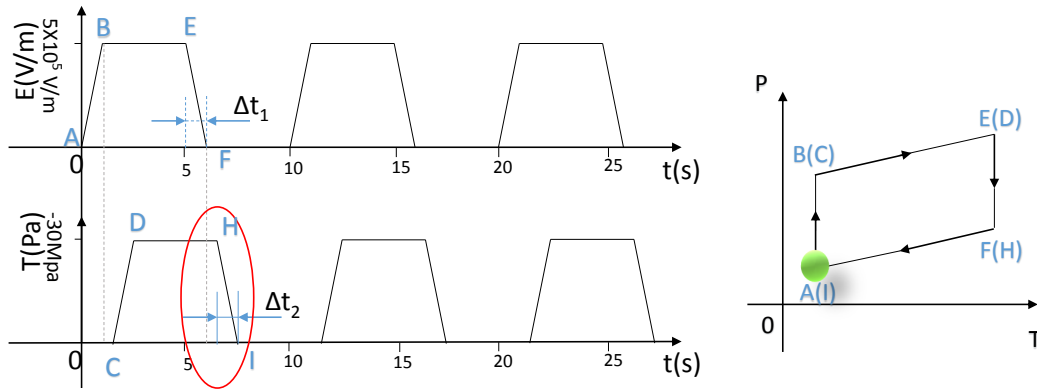


Figure 4.8: Temporal variations of the electric and mechanical excitations.

4.4.4 Simulation and experimental results

Fig. 4.9 presents first simulation/measurement comparison for dielectric Ericsson loops $P(E)$. The excitation conditions involved: an electric field of amplitude $3 \times 10^5 \text{ V/m}$, a frequency of 0.1Hz, and a mechanical stress of amplitude of 50Mpa.

This figure has been displayed in order to validate the good temporal correlation between the simulated and the measured Ericsson loops under high-amplitude excitations. In the remaining part of the result section, we focus on the evolution of the loop area versus the different manipulation parameters; we particularly insist on demonstrating that

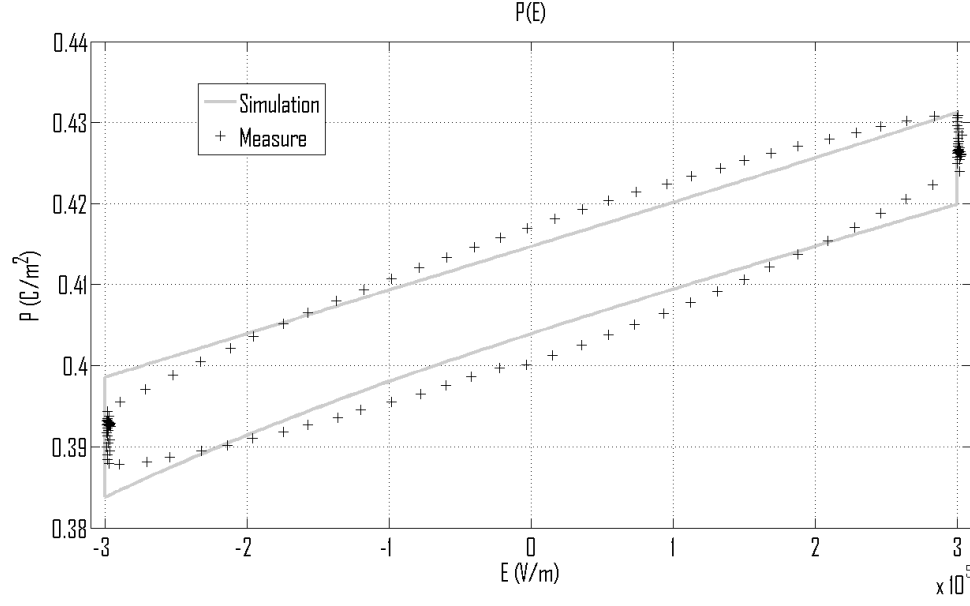


Figure 4.9: Temporal variations of the electric and mechanical excitations.

our model provides good results regardless of the factor considered. For instance, Fig. 4.10 illustrates a comparison between simulations ($n = 0.5$ and $n = 1$) and measurements of the loop area $\langle A \rangle$ as a function of the frequency of the electric field. The other factors were maintained constant (electric field amplitude: $3 \times 10^5 \text{ V/m}$, mechanical stress amplitude: 10 Mpa , mechanical Stress frequency: 0.1 Hz).

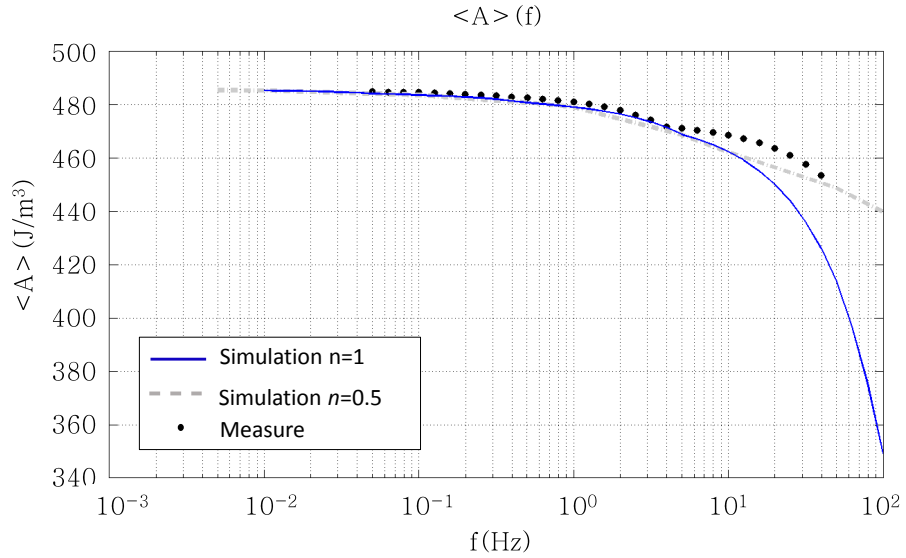


Figure 4.10: Comparison between simulations and measurements for Ericsson loops as a function of the frequency of the electric field.

The differences in accuracy between the fractional dimensions are particularly well illustrated in Figure 4.10. In fact, we can notice that for a fractional coefficient equal to 0.5, the rate of the loop area as the frequency increased remained very close to its

experimental counterpart, while the one of the integer derivation diverged.

Fig. 4.11 displays a comparison between simulations ($n = 0.5$) and measurements of the loop area $\langle A \rangle$ as a function of the frequency of the mechanical stress, while the other factors were maintained constant (electric field amplitude: $5 \times 10^5 \text{ V/m}$, electric field frequency: 0.1 Hz, mechanical stress amplitude: 10 Mpa).

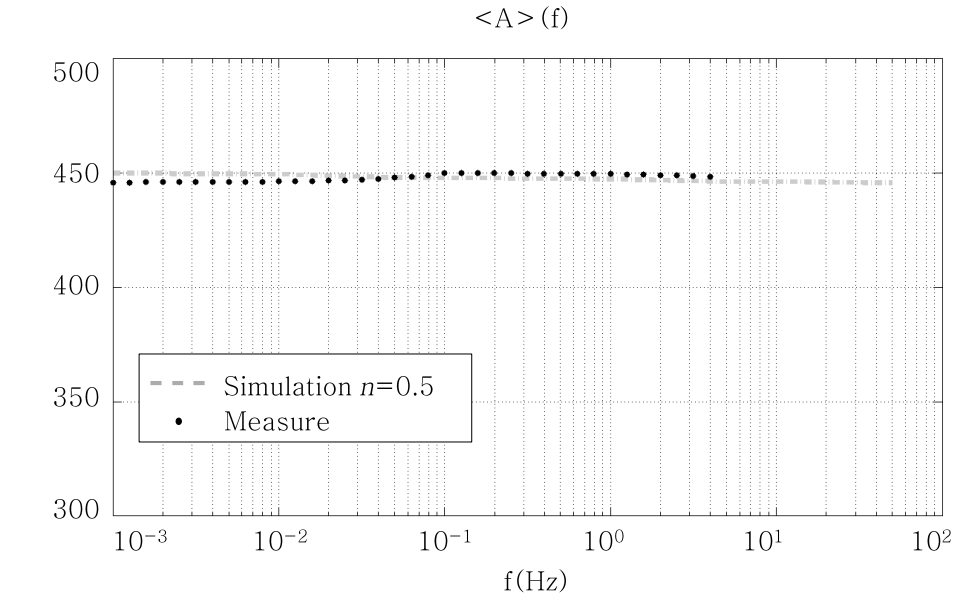


Figure 4.11: Comparison between simulations and measurements for Ericsson loops as a function of the frequency of the mechanical stress.

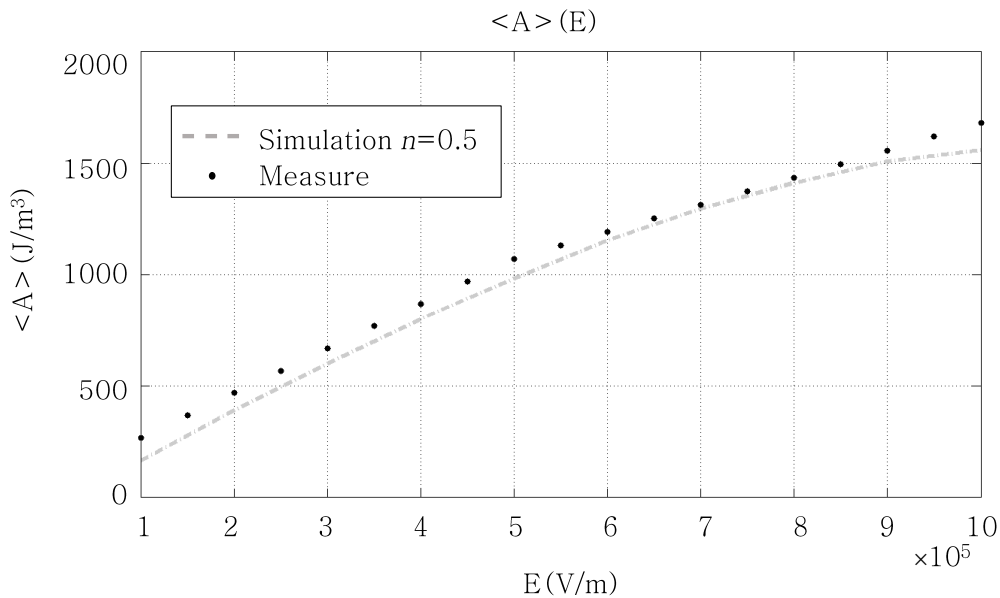


Figure 4.12: Comparison between simulations and measurements for Ericsson loops as a function of the amplitude of the electric field.

Figure 4.12 portrays a comparison between simulations ($n = 0.5$) and measurements

of the loop area $\langle A \rangle$ as a function of the amplitude of the electric field, while the other factors were maintained constant (electric field frequency: 0.1Hz, mechanical stress frequency: 0.1Hz, mechanical stress amplitude: 10Mpa).

Fig. 4.13 displays a comparison between simulations ($n = 0.5$) and measurements of the loop area $\langle A \rangle$ as a function of the amplitude of the mechanical stress, while the other factors were kept constant (electric field frequency: 0.1Hz, electric field amplitude: $3 \times 10^5 \text{V/m}$, mechanical stress frequency: 0.1Hz). Fig. 4.11, Fig. 4.12 and Fig. 4.13 indicate that the Ericsson loop was accurately taken into account by the model.

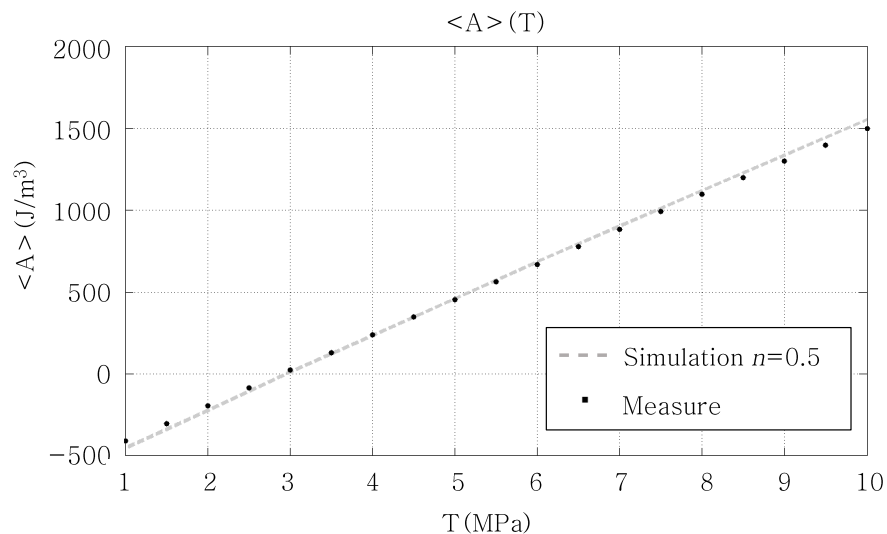


Figure 4.13: Comparison between simulations and measurements for Ericsson loops as a function of the amplitude of the mechanical stress.

The last set of results, displayed in Fig. 4.14, shows the variations in the amount of harvested energy. These 3D plots illustrate how the efficiency of the Ericsson loop is affected by the frequency of the excitation sources. We can observe here that the global surface of the 3D plots slowly shifts downwards, as the frequency was increased. This movement is directly linked to the fractional coefficient n of our model. In the future, we can imagine that this experimental result characteristic can be used as experimental proof to identify the fractional coefficient.

4.4.5 Discussion and conclusion

Mechanical vibrations are naturally accessible everywhere as an unlimited energy resource. The possibility of recycling this ambient energy and creating electrical generators with an unlimited lifetime is of major interest. By coupling the electric field and the mechanical excitation on Ericsson-based cycles, the amplitude of the harvested energy can be highly increased; this multiplication coefficient can reach a maximum value close to 100. However, this implies high electrical field levels, which induce non-linearity in the tested sample.

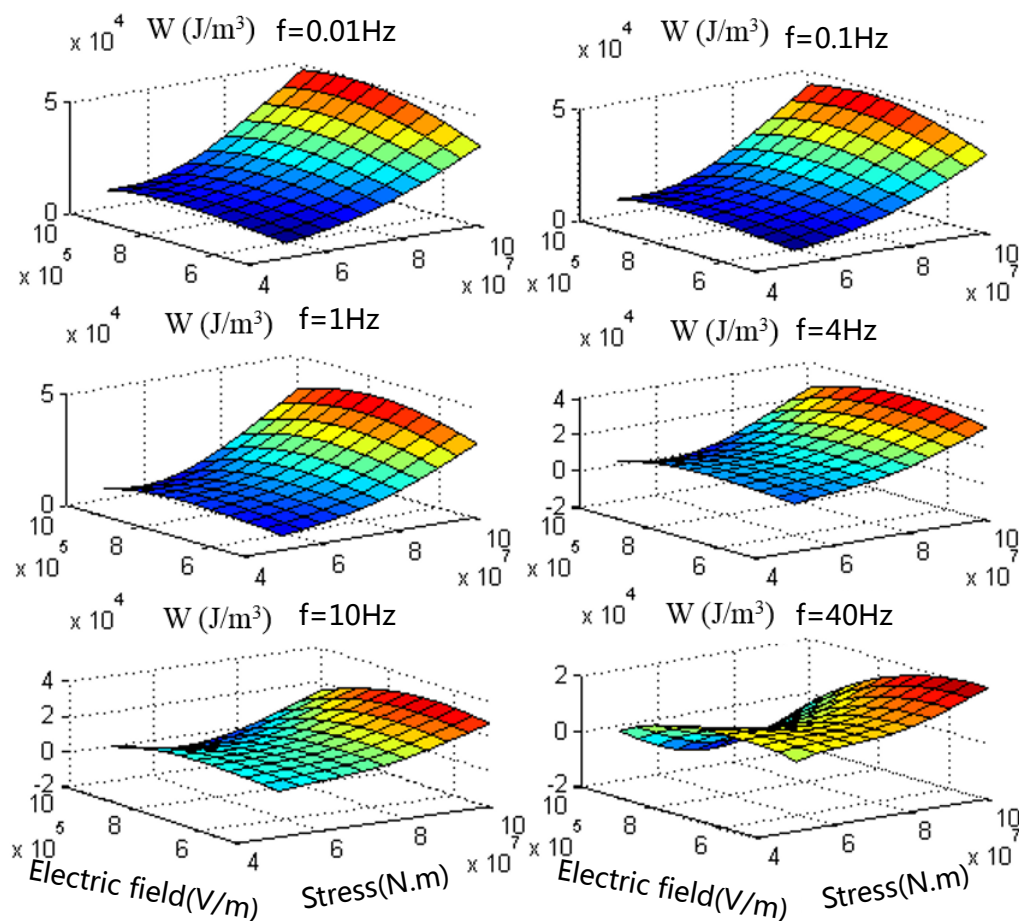


Figure 4.14: Energy variation of Ericsson loops versus mechanical stress and electric field excitation.

The present thesis describes how obtaining the adequate dynamic comparisons and simulation results when modeling the Ericsson loops with a dynamic model in which a fractional term for the dynamic part was taken into account. This model is particularly interesting since it constitutes a new tool to accurately define a correct estimation of the energy harvested by the Ericsson technique. However, the estimation is unfortunately lower than the optimistic evaluation previously described, mainly due to the dielectric losses through the active material.

The fractional derivation taken into account provides good results on a large frequency bandwidth, which is not the case with the usual integer derivation. This is particularly interesting in the case of the Ericsson technique since ambient energy is generally available as white noise, which is consistent with a large frequency distribution. [61, 62] We can imagine that in the future, this study and the fractional model will be extended and tested on other non-linear harvesting energy techniques, such as the SSD (single switch damping) method. Here again, active materials are usually highly excited which signifies a non-linearity in the system and a reduction of the amount of harvested energy.

4.5 Conclusion

A series of experiments have been carried out on the piezoceramic with mechanical excitation and hybrid of mechanical & electrical excitation. In the opening stage, mechanical drive was first introduced. This development in modeling piezoceramic introduces dynamic excitation description with high accuracy into quasi-static model. Unlike the usual impression about the quasi-static hysteretic phenomenon as a hysteresis loop, nonlinearity plays an important role and varies when the excitation condition changes, while the present model taking frequency factor into account makes it much more applicable in industrial. The nonlinearity phenomena of piezoceramic mainly dues to the wall movement. The nonlinearity of piezoelectric properties depend on the excitation condition. The hysteretic property differs on time domain in an unproportionate manner depending on the frequency change and amplitude variation. In a wide bandwidth excitation range, the dynamic counterpart using fractional derivative is applicable to the total polarization. It enlarges the model usage especially in an inconstant stimulation system. It precisely constitutes a connection between the mechanical stimulation and induced electrical outcome. Then a converse relation of this model was developed. The inverse model is especially useful in control system by use of mechanical stimulation. It controls the polarization or gets a specified one by altering the force. The combination of these two direct/inverse model is promisingly used in high power actuator and high sensitive piezoelectric sensor systems, where precision positioning and accuracy are required. The Ericsson loop energy harvesting method gives an instruction for energy harvesting. It highly increases the electromechanical conversion efficiency by combination of mechanical and electrical stimulation. The coordinated mechanical and electrical field stimulation works in turn. By correctly coupling of the coefficient nonlinearities of the piezoceramic, a high electromechanical conversion efficiency could be got and its application in transducer and energy harvester is promising. The present work used high external electric field is supplied by high-voltage amplifier.

Conclusions and perspectives

In this thesis, various aspects of Ferro-electricity have been approached; we have in particular focused our work on trying to describe and illustrate a dielectric polarization hysteresis model $P(E, T)$ accurate and employable on varying excitation (type, amplitude, frequency). We have checked and confirmed that fractional operators are particularly well adapted to model dielectric losses of piezoceramics. Comparisons model/simulation have demonstrated that usual operators (first order, constitute by entire derivatives) are always limited to a relatively weak frequency bandwidth. The approach based on fractional derivatives gives good simulation results even beyond the working frequency of classical piezoceramic systems. The model firstly developed to describe dielectric hysteresis behaviour under electric field has been extended and validated with success under mechanical excitation. Dedicated measuring bench has been developed during this PHD to validate such model. The frequency dependence of piezoceramic under mechanical stress has been relatively weakly studied, and the main reason is the difficulty to develop an accurate experimental bench leading to ceramic behaviour under extreme external conditions (high mechanical stress, high frequency). Another interesting feature of the measuring bench developed here, is its capability to operate under reverse condition, such as under imposed polarization. Here, the imposed mechanical stress waveform is calculated in simulation, and is used as excitation of the measuring bench. The major achievement of this thesis has been the development and the validation of the piezoceramic energy harvesting Ericsson loop technique. This technique gives promising perspectives, indeed it allows in special conditions to highly increase the amount of energy harvested. This technique has required also the development of dedicated measuring bench, able to impose synchronously high mechanical stress and high electric field. The development, the validation and the using of such measuring bench have constituted another important achievement of this PHD. To understand and to determine the real potential of Ericsson loop technique, we have needed a very accurate model able to correctly take into account the frequency dependence of piezoceramics. This is exactly the characteristics property of the fractional model previously introduced. Ericsson loop technique provides a perfect illustration of the utility of such model. The validation of the viability of Ericsson technique is very encouraging; it offers new perspective in the field of piezo energy harvesting systems. Finally, the good results obtained on comparison simulations/measures are really positive, and in the future it will be interesting to export all this fractional models and try their capabilities on

different materials or compositions such as PZT thin layers or matrix polymers. Indeed, due to the sample geometries of such materials the excitation levels are always extreme and lead usually to nonlinear behaviour. This relatively new materials are mainly used as sensors or for micro-positioning operation. In such circumstances, it is necessary to perfectly manage the physical behaviour of the sample in order to transmit the correct information. In the same way, based on these thesis experimental results, we can imagine the development of new innovating measuring benches, dedicated to characterized these new compositions and materials and provide experimental information necessary to new model validation.

Bibliography

- [1] E. Häslér, L. Stein, and G. Harbauer. Implantable physiological power supply with pvdf film. *Ferroelectrics*, 60(1):277–282, 1984.
- [2] J. F. Antaki, G. E. Bertocci, E. C. Green, A. Nadeem, T. Rintoul, R. L. Kormos, and B. P. Griffith. A gait-powered autologous battery charging system for artificial organs. *ASAIO journal*, 41(3):M588–M595, 1995.
- [3] FUJITSU SEMICONDUCTOR LIMITED. *FRAM Guide Book*, 6th edition, September 2010.
- [4] S. Qin and R. C. Wang. Geometric descriptions of distorted structures of abx3 type perovskite and application in structural prediction. *Acta Geologica Sinica*, 78(3):345–351, 6 2004.
- [5] C. M. Lu, M.X. Sun, Q. C. and Xu, and Y. F. Luo. Study on properties of pm-szt piezoelectric ceramics. *JOURNAL OF MATERIALS ENGINEERING*, 12:48–52, 2005.
- [6] Z. P. Wang and G. X. Li. Research situation on piezocrystal non-lead ceramics material. *INNER MONGULIA PETROCHEMICAL INDUSTRY*, 34(22):8–9, 2008.
- [7] D. L. Rousseau, RPSPS. P. Bauman, and SPS. Porto. Normal mode determination in crystals. *Journal of Raman Spectroscopy*, 10(1):253–290, 1981.
- [8] E. Defay, editor. *Integration of Ferroelectric and Piezoelectric Thin Films: Concepts and Applications for Microsystems*. Wiley-ISTE, March 21, 2011.
- [9] NEC-TOKIN. *Piezoelectric Ceramic*, vol.05 edition, 10 2013.
- [10] Meggitt Sensing Systems. *Material data for Ferroperm Piezoceramics (based on typical values)*, April 2011.
- [11] T. Ikeda. *Fundamentals of Piezoelectricity*. Oxford University Press, USA, July 19, 1990.
- [12] Ferroperm Piezoceramics A/S. *High Quality Component and Materials for the Electronic Industry*, May 2003.
- [13] Ieee standard on piezoelectricity. *ANSI/IEEE Std 176-1987*, 1988.
- [14] E. V. Kozyrev. Standing-wave structures. *Frontiers of Accelerator technology*, page 339, 1999.
- [15] G. SEBALD. *Nouveaux monocristaux à forte conversion piézoélectrique: croissance, modélisation et caractérisation*. PhD thesis, INSA Lyon, 2004.

- [16] H. J. Kim, K. Koo, S. Q. Lee, K.H. Park, and J. Kim. High performance piezoelectric microspeakers and thin speaker array system. *ETRI journal*, 31(6), 2009.
- [17] Y. Perriard and J. Fernandez Lopez. Modeling and optimization of ultrasonic linear motors. 2006.
- [18] D. A. Hall, M. Cain, and M. Stewart. Ferroelectric hysteresis measurement & analysis. In *Minutes of the NPL CAM7 IAG Meeting*, 1998.
- [19] Ieee standard definitions of primary ferroelectric terms. *ANSI/IEEE Std 180-1986*, 1986.
- [20] R. B. Mrad and H. Hu. Dynamic modeling of hysteresis in piezoceramics. In *Advanced Intelligent Mechatronics, 2001. Proceedings. 2001 IEEE/ASME International Conference on*, volume 1, pages 510–515. IEEE, 2001.
- [21] E. Boucher. *Elaboration et caractérisation de céramiques PZT bi-substituées et modélisation non-linéaire de leur comportement en contrainte et en champ électrique*. PhD thesis, INSA Lyon, 2002.
- [22] J. A. Paradiso and T. Starner. Energy scavenging for mobile and wireless electronics. *Pervasive Computing, IEEE*, 4(1):18–27, 2005.
- [23] M. Lallart. *Amélioration de la conversion électroactive de matériaux piézoélectriques et pyroélectriques pour le contrôle vibratoire et la récupération d'énergie-Application au contrôle de santé structurale auto-alimenté*. PhD thesis, INSA Lyon, 2008.
- [24] S. Chalasani and J. M. Conrad. A survey of energy harvesting sources for embedded systems. In *Southeastcon, 2008. IEEE*, pages 442–447. IEEE, 2008.
- [25] Thorlabs. Source of vibration, 6 2014.
- [26] D. A. Hall. Review nonlinearity in piezoelectric ceramics. *Journal of materials science*, 36(19):4575–4601, 2001.
- [27] B. Ducharne, B. Zhang, D. Guyomar, and G. Sebald. Fractional derivative operators for modeling piezoceramic polarization behaviors under dynamic mechanical stress excitation. *Sensors and Actuators A: Physical*, 189:74–79, 2013.
- [28] B. Zhang, B. Ducharne, D. Guyomar, and G. Sebald. Energy harvesting based on piezoelectric ericsson cycles in a piezoceramic material. *The European Physical Journal Special Topics*, 222(7):1733–1743, 2013.
- [29] B. Zhang, B. Ducharne, and D. Guyomar. Inverse model of the piezoelectric ceramic polarization under wide bandwidth mechanical excitations with fractional derivative consideration. *Optical and Quantum Electronics*, 46(1):103–110, 2014.
- [30] R. C. Smith and C. L. Hom. Domain wall theory for ferroelectric hysteresis. *Journal of Intelligent Material Systems and Structures*, 10(3):195–213, 1999.
- [31] N. Aurelle, D. Guyomar, C. Richard, P. Gonnard, and L. Eyraud. Nonlinear behavior of an ultrasonic transducer. *Ultrasonics*, 34(2):187–191, 1996.
- [32] G. Sebald, E. Boucher, and D. Guyomar. A model based on dry friction for modeling hysteresis in ferroelectric materials. *Journal of applied physics*, 96(5):2785–2791, 2004.

-
- [33] R. C. Miller and A. Savage. Motion of 180 domain walls in metal electroded barium titanate crystals as a function of electric field and sample thickness. *Journal of Applied Physics*, 31(4):662–669, 1960.
 - [34] R. C. Smith and Z. Ounaies. A domain wall model for hysteresis in piezoelectric materials. *Journal of Intelligent Material Systems and Structures*, 11(1):62–79, 2000.
 - [35] D. Guyomar, B. Ducharne, and G. Sébald. Time fractional derivatives for voltage creep in ferroelectric materials: theory and experiment. *Journal of Physics D: Applied Physics*, 41(12):125410, 2008.
 - [36] D. Guyomar, B. Ducharne, G. Sebald, and D. Audiger. Fractional derivative operators for modeling the dynamic polarization behavior as a function of frequency and electric field amplitude. *Ultrasonics, Ferroelectrics and Frequency Control, IEEE Transactions on*, 56(3):437–443, 2009.
 - [37] M. Ismail, F. Ikhouane, and J. Rodellar. The hysteresis bouc-wen model, a survey. *Archives of Computational Methods in Engineering*, 16(2):161–188, 2009.
 - [38] D. C. Jiles and D. L. Atherton. Theory of ferromagnetic hysteresis. *Journal of magnetism and magnetic materials*, 61(1):48–60, 1986.
 - [39] M. Kuczmann. Dynamic preisach hysteresis model. *Journal of advanced research in physics*, 1(1), 2010.
 - [40] Z. Q. Chen, C. Guo, J. X. Zhao, and Z. Z. Yuan. Modeling and control of hysteretic systems based on preisach model. *CONTROL ENGINEERING OF CHINA*, 13(4):304–306, 2006.
 - [41] X. J. Dang and Y. H. Tan. Study on similar diagonal dynamic neural network hysteresis model for piezoceramic actuator based on preisach model. *CHINESE JOURNAL OF MECHANICAL ENGINEERING*, 41:7–12, 2005.
 - [42] L. Cima and E. Laboure. Experimental preisach density used for characterization and modelling of ferroelectric active sensor integrating temperature and aging dependence. In *Proceedings-IEEE International Symposium on Applications of Ferroelectrics*, pages 223–226, 2002.
 - [43] Y. Bernard, E. Mendes, and Z. Ren. Determination of the distribution function of preisach’s model using centred cycles. *COMPEL: The International Journal for Computation and Mathematics in Electrical and Electronic Engineering*, 19(4):997–1006, 2000.
 - [44] D. Guyomar, B. Ducharne, and G. Sebald. Dynamical hysteresis model of ferroelectric ceramics under electric field using fractional derivatives. *Journal of Physics D: Applied Physics*, 40(19):6048, 2007.
 - [45] D. Guyomar, B. Ducharne, and G. Sebald. The use of fractional derivation in modeling ferroelectric dynamic hysteresis behavior over large frequency bandwidth. *Journal of Applied Physics*, 107(11):114108–114108, 2010.
 - [46] B. Ducharne, B. Zhang, G. Sebald, and D. Guyomar. Fractional operator for hysteresis and complexe dielectric permittivity. In *Proc. 2014 IEEE 23rd international Symposium on Applications of Ferroelectrics (ISAF)*, 2014.
-

- [47] K. S. Cole and R. H. Cole. Dispersion and absorption in dielectrics i. alternating current characteristics. *The Journal of Chemical Physics*, 9(4):341–351, 1941.
- [48] K. S. Cole and R. H. Cole. Dispersion and absorption in dielectrics ii. direct current characteristics. *The Journal of Chemical Physics*, 10(2):98–105, 1942.
- [49] C. J. Lin and S. R. Yang. Precise positioning of piezo-actuated stages using hysteresis-observer based control. *Mechatronics*, 16(7):417–426, 2006.
- [50] G. Song, J. Zhao, X. Zhou, and J. A. De Abreu-García. Tracking control of a piezo-ceramic actuator with hysteresis compensation using inverse preisach model. *Mechatronics, IEEE/ASME Transactions on*, 10(2):198–209, 2005.
- [51] M. L. Trawick, M. Megens, D. E. Angelescu, C. Harrison, D. A. Vega, P. M. Chaikin, R. A. Register, and D. H. Adamson. Correction for piezoelectric creep in scanning probe microscopy images using polynomial mapping. *Scanning*, 25(1):25–33, 2003.
- [52] H. Kaizuka. Application of capacitor insertion method to scanning tunneling microscopes. *Review of Scientific Instruments*, 60(10):3119–3122, 1989.
- [53] D. Croft, G. Shed, and S. Devasia. Creep, hysteresis, and vibration compensation for piezoactuators: atomic force microscopy application. *Journal of Dynamic Systems, Measurement, and Control(Transactions of the ASME)*, 123(1):35–43, 2001.
- [54] R. C. Smith, M. V. Salapaka, A. Hatch, J. Smith, and T. De. Model development and inverse compensator design for high speed nanopositioning. *Proceedings of the 41st IEEE Conference on Decision and Control 2002*, (December):3652–3657, 2002.
- [55] D. Guyomar, B. Ducharne, and G. Sebald. High frequency bandwidth polarization and strain control using a fractional derivative inverse model. *Smart Materials and Structures*, 19(4):045010, 2010.
- [56] D. Guyomar, A. Hajjaji, G. Sebald, and K. Yuse. Stress/electrical scaling in ferroelectrics. *Journal of Applied Physics*, 105(12):124103–124103, 2009.
- [57] D. A. Hall and P. J. Stevenson. High field dielectric behaviour of ferroelectric ceramics. *Ferroelectrics*, 228(1):139–158, 1999.
- [58] *Piezoelectric Ceramics: Principles and Applications*. APC International, Ltd., December 2011.
- [59] FUJI Ceramics corporation. *Piezoelectric Ceramics*.
- [60] K. Kuhnen. Modeling, identification and compensation of complex hysteretic nonlinearities: A modified prandtl-ishlinskii approach. *European Journal of Control*, 9(4):407–418, 2003.
- [61] F. Cottone, H. Vocca, and L. Gammaitoni. Nonlinear energy harvesting. *Physical Review Letters*, 102(8):080601, 2009.
- [62] G. Litak, M. I. Friswell, and S. Adhikari. Magnetopiezoelectric energy harvesting driven by random excitations. *Applied Physics Letters*, 96(21):214103–214103, 2010.

List of Figures

1.1	illustration of the piezoelectric effect.	2
1.2	(a). ABO_3 crystal structure [3] (b). $CaTiO_3$ structure. [4]	3
1.3	$PZT(Pb(Zr,Ti)O_3)$ crystal structure [3]	4
1.4	the 32 crystal classes denominations [8]	5
1.5	Crystal grain with respect to electric field [9]	6
1.6	Relations of mechanical, electric and thermal properties in a crystal [11] . .	8
1.7	Coordinate system in the piezoceramic analysis [12]	9
1.8	Equivalent electrical circuit of a piezoceramic.	12
1.9	Illustration of different electric element polarization under electric field . . .	15
1.10	P-E hysteresis loop for a ferroelectric piezoceramic [18]	15
1.11	Development of disk capacity, CPU speed, available RAM, wireless transfer speed, battery energy density from 1990 to 2002 [22]	17
1.12	Progress of some chips' energy consumption standard [23]	18
1.13	The Camel Fridge project to deliver medicines to the remote villages in Africa (Photo from http://inhabitat.com/)	18
1.14	Common vibration in a laboratory, [25]	20
2.1	$S(E)$ curve of a piezoceramic. [26]	24
2.2	Illustration of the quasi-static analog mechanical dry friction.	27
2.3	Illustration of the anhysteretic curve translation.	28
2.4	Translation of the E_{cn} value of the anshyeretic curve corresponding to dif- ferent ferroelectric domains.	30
2.5	Translation of the anhysteretic curve.	30
2.6	(a) First polarization curve (Black), perfect dielectric curve (Grey), for a P188 sample, (b) Distribution (Spectrum) of elementary loops.	31
2.7	(a).Comparison measure/simulation for quasi-static hysteresis loop. (b). Comparison simulation/measure at 2mHz for reversal curves.	32
2.8	Algorithm of the quasi-static direct P(E) model.	33
2.9	Hysteresis operator $\gamma_{\alpha\beta}[u(t)]$	34
2.10	Comparison measure/simulation for hysteresis loop area (frequency)	35
2.11	Gamma function in real axis	37
2.12	Constant Phase Element in the analogy electrical circuit [36]	38
2.13	Comparison measure/simulation for hysteresis loop area as the frequency is increasing.	39
2.14	Comparison measure/simulation for hysteresis loop area as the frequency is increasing.	40
2.15	Hysteresis loop area versus the frequency $A_{<f>}$	41

2.16	(a) A comparison of measured data/simulation on a quasi-static major hysteresis loop, using the quasi-static inverse model 1.(b) The associated electric field.	43
2.17	$E_{static}(P)$ inverse model	43
2.18	Inverse model $T(P)$	45
3.1	Illustration of the procedure for the conditionings of the piezoceramic samples.	49
3.2	Polarizing bench under high voltage electric field.	50
3.3	Schematic diagram of capacitive displacement sensor and polarization current amplifier used to measure the electromechanical activities and dielectric polarization of a piezoceramic.	52
3.4	Photo of capacitive displacement sensor and polarization current amplifier used to measure the electromechanical activities and dielectric polarization of a piezoceramic.	54
3.5	Schematic diagram measure of electric polarization behavior under mechanical excitation of a piezoceramic.	55
3.6	Photo of the measure of electric polarization behavior under mechanical excitation of a piezoceramic.	56
3.7	Schematic diagram of hybrid measuring bench, simultaneous control of the external electrical and mechanical excitation.	57
3.8	Photo of hybrid measuring bench, simultaneous control of the external electrical and mechanical excitation.	58
3.9	Temporal variation of electrical and mechanical excitation in order to reproduce Ericsson-based cycles conditions.	58
3.10	Comparison measure/simulation, for 3 decades of frequency on P188 piezoceramic	59
3.11	Comparison measure/simulation, for 3 decades of frequency on PZT 5A piezoceramic	60
3.12	Comparison measure/simulation, for 3 decades of frequency on C2 piezoceramic	61
3.13	Comparisons between measurements and simulations for $0.02 < f < 1$ Hz under the sum of a constant mechanical static stress and a sinus dynamical mechanical stress of constant maximum value.	61
3.14	Comparisons between measurements and simulations for $f = 50$ mHz and $f = 500$ mHz under a constant mechanical static stress for 3 maximum dynamical mechanical stress values.	63
3.15	Comparison between simulations and measurements for Ericsson loops.	63
4.1	Comparisons between measurement and simulation for 1 Hz under the sum of a constant mechanical static stress and a sinus dynamical mechanical stress.	68
4.2	$\langle A \rangle (freq)$ curve under electric field stress (b). $\langle A \rangle (freq)$ curve under high mechanical stress.	69
4.3	Block diagram of the inverse T(P) model	71
4.4	Comparisons between the imposed and the obtained polarization $P(T)$, and the corresponding mechanical excitations, $T(t)$, for increasing frequencies	72
4.5	Comparisons between the imposed and the obtain Polarization $P(t)$, and the corresponding Mechanical excitations, $T(t)$, for triangular type waveform excitation.	73
4.6	Comparisons between the imposed and the obtain polarization $P(T)$, and the corresponding mechanical excitations	74

4.7	Harvesting basic technique, piezo road	77
4.8	Temporal variations of the electric and mechanical excitations.	78
4.9	Temporal variations of the electric and mechanical excitations.	79
4.10	Comparison between simulations and measurements for Ericsson loops as a function of the frequency of the electric field.	79
4.11	Comparison between simulations and measurements for Ericsson loops as a function of the frequency of the mechanical stress.	80
4.12	Comparison between simulations and measurements for Ericsson loops as a function of the amplitude of the electric field.	80
4.13	Comparison between simulations and measurements for Ericsson loops as a function of the amplitude of the mechanical stress.	81
4.14	Energy variation of Ericsson loops versus mechanical stress and electric field excitation.	82

List of Tables

1.1	Material technic data [10]	7
1.2	Constant boundary condition [12]	10
1.3	Subscript corresponding to the electrical and mechanical indication [12] . .	11
1.4	Typical ferroelectric material applications [21]	16
1.5	Energy harvesting sources [24]	19
1.6	Vibration frequency and amplitude in a laboratory and daily life, [25] . . .	21
2.1	Comparison of our model with Preisach model	34
3.1	Main characteristics of standard P188 ceramic given by the manufacturer [29]	49
3.2	Main characteristics of standard PZT5A ceramic given by the manufacturer [10]	51
3.3	Main characteristics of standard C2 ceramic given by the manufacturer [59]	51
3.4	Simulation optimum parameters, for the P(E) dielectric model	62

FOLIO ADMINISTRATIF

THESE SOUTENUE DEVANT L'INSTITUT NATIONAL DES SCIENCES APPLIQUEES DE LYON

NOM : **ZHANG**

(avec précision du nom de jeune fille, le cas échéant)

DATE de SOUTENANCE : **Mercredi, 2 juillet 2014**

Prénoms : **Bin**

TITRE : **Model for coupled ferroelectric hysteresis using time fractional operators: Application to innovative energy harvesting.**

NATURE : **Doctorat**

Numéro d'ordre : 2014ISAL0065

Ecole doctorale : **MECANIQUE, ENERGETIQUE, GENIE CIVIL, ACOUSTIQUE(MEGA)**

Spécialité : **Acoustique**

RESUME : Les systèmes de récupération d'énergies basées sur les vibrations mécaniques environnantes suscitent l'intérêt depuis de nombreuses années. Les propriétés des matériaux (coefficients de couplage...) et la mise au point de nouvelles méthodes de collecte de l'énergie ont beaucoup évolué. Augmenter l'efficacité de la conversion d'énergie est primordial, mais celle-ci pour être bien maîtrisée, passe par la mise au point de modèles précis et notamment par la prise en compte des lois régissant les matériaux piézoélectriques. En effet, ces matériaux sont à la base des couplages mécano/électriques et il est capital de comprendre comment ils fonctionnent quelque soit l'excitation externe.

L'augmentation des niveaux de puissance, couplée à la miniaturisation des systèmes impliquent des sollicitations extrêmes sur les matériaux piézoélectriques utilisés, et donc de fortes non-linéarités au niveau des lois de couplages. En outre, la mise au point de techniques de récupération d'énergie large bande implique une grande gamme de fréquence d'utilisation. Un modèle précis du matériau ferroélectrique est indispensable pour établir des critères de conception des prototypes et leur optimisation.

Dans cette thèse, un modèle précis, temporel, large bande tenant compte de l'ensemble des non-linéarités d'une céramique piézoélectrique a été développé. L'utilisation d'opérateurs fractionnaires a permis d'augmenter fortement la bande de fréquence de validité du modèle. Le modèle permet notamment de prévoir l'évolution de la polarisation diélectrique ainsi que le déplacement mécanique de l'échantillon testé et ceci quelque soit le type de stimulation (contrainte mécanique pure, champ électrique et même excitation hybride électriques/mécaniques). La dérivée fractionnaire a dans un premier temps été utilisée pour l'hystérésis sous excitation électrique pour décrire le comportement dynamique de la polarisation diélectrique. En effet, au delà d'un seuil de fréquence, lorsque l'état du matériau n'est plus quasi-statique, une contribution dynamique apparaît. Cette contribution joue un rôle primordial lorsque les niveaux de fréquence et d'amplitude sont élevés. La même étude a ensuite été menée sous contrainte mécanique, et le même opérateur fractionnaire a été utilisé avec succès. Nous avons entre autre constaté que sur un même échantillon les paramètres de simulation établis sous champ électrique étaient conservés sous contrainte mécanique. Ensuite, un modèle inverse permettant d'imposer la forme d'onde de la polarisation ou du déplacement a été proposé. Pour une polarisation ou un déplacement donné, le modèle inverse permet de déterminer avec précision l'effort mécanique à appliquer sur la céramique piézo-électrique. Ces modèles sont nécessaires pour optimiser une forme d'onde de contrainte mécanique ou électrique et obtenir un rendement supérieur des systèmes récupérateurs d'énergie. En effet, une nouvelle technique couplée champ électrique/contrainte mécanique de récupération d'énergie est présentée à la fin de la thèse, technique qui nous a permis de valider l'utilisation du modèle. L'utilisation du modèle permet d'optimiser la mise au point d'un prototype mais également d'obtenir la valeur exacte du rendement de la méthode en rendant compte notamment des pertes diélectriques. Dans la thèse, le modèle sous ses différentes variantes est décrit de manière exhaustive.

MOTS-CLES : **récupération d'énergies, dérivé fractionnaire, couplée champ électrique/contrainte, piézoceramic, non-linéarités**

Laboratoire (s) de recherche : **Laboratoire de Génie Electrique et Ferroélectricité (LGEF) – INSA Lyon**

Directeur de thèse: **Pr. Daniel GUYOMAR**
Co-directeur de thèse : **Dr. Benjamin DUCHARNE**

Président de jury : **Pr. Jean-François DEU**

Composition du jury : **Pr. Yves BERNARD Pr. Jean-François DEU Dr. Benjamin DUCHARNE**
Pr. Daniel GUYOMAR Pr. Grzegorz LITAK Dr. Pierre MELCHIOR